Members of the Council of the West European Confederation of Maritime Technology Societies (WEMT)

Skipsteknisk Selskab, Copenhagen
Finnish Society of Naval Architects, Helsinki
Association Technique Maritime et Aeronautique, Paris
Association of Naval Architects of Greece, Piraeus
Associazione Italiana di Technica Navale, Napels
Nederlandse Vereniging van Technici op Scheepvaartgebied, Rotterdam
Koninklijk Instituut van Ingenieurs/Maritieme Techniek, The Hague
Norske Sivilingeniorers Forening, Oslo
Society of Polish Naval Architects and Marine Engineers, Gdansk
Colegio de Engenharia Naval, Lisbon
Asociacion de Ingenieros Navales de España, Madrid
Royal Institution of Naval Architects, London
Institute of Marine Engineers, London

Gold Medal Awards 1997

West European Confederation of Maritime Technology Societies

1997
Delft University Press

Published and distributed by:

Delft University Press
Mekelweg 4
2628 CD Delft
The Netherlands

tel. +31.15.2783254
fax +31.15.2781661
e-mail: DUP@DUP.TUDelft.NL

Cover: Harry N. Sierman

ISBN 90-407-1534-3

Printed in The Netherlands

Contents

Preface

The *Gold Medal Awards 1997* is published by the Council of the West European Confederation of Maritime Technology Societies (WEMT) in order to show the best paper produced by a member of each society participating in WEMT. However, because of the short preparation time not all the members of WEMT could participate this time.
A publication in English opens up these papers to all the members of the relevant societies because otherwise they would have been published in the national language only.
Moreover, such a publication if selectively distributed, makes the ability of the members of the societies concerned better known to a wider public with an interest in maritime technology.
Improved knowledge of as well as more interest in the prospects of maritime technology in a wider public might support het present position of naval architects and marine engineers, actually the brainpower in maritime developments. With that support and together with other professions needed to be engaged in maritime industry the present situation with respect to the maritime market in Europe and abroad could be improved again.

Competition, whether fair or unfair, will be a fact of live in this world and to beat the competition all organisations engaged in the maritime industry have to set all sails. So are the societies of naval architects and/or marine engineers.
'Knowledge is power' is an old saying but still in force today and that we have to develop to the limits of our ability by research and development. Every opportunity to improve our knowledge should be grabbed by participation in either national or European research directed at application in the maritime industry.
However, that only will not be sufficient because knowledge and experience should also be brought forward with authority at all levels of concern in society. It is to each one of us to support that task as well.

Whenever, the publication of *Gold Medal Awards* can contribute to the aims as described above, it will be worth the effort.

Council of WEMT
p.p. ir. W. Spuyman,
secretary

Rotterdam, October 1997

Global Strenght Asessment of Naval Surface Vessels in Rough Sea

R. Damonte, R. Porcari, L. Sebastiani,
CETENA S.p.A.

B. Spanghero
Italian Navy

Offered for publication by Associazione Italiana di Tecnica Navale

Abstract

Rational ship structural design needs stress analyses to be carried out with a certain degree of approximation: this means an adequate representation of ship structures and realistic assumption on loads combinations.
As far as structural modelling is concerned finite element models for the stress analysis of the whole ship are more and more frequently adopted, allowing good insight in structural behaviour. Because of uncertainties of the loads the ship has to withstand during her life, the effectiveness of direct calculation considerably depends not only on goodness of structural modelling, but also on the evaluation of environmental loads and ways to apply them on structures.
According to this perspective, a joint effort between the Italian Navy and CETENA is in progress for the development of a structural design procedure totally computer-based able to analyse complex ship structures and to support relevant design.
In this paper the fundamental steps of this procedure are described focusing the attention to structural and seakeeping packages which are going to be integrated in order to allow the user to easily manage the whole procedure.
Structural module is mainly based on a F.E. package oriented to global analysis of stiffened shell structures and therefore suitable for preliminary structural design, while the seakeeping module is based on a linear strip theory code integrated with a statistic processor.

1. Introduction

Wave loading evaluation is fundamental for the strength assessment of the ship hull. The common seagoing experience demonstrated that design procedures based on traditional scantling rules held to non optimised structures, often too much conservative for the large amount of structural members, but sometimes critical for a certain number of details.
Traditionally, a design bending moment has been used by calculating the value deriving from balancing the ship on a wave with length equal to that of the ship and height equal to L/20. This empirical approach may be not directly applicable in the case of new ships designed for different operation and sometimes characterised by different structural arrangement. In these cases, in order to assess structural strength of the hull, it is extremely important to define real loading to be applied to the hull structural model. Furthermore, in the case of innovative designs, direct strength analysis of the hull structure are recommended; such analysis strongly depends on loads and loading condition evaluation, which calculation needs to be carried out by suitable seakeeping analysis. The complexity of the matter makes extremely heavy the treatment of all the calculation steps as separate items, and a strong integration among them allows to obtain better results and an easier use of the procedure.
Within the frame of a rational ship structural design for naval vessels, Italian Navy and CETENA have been working for some years on the development of a strength assessment procedure based on commercial and home made software codes. This integrated procedure allows the user to design the whole structure on the basis of a rational approach which takes into account the ship response in rough sea. A series of structural load cases for each cargo loading condition is generated on the basis of hydrodynamic analysis and may be investigated by means of the finite element technique in order to identify critical response of the structure.
The purpose of this paper is to describe the fundamental steps of this procedure focusing the attention on seakeeping and structural packages and their integration.

2. Integrated computational procedure

The procedure, named POS2, is articulated in several steps, grouped into three main types of analysis: *hydrodynamic analysis, load calculation and loading condition definition, structural analysis* and it is based on the concept of equivalent design wave, reported by some authors [1, 2, 3]. The overall flow diagram of the computational procedure is shown in Fig. 1, the main steps being:

1. hydrodynamic modelling and calculation of Linear Transfer Functions of motions and global loads according to strip theory;
2. prediction of expected maximum loads in the ship life;

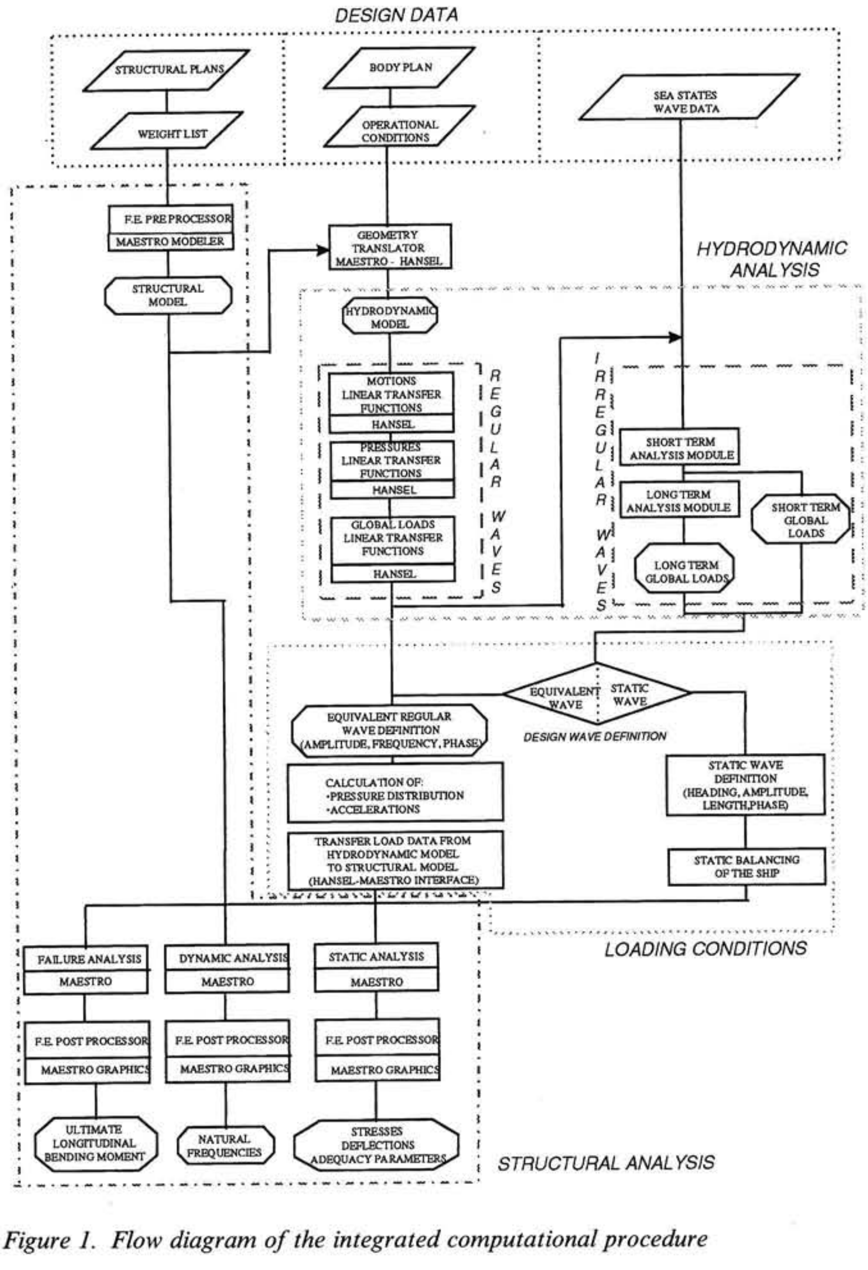

Figure 1. Flow diagram of the integrated computational procedure

3. determination of equivalent regular design wave;
4. calculation of pressure distribution and accelerations for equivalent wave to be applied to structural model;

5. global structural analyses by F.E. code (static, ultimate strength, natural frequencies);
6. local structural analysis by F.E. codes.

2.1 Hydrodynamic analysis

The core of the hydrodynamic analysis package (hereafter referred to as **HANSEL** acronym of **H**ydrodynamic **AN**alysis for **SE**a **L**oads) the *NSRDC Ship-Motion and Sea-Load Computer Program* [4] which is a linear frequency-domain seakeeping code based on the *strip-theory* of Salvesen, Tuck and Faltinsen [5] and on the Frank's *close-fit* technique [6] for the modelling of the sectional hydrodynamic quantities.

HANSEL is able to predict the motions and global dynamic loads for a ship in six-degrees-of-freedom (6DOF) advancing at constant speed with arbitrary heading in regular waves. More specifically the module computes amplitudes and phases for surge, sway, heave, roll, pitch and yaw motions and the vertical and horizontal shear forces, bending moments, and torsional moments. Furthermore the program computes at any point on the submerged portion of the hull the hydrodynamic pressure due to the motions and the incoming wave.

According to the Frank's *close-fit* technique, each cross-section of the ship is modelled by means of a polygonal based on a system of offset points properly chosen along the girth. At the middle-point of each segment a pulsating source is placed which superimposed effect represents the two-dimensional flow disturbance caused by the ship/wave interaction.

As regards the pressure distribution, it must be noted that in deriving the expression for the wave diffraction force use is made of the so-called Haskind's theorem (i.e. Green's second identity) so that the expression is only applicable to the total force and not to the local disturbance. In the present methodology the diffraction part of the hydrodynamic pressure has been approximated by a uniform sectional pressure which when integrated over the section is equal to the sectional diffraction forces. This is a sound approximation in many cases, as usually the diffraction component is a minor part of the total disturbance.

The determination of the global dynamic loads at specified ship stations requires the definition of the longitudinal weight distribution. It should be noted that for the computation of the torsional moment the specific knowledge of the roll radius of gyration for each cross-section is requested.

HANSEL package has been organised as a suite of three calculation modules in-sequence:

1. RW – regular waves module	– Linear Transfer Functions of local/ global loads
2. STS – *short-term* statistics module	– RMS values of local/global loads in a sea state
3. LTS – *long-term* statistics module	– Extreme values of local/global loads in a cluster of sea states

2.1.1 Linear Transfer Functions

As regards RW module three basic categories of Linear Transfer Functions (LTFs) are of relevance for the structural analysis, namely: rigid-body accelerations at specified ship points, global dynamic loads at specified ship stations, hydrodynamic pressures at specified points of the hull wetted surface. The LTF of a generic seakeeping quantity X pertaining to these categories is defined in terms of its amplitude and phase with respect to the incident wave ζ with its crest at the ship LCG:

$$X(t) \quad = X_M \cdot \cos(\omega t - X_P) \tag{1}$$

$$\zeta(x,y;t) = a \cdot \cos(\omega t - k\ x \cos\beta - k\ y \sin\beta) \tag{2}$$

whereas ω is the *encounter* frequency of the train of regular waves, k is the wave number and β is the incoming wave direction angle with respect to the bow (head sea=180°).

2.1.2 Short-term statistics

Once the relevant LTFs have been evaluated as a function of ship speed, wave heading and wave frequency, spectral theory can be invoked to carry out the *short-term* statistics of the various seakeeping quantities.

The random nature of the sea environment implies that it is not possible to attribute an unique deterministic value to the wave-induced responses of the ship but they can only be statistically characterised, i.e. in probabilistic terms. The basic hypothesis of spectral theory is that sea waves can be thought as a *zero-mean homogeneous stationary ergodic Gaussian* aleatory process; linearity assumption hence ensures that also ship response in waves will enjoy the same privileges. *Homogeneous* means that the statistical nature of the process will be the same within the spatial area (*fetch*) interested by the sea state, *stationary* means that the statistical nature of the process will not change in time for the duration of the sea state (this implicitly assumes a *fully-developed* sea), *ergodic* means that the statistical average, which should be in principle performed with respect to the abstract ensemble of all the possible *realisations* of the process, can be identified with the much more practical temporal average, *Gaussian* means that the values of the process are statistically distributed according to Gaussian (*normal*) law.

The latter assumption ensures that a generic wave-induced ship response X(t) in a sea state is statistically determined by its RMS (*Root Mean Square or Standard Deviation*) value RMS_X whilst the first three assumptions allow to easily determine such value in frequency-domain as the square-root of the integral of the response amplitude spectrum $S_X(\omega)$:

$$RMS_X = \sqrt{\int_0^\infty S_X(\omega)\ d\omega} \tag{3}$$

Furthermore, linearity assumptions provides a relationship between the response amplitude spectrum and the sea wave spectrum $S_\zeta(\omega)$ through the LTF:

$$S_X(\omega) = X_M^2(\omega) \cdot S_\zeta(\omega) \tag{4}$$

Each sea state is modelled by means of JONSWAP 3-parameters wave spectrum, specified in terms of Significant Wave Height (H_S), Modal (or Peak) Wave Period (T_0) and Enhancement (or Peak) Factor (γ). Both uni-directional (*long-crested*) sea and multi-directional or confused (*short-crested*) sea are accounted for. In the latter case the sea state can be thought of as the superposition of monochromatic uni-directional waves so that its sea spectrum will be in principle a two-variable $S_\zeta(\omega,\theta)$ function. Invoking separability assumption, such spectrum can be decomposed as:

$$S_\zeta(\omega,\theta) = S_\zeta(\omega) \cdot S_\beta(\theta) \tag{5}$$

A *cosine-squared spreading function* is further adopted to represent the distribution of the wave energy over the wave headings:

$$S_\beta(\theta) = 2/\pi \cos^2(\beta-\theta) \tag{6}$$

2.1.3 Long-term statistics

Whilst *short-term* statistics refer to the statistical determination of wave-induced ship response for short duration of time, i.e. for the duration of an individual sea state, *long-term* statistics is relevant to longer laps of time during which more sea states are likely to be encountered. Long-term statistics require to specify a geographical area and a period of time for the mission of the ship. By means of statistical tables is then possible to associate to the ship mission a cluster of sea states with their probability of occurrence.

Duality principle can be invoked to reduce long-term statistics to the *weighted* average of the short-term statistics with respect to the sea states cluster considered. In particular the probability that the generic wave-induced ship response X(t) exceeds a certain threshold value x in the long-term will be given by:

$$P[X>x]=\Sigma_i\, w_i \cdot p_i(x) \tag{7}$$

whereas the summation is extended to all the associated sea states, w_i is the probability of occurrence of the i-th sea state and p_i is the exceeding probability in the short-term for the i-th sea state which is provided by:

$$p_i(x) = EXP[\,-(x\,/\,2RMS_X)^2\,] \tag{8}$$

The long-term probability can be related to the number of cycles N_{extr} within which the response X(t) exceeds at least once the threshold value X_{extr} during the expected service life T_{sl} of the ship:

$$P[X>X_{extr}]=1/\,N_{extr} \tag{9}$$

whereas:

$$N_{extr} = T_{sl}\,/\,T_z \tag{10}$$

having denoted with T_z the characteristic period of the response i.e. its *zero-crossing* period.

2.2 Loads and loading conditions definition

The core of the structural analysis package is the MAESTRO code. In the following the interaction between MAESTRO and HANSEL packages is outlined to provide the desired design loads on the ship.

2.2.1 Definition of the loads on the structural model

The most critical aspect in linking the hydrodynamic analysis package with the structural analysis package is probably to properly transfer the hydrodynamic loads to the structural model.

This topic is closely related to the strategy adopted for the structural analysis. The underlying philosophy of the present global approach to ship scantling is the use of a *design wave* which means that the hydrodynamic/structure linking is rationally accomplished by defining a suitable *equivalent* regular wave and by using the corresponding values of the hydrodynamic pressures as the proper local loads to be applied to the FEM mesh of the ship. In this case the problem arises of how interfacing the hydrodynamic 2D mesh with the structural 3D mesh.

Hydrodynamic pressures are computed at the middle points of the straight-line segments joining the offset points of each transverse section of the ship. It is assumed that the FEM mesh is built-up by means of quadrilateral elements only and that the hydrodynamic offset points do coincide with a sub-set of the nodal points defining the FEM mesh. This way a practical linear interpolation scheme can be devised to transfer the hydrodynamic values to the structural nodal points.

Besides the hydrodynamic pressures, it is also necessary to feed the structural model with the proper inertia loads. By assuming a *lumped-mass* modelling of the weight distribution is adopted for the structural analysis, it is thence possible to associate to each individual centre of gravity the wave-induced rigid-body accelerations by properly combining the 6DOF COG LTFs calculated by HANSEL package.

The waves exert their action on the ship through the fluid pressure normally applied on the immersed portion of the hull and, as a consequence of this action, the ship undergoes oscillatory motions. At each instant of time the ship is globally in dynamic equilibrium, since the resultant of the hydrodynamic forces exactly counterbalances the inertia force:

$$\underline{F_{diff}} + \underline{F_{inc}} + \underline{F_{rad}} + \underline{F_{reac}} - m\,\underline{\ddot{x}} = \underline{0} \tag{11}$$

whereas the total hydrodynamic force is split into its individual components: diffracted wave force (resulting from the reflection of the incident wave by the standing ship), incident wave or *Froude-Krylov* force, radiated wave force and reaction force (associated with the resistance opposed by the fluid to the oscillatory motions of the ship). The above statement can be as well expressed in terms of hydrodynamic pressures:

$$\int_{hull} (p_{diff} + p_{inc} + p_{rad} + p_{hyd})\,\underline{N}\,dS - m\,\underline{\ddot{x}} = \underline{0} \tag{12}$$

Whilst such dynamic equilibrium is imbedded in the mathematical model for the seakeeping behaviour of the ship, there is nothing to warrant that it will be maintained when transferring the wave loads from the hydrodynamic model to the structural model.

While retaining the inertia loads as resulting from the structural model it is thence necessary *a trial-and-error* procedure to adjust the nodal values of the hydrodynamic pressure on the FEM mesh until dynamic equilibrium for the structural model is reached.

2.2.2 Definition of the loading conditions

The present approach for the definition of the loading conditions is based on the concept of *equivalent design wave*.

To this regard it is assumed that a set of representative global dynamic loads has been identified, referred to as Dominant Load Components (or DLC).

For each DLC the HANSEL package will evaluate the *long-term* value associated with the proper probability level.

It is thence possible to define for each DLC an equivalent regular wave:

$$\zeta(t) = a \cdot \cos(\omega\, t - \delta) \tag{13}$$

so that:

a = ratio between the *long-term* value and the *maximum* amplitude of the LTF,
ω_0 = *peak* frequency of the LTF,
δ = phase of the LTF corresponding to the *peak* frequency.

The hydrodynamic pressure to be applied at the i-th nodal point of the FEM mesh will be thence given by:

$$p_i(t) = a \cdot p_{Mi} \cdot \cos(\omega_0\, t_0 - p_{Pi} - \delta) \tag{14}$$

whereas t_0 is the time instant corresponding to the maximum value of the response of the DLC induced by the equivalent regular wave.

The same considerations hold about the rigid-body accelerations for the definition of the inertia loads in the structural model.

Notwithstanding the above approach is surely a rational and consistent procedure to carry out a structural analysis based on the direct calculation of the wave-induced loads on the ship, it is still common practice in the design offices of many shipyards the recourse to the *static wave* for the definition of the design loads. As a matter of fact, such *hydrostatic* approach, even if lacking a real scientific basis, has been thoroughly calibrated and assessed by years of experience, so that it cannot be expected to be replaced at once by quite recent innovative design methodologies such as the one above outlined.

Considering this fact, POS2 package allows to optionally carry out the structural analysis of the ship according to this well-proven traditional procedure but provides a more rational foundation for the definition of the *static wave*.

In particular such steady wave is characterised by amplitude, wave length and phase. Wave length and phase will be chosen as for the *equivalent* wave, while amplitude will be determined so to ensure at the *Midship Section* a *hydrostatic* global load equal to its *long-term* value as calculated by the HANSEL package.

This will obviously require an iterative scheme on the wave amplitude until the desired hydrostatic condition is reached.

As MAESTRO package currently does not provide a specific option for the automatic imposition of the equilibrium, an *ad hoc* module for balancing on the static wave will be developed.

2.3 Structural analysis

2.3.1 Global analysis

The structural response to the quasi static loads derived from hydrodynamic analysis is calculated via Finite Element Analysis in terms of stresses and deflections.
The procedure is oriented to the global analysis of the hull structures, that means to model the overall stiffness and global strength distribution in the primary members of the hull.
The use of a quite coarse global model allows to establish the most severely stressed areas and to provide relevant boundary conditions for possible more detailed analyses. In particular, each equivalent design wave associated to a Dominant Load Component allows to assess the structural strength for a specific demand. For this reason assumption of different Dominant Load Components and relevant equivalent waves has to cover the envelope of most severe conditions the ship will experience during her life. This means that, in general, loading conditions to be adopted need to be tailored on each vessel, as a function of specific structural arrangement.
The finite element code adopted in the procedure is MAESTRO /7/, /8/ with the relevant pre and post processors programs. MAESTRO is a commercial code for structural analysis, design and optimisation of ship structures. Its key feature consists in the capability to model a complex stiffened shell structure, like a ship, with a few structural elements. The elements have an 'ad hoc' formulation to represent the behaviour of the elements typical to ship structures (stiffened panels, girders and so on), allowing the user to perform design and evaluation of ship structures in a quick and simple manner through a F.E. solver.
Figs. 2 and 3 show MAESTRO 3D global models of a Guided Missiles Destroyer (DDG) and of a Replenishment Ship (AOR) hull structures.
MAESTRO package is organised in the following calculation modules:

1	Finite elements pre-processor module	(MAESTRO Modeler)
2	Finite elements post-processor module	(MAESTRO Graphics)
3	Module for Static Structural Analysis	(MAESTRO)
4	Module for Dynamic Structural Analysis	(MAESTRO ADIN)
5	Module for Ultimate Strength Analysis	(MAESTRO COLL)
6	Module for Detailed Stress Analysis	(MAESTRO DSA)

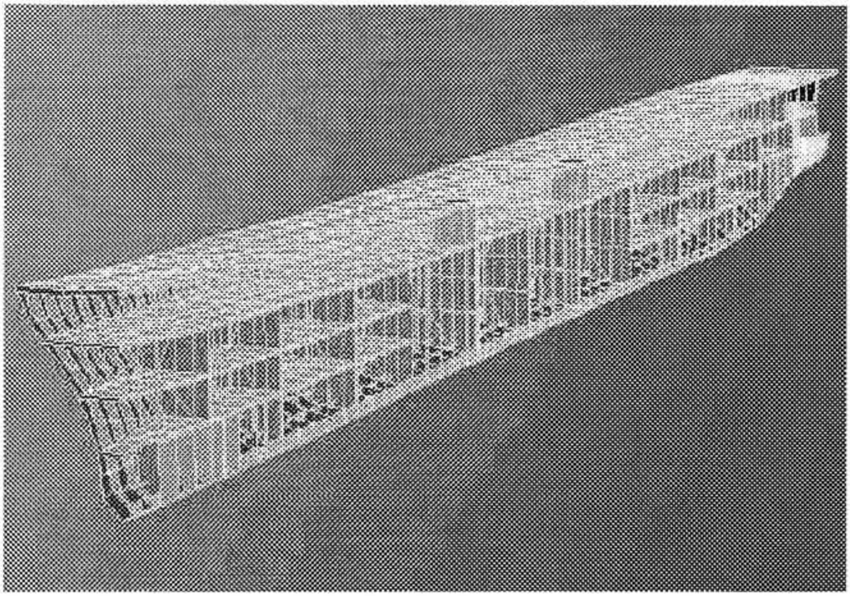

Figure 2. MAESTRO global model of DDG hull structure

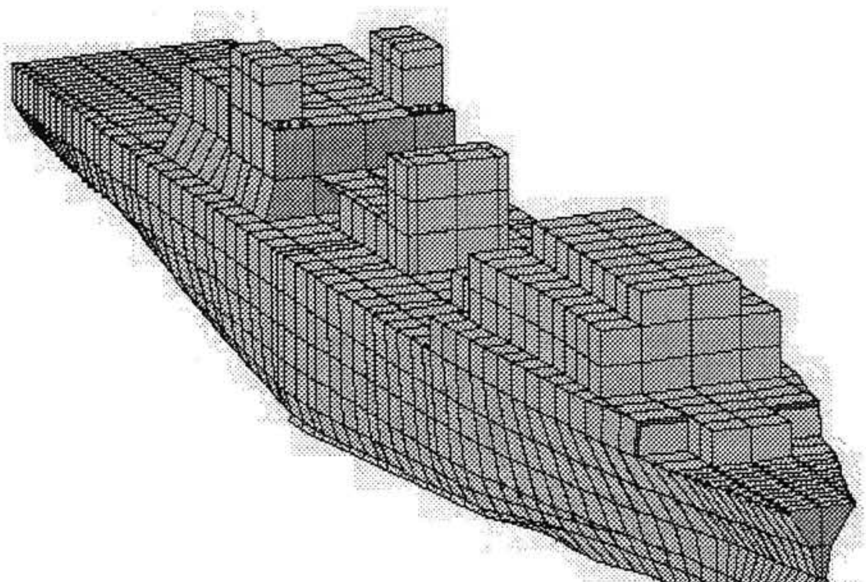

Figure 3. MAESTRO global model of AOR structure

2.3.2 Local stress analysis

MAESTRO provides the capability to perform detailed stress analyses in conjunction with global analysis, this may be obtained including detailed models of localised areas of interest directly into the global model by means of the superelement technique or using distinct detailed models in a top-down analysis. Of course any finite element code may be used for detailed analysis, made sure that all acting critical load situations, including secondary loads, are modelled. In any case detail structural design and analysis is generally a separate process performed at a later design stage.

2.3.3 Ultimate strength analysis

As this procedure includes the evaluation of the ship behaviour under extreme design loads, it is worth having a package for the ultimate strength analysis, able to compute at least the ultimate longitudinal bending moment, taking into account non linear behaviour of decks and bottom panels under in plane compressive loads.
Furthermore, information on ultimate strength of structure and on extreme loads are necessary to move towards a reliability based design, that is an almost mature approach to be introduced in the shipbuilding community.
With regards to this item, MAESTRO contains a specific routine for ultimate bending moment evaluation based on the Adamchak's approach [9].
The ultimate strength evaluation can be integrated into the MAESTRO design process in two ways: as a final check of the design or as an obligatory step, and as a possible constraint, in an optimisation process.
The hull girder collapse calculation is based upon following main assumptions:

- the frames are strong enough to be considered as a support of the panels, so transverse collapse is excluded;
- longitudinal collapse occurs only between two adjacent frames;
- longitudinal girders are strong enough to be considered as a support for the panels,
- longitudinal girders failure is due to yielding only;
- the critical structural member for inter frame collapse is the stiffened panel.

Under these assumptions, the moment-curvature relationship is calculated step by step as follows.
For each increment of curvature ΔK the strain increment for each element i is computed with the simple bending beam theory assuming a linear distribution through the cross section:

$$\Delta\varepsilon_i = y_i \cdot \Delta K \qquad (15)$$

where y_i is the distance of the i-element from the instantaneous cross-section neutral axis.

The corresponding bending moment acting on the section is:

$$M = \sum_i (A_i \cdot \sigma_i \cdot y_i) \tag{16}$$

where:
A_i = effective sectional area of the elements,
σ_i = stress related to the strain ε_i via the stress-strain curve, characteristic for the element.

Since the stress distribution may be non linear, the position of the instantaneous neutral axis must be computed by a separate iterative process. The position of the neutral axis is varied until the following equation is satisfied:

$$N = \sum_i (A_i \cdot \sigma_i) = 0 \tag{17}$$

The cumulative strain of the *i*-element results as:

$$\varepsilon_i = \sum_j y_{ij} \cdot \Delta K_j \tag{18}$$

and cumulative curvature:

$$K = \sum_j \Delta K_j \tag{19}$$

Using the above approximation the calculation of the hull girder collapse is influenced by the evaluation of the non linear behaviour of interframe stiffened panels subjected to in-plane loads. To obtain a suitable value in a quick way, the code uses simplified design formulas based on the beam-column approach. The failure equations for the collapse modes included into MAESTRO code can be found in [8].

4. Future developements and conclusions

The validation of the described procedure, currently under development as far as the integration of different modules is concerned, can be achieved by means of the assessment of real loading experienced by seagoing ships.
For this reason a project for the structural monitoring of ships at sea is currently under launching by the Italian Navy.
A monitoring system installed on board shall be able to provide ship motions and hull stress information on which basis the validation of the above mentioned theoretical procedure could start.
The knowledge of realistic loading histories shall contribute not only in checking the ship response to extreme loads, but will be also extremely important to

investigate the fatigue behaviour of structures due to the cumulative contribution of all significant cyclic loads. In fact most common structural problems experienced by ships after prolonged operations at sea consist in fatigue cracking; although generally fatigue cracks do not represent a safety problems, they can originate considerable costs for repair.

5. References

[1] Liu, D., Spencer, J., Itoh, T., Kawachi, S., Shigematsu, K.
"Dynamic Load Approach in Tanker Design"
SNAME Transactions, Vol. 100, 1992, pp. 143-172

[2] Payer, H.G., Fricke, W.
"Rational Dimensioning and Analysis of Complex Ship Structures"
SNAME Transactions, Vol. 102, 1994, pp. 395-417

[3] Valsgœrd, S., Svensen, Tor E., Thorkildsen, H.
"A Computational Method for Analysis of Container Vessels"
SNAME Transactions, Vol. 103, 1995, pp. 371-393

[4] Meyers, W. G. et al.
"Manual NSRDC ship-motion and sea-load computer program"
NSRDC Rep. n. 3376, February 1975

[5] Salvesen, N., Tuck, E.O., Faltinsen, O.
"Ship motions and sea LOADS"
Trans. SNAME 1970, vol. 78, pp. 250-287

[6] Frank, W.
"Oscillation of cylinders in or below the free-surface of deep-fluids"
NSRDC Rep. n. 2357, 1967

[7] Hughes, O.
MAESTRO user manuals
V. 5.4-4, November 1990; V. 6.0, February 1992; V. 6.01, November 1992; V. 6.2, September 1993

[8] Hughes, O.
Ship structural design
Wiley – Interscience Publication, 1983

[9] Adamchak, J. C.
ULTSTR: a program for estimating the collapse moment of a ship's hull under longitudinal bending.
DTNSRDC, Bethesda; October 1982

Fluid Momentum in Ship Hydrodynamics

W. Beukelman,
Ass. Professor of Ship Hydromechanics
Delft University of Technology

Offered for publication by Nederlandse Vereniging van Technici op Scheepvaart gebied

Introduction

The rate of change of fluid momentum is a very significant characteristic to determine important phenomena in ship hydrodynamics such as motions in waves, slamming, lift forces on hull and rudder, manoeuvring derivatives, etc.
Three of these phenomena will be considered closer here, especially the calculation methods viz.:

- slamming
- lift production of the hull
- manoeuvring

For *slamming* the impact force is determined with aid of fluid momentum exchange and strip theory including forward speed influence.
To determine the *lift forces* and *-moments* and also the *hydrostatic-* and *dynamic manoeuvring coefficients* the ship hull is considered to be a low aspect-ratio surface piercing wing. The determination is based upon potential theory making use of the variation of the added mass impulse or the rate of change of fluid momentum.
Transformation from seakeeping to manoeuvring notation is used to arrive at expressions for sway and yaw derivatives applicable for both *deep* and *shallow water*.
Reduction of waterdepth causes a strong increase of lift and consequently also of manoeuvring derivatives.
The calculated results are related to the linear part of the coefficients, which means validity only at small drift angles or angles of attack. As an example comparisons with experiments are presented for the cases considered.

1 Slamming

The impact pressure is mainly determined by the velocity normal to the hull. In case of a ship with a flat bottom, the impact pressures on the bottom can be determined if the velocities normal to the bottom are known. This case will be considered here [I].
The hydrodynamic force per unit length on a strip of an oscillating ship will be

$$F' = F'_1 + F'_2 + F'_3 \quad = \quad -2\rho\, g\, y_w s - N'\dot{s} - \frac{d}{dt}(\, m'\dot{s}\,) \tag{1}$$

in which ρ = density of water
g = acceleration of gravity
y_w = half width of the cross-section at the moment of touching the water surface
m' = the sectional added mass

N' = the sectional damping
s = $s_a \cos \omega t$ = the vertical displacement

The first term F'_1 is of minor importance because the vertical displacement s is very small during the time that the maximum slam pressure is built up. The contribution of the second term, F'_2, is also negligible on account of the small damping proportional to the first power of the vertical velocity. What remains is the third term, F'_3, representing the *fluid momentum exchange* of the section considered.
The resulting slam pressure may be written as

$$p = \frac{1}{2y_w} \left(+ \frac{dm'}{ds} \dot{s}^2 + m'\ddot{s} \right) \tag{2}$$

From eq. (2) it appears that:
1. the slam pressure is inversely proportional to the wetted width, $2y_w$
2. the second term is proportional to the squared vertical velocity and showing also that the increase of added mass with depth is very important

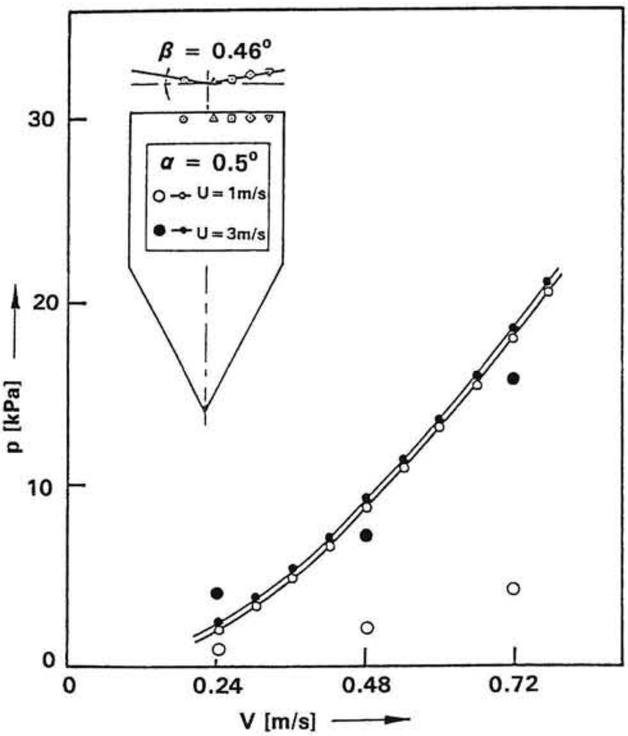

Figure 1. Test points (● o) and predicted results (-●-, -o-) of peak pressure as function of vertical velocity V [1]

3. the third term may become very significant if the vertical acceleration is high. This may be the case if a component arises due to the forward velocity of the ship.

In case of forward speed U with a trim angle α (bow up) the vertical impact speed will be

$$V = \dot{s} - U\sin\alpha \tag{3}$$

An extension of this method taking into account more significant forward speed influence and 3-D effects is presented in part II of I. An example of measured and calculated impact pressures dependent on the vertical speed V is presented in Figure 1 from [I] (part II) for a dead rise angle $\beta = 0.46°$ and a trim angle $\alpha = 0.50°$. Most existing calculation methods show too high pressure predictions. A strong increase of peak pressures with dead rise angles could be established up to 1.15° dead rise angle.

2 Transverse forces

The calculation of the transverse force is also based on the *exchange* of *fluid momentum* according to method as proposed by Jones [2] to determine the lift forces on a wing profile. For zero drift angle the transverse force is equal to the lift force (Figure 2). The hydrostatic and hydrodynamic manoeuvring coefficients are derived from the transverse forces and moments. In this way a ship is considered to be a wing profile with a low aspect ratio.

The derivative of the local normal or transverse force N may be set equal to the time-derivative of the local added mass impulse in transverse direction or the fluid momentum exchange and can be written as

$$\frac{dN}{dx} = \frac{d}{dt}(m'v) \tag{4}$$

with: m' = the added mass per unit length
v = + $U\beta$ as the transverse component of the flow speed – U
β = drift angle or angle of attack

Equation (4) may be developed into

$$\frac{dN}{dx} = \frac{dm'}{dx}\frac{dx}{dt}v + m'\frac{dv}{dx}\frac{dx}{dt} \tag{5}$$

Keeping in mind that $dv/dx = 0$ and $dx/dt = -U$ (being the fluid flow speed on the wing which is opposite to the wing-model speed U) the expression becomes:

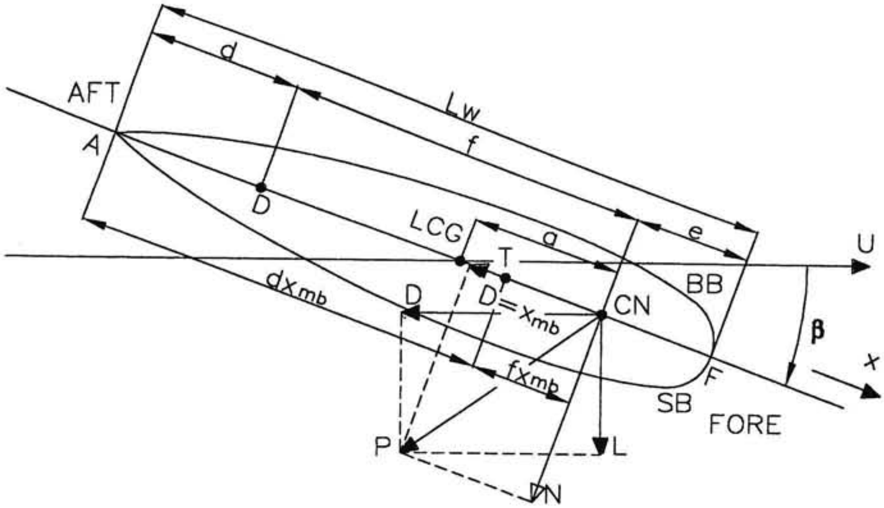

Figure 2. Forces acting on the wing section

$$\frac{dN}{dx} = -U^2\beta\,\frac{dm'}{dx} \tag{6}$$

and $\quad dN = -U^2\beta dm' \qquad (7)$

The total normal force on the wing model will be obtained by integration of dN over the length/chord of the wing as:

$$N = \int_A^F dN = -U^2\beta \int_A^F dm' = \tag{8}$$

$$[\,N_F - N_A\,] = -U^2\beta\,[m'_F - m'_A] \tag{9}$$

If $m'_F = m'_A = 0$ which is generally the case, the total transverse force will be zero. This phenomenon is quite in accordance with D'Alembert's paradox on the assumption that the flow is irrotational in an ideal fluid without viscosity, vortex sheets and separation. Only for a body with a tail fin at the end, so $m'_A \neq 0$, the situation is fundamentally different as stated by Newman in [3].
It is well known, however, that viscosity is required to start the potential lift production. Jones [2] put forward that with the aid of the Kutta-condition it may easily be shown that sections of the wing behind the section of the greatest width develop no lift. Katz and Plotkin even showed in [4] that there will be no lift if $b(x)$ is constant with x. Integration up to the section with the maximum width should then be sufficient.
If the integration in eq. (8) is carried out from the forward point (F) to the sec-

tion with the maximum beam *(mb)* and if $m'_F = 0$, it then holds that the transverse force may be written as

$$N = -U^2 \beta m'_{x_{mb}} \tag{10}$$

The sectional added mass m' was determined using a method based upon potential theory only as presented by Keil in [5] including the influence of restricted waterdepth. The sectional added mass m' may also be obtained by a diffraction method i.e. Delfrac of Pinkster as presented by Dmitrieva in [6]. The advantage of this method is that wall influence or influence of other obstacles in the neighbourhood may be taken into account.

3 Lift production

Here the lift production at zero drift angle β will be considered for which case holds that the lift force L is equal to the transverse force N. For other drift angles the longitudinal force T should be accounted for to find the lift force L and drag D as denoted in Figure 2. If the lift force coefficient is presented as

$$C_L = \frac{L}{\frac{1}{2}\rho U^2 L_w T} \tag{11}$$

the slope of the lift curve at $\beta = 0$ may be written as

$$\frac{\partial C_L}{\partial \beta} = \frac{m'_{x_{mb}}}{\frac{1}{2}\rho L_w T} \tag{12}$$

in which L_w = the length of the wing or ship and
T = draught.

The moment of the local transverse force with respect to the origin of a body-fixed right hand coordinate system xyz (x longitudinal, positive in forward speed direction at $\beta = 0°$, y transverse, positive to the right or starboard side SB, z positive downwards) may be expressed as follows:

$$dM = \frac{dN}{dx}\, x\, dx \tag{13}$$

With the origin of the coordinate system situated at D (Figure 2) and substituting eq. (6) into (13) the total moment of the transverse force on the wing model with respect to D will be:

$$M = \int_D^F dM = -U^2\beta \int_D^F x\, dm' = \tag{14}$$

or

$$M = -U^2\beta \{xm' \Big|_D^F - \int_D^F m'\, dx\}$$

It follows with

$$m'_F = 0$$

$$M = U^2\beta m_D \tag{15}$$

Following the reasoning as used for the transverse/lift force D should be chosen as located at x_{mb} (Figure 2)

$$m_{x_{bm}} = m_D = \int_{D=x_{mb}}^{F} m'\, dx$$

is the added mass from F to x_{mb}. This moment with respect to LCG delivers the well known destabilizing Munk-moment for a body with a drift angle at a steady translation. The distance Fx_{mb} from x_{mb} to CN (See Figure 2) is found as follows:

$$f_{x_{mb}} = \frac{M}{N} = \frac{U^2\beta m_{x_{mb}}}{U^2\beta m'_{x_{mb}}} = \frac{m_{x_{mb}}}{m'_{x_{mb}}} \tag{16}$$

The distance e from CN to the forward wing point will be:

$$e = Lw - d_{x_{mb}} - f_{x_{mb}} = L_w - d_{x_{mb}} - \frac{m_{x_{mb}}}{m'_{x_{mb}}} \tag{17}$$

and

$$\frac{e}{L_w} = \frac{(L_w - d_{x_{mb}} - \frac{m_{x_{mb}}}{m'_{x_{mb}}})}{L_w} \tag{18}$$

The moment of the transverse force or lift force at $\beta = 0$ with respect to F is:

$$M_e = N_e = U^2\beta m'_{x_{mb}} (L_w - d_{x_{mb}} - \frac{m_{x_{mb}}}{m'_{x_{mb}}}) \tag{19}$$

and the moment coefficient

Square Tips, H = 2.50 m, T = 0.30 m

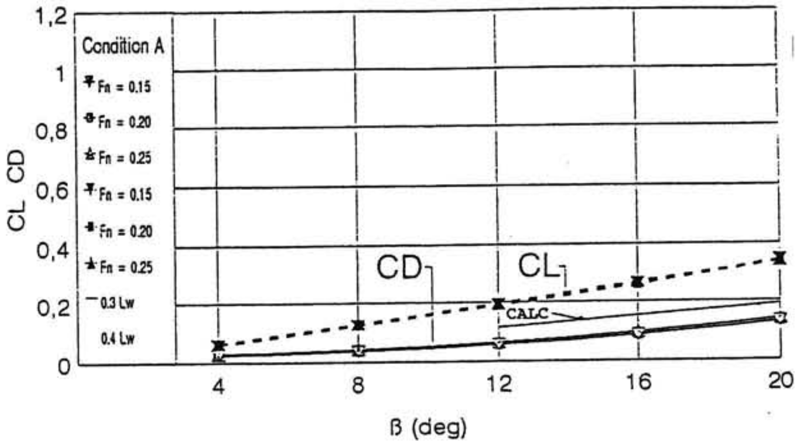

Square Tips, H = 0.48 m, T = 0.30 m

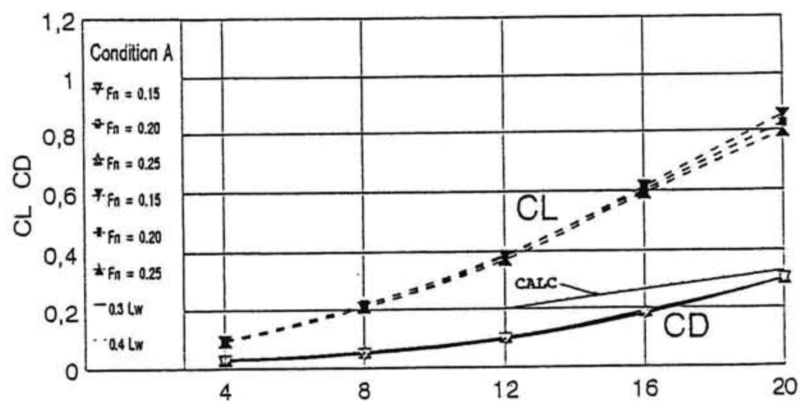

Figure 3. Lift and drag coefficients

$$C_{M_e} = \frac{M_e}{\frac{1}{2}\rho U^2 L_w^2 T} = \frac{m'_{x_{mb}}\beta}{\frac{1}{2}\rho L_w T}\,\frac{e}{L_w} \tag{20}$$

The slope of the moment curve at $\beta = 0$ is found to be as follows:

$$\frac{\partial C_{M_e}}{\partial \beta} = \frac{m'_{x_{mb}}}{\frac{1}{2}\rho L_w T} * \frac{e}{L_w}$$

$$= \frac{\partial C_L}{\partial \beta}\frac{e}{L_w} \tag{21}$$

Tests with a wing model as reported in [7] show that lift and drag increase strongly if the waterdepth reduces. See as an example Figure 3. Calculated values confirm this very well. Using faired tips at the bilge in stead of square tips decreases drag and lift considerably. Experimental results with faired tips approach for both lift and moment the calculated linear values in case of zero angle of attack β.

4. Manœuvring

4.1 General

The manoeuvring coefficients will be calculated with aid of the seakeeping coefficients. See for a description [8]. These coefficients generally are built up from terms with sectional fluid added mass (m') and damping coefficient ($N' - U\,dm'/dx$). For manoeuvring it is assumed that the oscillation frequency is zero (static measurements) or very low at oscillation so that the damping $N' \rightarrow o$. The term $U\,dm'/dx$ of the damping coefficient will deliver the transverse forces as shown before. For this reason terms with $U\,dm'/dx$ will be integrated from the forward point (F) to the section with the maximum beam (mb). This holds also for terms with m' following from $U\,dm'/dx$ by partial integration. Terms with pure added mass m' will be integrated over the whole model length L_w as shown experimentally in the past. The relation between seakeeping and manoeuvring has to be considered to find expressions for the manoeuvring coefficients. The most remarkable difference is the choice of the vertical axis z, positive upwards in seakeeping and downwards for manoeuvring. Hence the transverse axis is also different in direction, positive to BB for seakeeping and to SB for manoeuvring.

4.2 Sway

The equation of motion for the swaying motion related to seakeeping may be written as

$$(m_w + a_{yy})\, \ddot{y} + b_{yy}\, \dot{y} = Y_a \sin (\omega t + \epsilon) \tag{22}$$

Substituting $y = y_a \sin \omega t$ delivers for the quadrature component of the side-force:

$$b_{yy}\,\omega\,y_a = -\,Y_a \sin\epsilon \tag{23}$$

The sway oscillation for manoeuvring may be presented as

$$(\,Y_{\dot v} - m_w\,)\dot v + Y_v v = Y_a \sin(\,\omega t + \epsilon\,) \tag{24}$$

from which follows

$$Y_v\,\omega\,y_a = -\,Y_a \sin\epsilon \tag{25}$$

The sign for this force is opposite to that found for manoeuvring due to the difference in the direction of the y-axis. In the above equations are:

M_w = mass of the wing
A_{yy}, b_{yy} = seakeeping coefficients for resp. added mass and damping
$Y_{\dot v}$, Y_v, = manoeuvring coefficients for resp. added mass and damping

With aid of the expressions for the seakeeping coefficients as presented in [8], it follows with (22), (23) and (25) that

$$Y_v = -\,b_{yy} = U\int_{x_{mb}}^{F} \frac{dm'}{dx}\,dx = -Um'_{x_{mb}} \tag{26}$$

In non-dimensional form the expression becomes:

$$Y'_v = \frac{Y_v}{\frac{1}{2}\rho L_w^2 U} = -\frac{m'_{x_{mb}}}{\frac{1}{2}\rho L_w^2} \tag{27}$$

In the same way is found:

$$Y_{\dot v} = -\,a_{yy} = -\int_A^F m'dx \tag{28}$$

which becomes in non-dimensional form:

$$Y'_{\dot v} = -\frac{1}{\frac{1}{2}\rho L_w^3}\int_A^F m'dx \tag{29}$$

The other coefficients may be determined in the same way. An overview of the sway coefficients is presented in Table I.

Table I. *Overview of Sway coefficients*

$Y_v = U \int_{x_{mb}}^{FPP} \frac{dm'}{dx} dx$	$Y'_v = \frac{Y_v}{\frac{1}{2}\rho L_w^2 U}$	
$= - U m'_{x_{mb}}$	$= \frac{- m'_{x_{mb}}}{\frac{1}{2}\rho L_w^2}$	
$Y_{\dot{v}} = - \int_{APP}^{FPP} m'dx$	$Y'_{\dot{v}} = \frac{Y_{\dot{v}}}{\frac{1}{2}\rho L_w^3}$	$= - \frac{1}{\frac{1}{2}\rho L_w^3} \int_{APP}^{FPP} m'dx$
$N_v = U \int_{x_{mb}}^{FPP} \frac{dm'}{dx} xdx$	$N'_v = \frac{N_v}{\frac{1}{2}\rho L_w^3 U}$	
$= U [- x_{mb} m'_{x_{mb}} - \int_{x_{mb}}^{FPP} m'dx]$		$= \frac{1}{\frac{1}{2}\rho L_w^3} [- x_{mb} m'_{x_{mb}} - \int_{x_{mb}}^{FPP} m'dx]$
$N_{\dot{v}} = - \int_{APP}^{FPP} m'xdx = Y_{\dot{r}}$	$N'_{\dot{v}} = \frac{N_{\dot{v}}}{\frac{1}{2}\rho L_w^4}$	$= - \frac{1}{\frac{1}{2}\rho L_w^4} \int_{APP}^{FPP} m'xdx = Y'_{\dot{r}}$

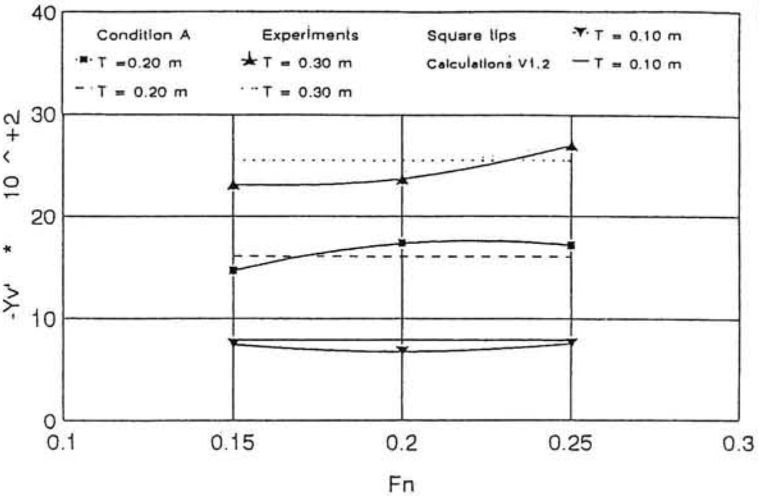

Figure 4. Measured and calculated $-Y_v$ as function of forward speed

As an example:
Figure 4 shows the measured and calculated values of $-Y'_v$ as function of forward speed Fn for $H/T = 1.2$, H = Waterdepth, T = draught.

4.3 Yaw

Yaw in manoeuvring may be divided in sway and yaw with a mutual phase difference of 90 degrees.

The velocity vector of LCG is tangent to the swaying path of LCG which is achieved by adjusting a phase angle Φ between a fore and aft leg in case of an oscillator [8], so that

$$tg\,\frac{\Phi}{2} = \frac{l\omega}{2U} \tag{30}$$

with l = the distance between oscillator legs.
The force equation for sway/yaw may be written as:

$$(m_w + a_{yy})\,\ddot{y} + b_{yy}\,\dot{y} + d_{y\psi}\,\ddot{\psi} + e_{y\psi}\,\dot{\psi} = -\,Y_a\cos(\,\omega t + \varepsilon\,) \tag{31}$$

The force here is taken in phase with the yawing angle Ψ and negative in sign in view of the manoeuvring notation. Substitution of $y = y_a \sin \omega t$ and

$$\psi = \psi_a \cos \omega t = \frac{2y_a}{l}\sin\frac{\Phi}{2}\cos \omega t \tag{32}$$

in (31) and using the pure yawing motion equation

$$Y_{\dot r}\dot r + (Y_r - m_w U)\mathrm{r} = Y_a \cos(\omega t + \varepsilon) \tag{33}$$

yields

$$(Y_r - m_w U) = \frac{Y_a \sin \varepsilon}{\psi_a \omega} = \frac{-\omega^2 (m_w + a_{yy})\, y_a - e_{y\psi}\omega\, \psi_a}{\psi_a \omega}$$

$$or \;\; Y_r = -e_{y\psi} - \frac{\omega (m_\omega + a_{yy})\, l}{2 \sin \frac{\Phi}{2}} + m_w U \tag{34}$$

$$If \;\; \omega \to 0 \;\; then \; \sin \frac{\Phi}{2} \to tg\, \frac{\Phi}{2} \to \frac{\Phi}{2} \to \frac{l\omega}{2U}$$

which results into

$$Y_r = -e_{y\psi} - U a_{yy} \tag{35}$$

Using the seakeeping expressions for $e'_{y\psi}$ and a'_{yy} as presented in [8] and taking $N' \to 0$ for $\omega \to 0$ yields

$$Y_r = U\left[\int_{x_{mb}}^{F} \frac{dm'}{dx}\, x\, dx + \int_{A}^{F} m'\, dx\right] \tag{36}$$

In non-dimensional form after partial integration is found

$$Y'_r = \frac{Y_r}{\frac{1}{2}\rho L_w^3 U} = \frac{1}{\frac{1}{2}\rho L_w^3}\left[-x_{mb}\, m'_{x_{mb}} - \int_{x_{mb}}^{F} m'\, dx + \int_{A}^{F} m'\, dx\right] \tag{37}$$

The in-phase relation of equation (31) and (33) gives in the same way:

$$Y_{\dot r} = -d_{y\psi} + \frac{b_{yy}\, U}{\omega^2} \tag{38}$$

and after taking $N' \to 0$ for $\omega \to 0$ there remains

$$Y_{\dot r} = -\int_{A}^{F} m' x dx = N_{\dot v} \tag{39}$$

Non-dimensional presentation gives:

$$Y'_{\dot{r}} = N'_{\dot{v}} = -\frac{1}{\frac{1}{2}\rho L_w^4} \int_A^F m'x dx \tag{40}$$

The other coefficients may be determined in the same way.
In the above equations are
$d_{y\psi}, e_{y\psi}$ = seakeeping moment coefficients for resp. added mass and damping
$Y_{\dot{r}}, Y_r$ = yaw moment coefficients for resp. added mass and damping

If for yawing the velocity vector of LCG is not tangent to the swaying path of LCG the yaw coefficients may change rather strongly. In [8] a counter phase of 180° has been considered showing these very strong alterations in value. An overview of the yaw coefficients is presented in Table II.

4.4 Semi-empirical methods

In the past several attempts have been made to find empirical expressions for the manoeuvring coefficients at ships based on measured values from planar motion and rotating arm experiments.
Mentioned here are Norrbin (1971) [9], Gerritsma e.a. (1974) [10], Inoue e.a. (1981) [11]. Clarke e.a. (1982) [12] compared several empirical formulas against scatter plots of velocity derivatives.
Clarke used multiple linear regression analysis to develop empirical formulas to explain the variation in the available data for the velocity derivatives and also the acceleration derivatives.
His resulting four equations for velocity derivatives were obtained from the pooled data and are, together with the remaining equations for acceleration derivatives, also presented in [13].

In Table III the experimental results of the manoeuvring derivatives for the shiplike condition $T = 0.10$ m, $H = 2.50$ m (deep water) are compared with the present calculation results and the semi-empirical methods mentioned above.

Table II. *Overview of Yaw coefficients*

$Y_r = U\,[\int_{x_{mb}}^{FPP} \frac{dm'}{dx}\,x dx + \int_{APP}^{FPP} m'dx\,]$	$Y_r' = \frac{Y_r}{\frac{1}{2}\rho L_w^3 U}$
$= U\,[-x_{mb}\, m'_{x_{mb}} - \int_{x_{mb}}^{FPP} m'dx + \int_{APP}^{FPP} m'dx\,]$	$= \frac{1}{\frac{1}{2}\rho L_w^3}\,[-x_{mb} m'_{x_{mb}} - \int_{x_{mb}}^{FPP} m'dx + \int_{APP}^{FPP} m'dx\,]$
	$= N'_v - Y'_{\dot v}$
$Y_{\dot r} = -\int_{APP}^{FPP} m'xdx = N_{\dot v}$	$Y'_{\dot r} = \frac{Y_{\dot r}}{\frac{1}{2}\rho L_w^4} = -\frac{1}{\frac{1}{2}\rho L_w^4}\int_{APP}^{FPP} m'xdx = N'_{\dot v}$
$N_r = U\,[\int_{x_{mb}}^{FPP} \frac{dm'}{dx}\,x^2 dx + \int_{APP}^{FPP} m'xdx\,]$	$N'_r = \frac{N_r}{\frac{1}{2}\rho L_w^4 U} = \frac{1}{\frac{1}{2}\rho L_w^4}\ *$
$= U\,[-x^2_{mb}\, m'_{x_{mb}} - 2\int_{x_{mb}}^{FPP} m'xdx +$	$*\ [-x^2_{mb}\, m'_{x_{mb}} - 2\int_{x_{mb}}^{FPP} m'xdx + \int_{APP}^{FPP} m'xdx\,]$
$+ \int_{APP}^{FPP} m'xdx\,]$	$= \frac{1}{\frac{1}{2}\rho L_w^4}[-x^2_{mb}\, m'_{x_{mb}} - 2\int_{x_{mb}}^{FPP} m'xdx\,] - Y'_{\dot r}$
$N_{\dot r} = -\int_{APP}^{FPP} m'x^2dx$	$N'_{\dot r} = \frac{N_{\dot r}}{\frac{1}{2}\rho L_w^5} = -\frac{1}{\frac{1}{2}\rho L_w^5}\int_{APP}^{FPP} m'x^2dx$

Table III. *Comparison of measured, calculated and semi-empirical values for the coefficients*

Condition A $T = 0.10$ m, $H = 2.50$ m

Manoevring Coefficients	Fn	Experiment: Square Tips	Experiment: Faired Tips	Present calculation	Semi-empirical methods: Clarke (1982)	Inoue (1981)	Norrbin (1971)	Gerritsman, Beukelman Glansdorp (1974)
$-Y_{\dot{v}}'$	.15	0.92	0.51	0.89	0.77	0.90	0.90	0.90
	.20	1.04	0.30					
$*10^2$	.25	1.25	0.62					
$-Y_v'$	.15	2.15	1.39	0.97	1.17	0.96	1.08	0.96
	.20	2.18	1.18					
$*10^2$	.25	2.02	1.50					
$-N_{\dot{v}}'$	.15	−0.11	−0.09	−0.05	0.02	−0.05	−0.05	−0.05
	.20	−0.13	−0.05					
$*10^2$	.25	−0.11	−0.17					
$-N_v'$	.15	0.46	0.26	0.40	0.37	0.39	0.38	0.68
	.20	0.46	0.22					
$*10^2$	.25	0.57	0.28					
$-Y_{\dot{r}}'$	.15	−0.05	0.05	−0.05	0.04	−0.05	−0.05	−0.05
	.20	0.16	0.12					
$*10^2$	.25	0.12	0.21					
$-Y_r'$	.15	−0.47	−0.31	−0.50	−0.27	−0.37	−0.24	−0.24
	.20	−0.38	−0.21					
$*10^2$	.25	−0.66	−0.33					
$-N_{\dot{r}}'$	.15	0.01	0.10	0.07	0.04	0.07	0.07	0.07
	.20	−0.03	0.10					
$*10^2$	.25	−0.07	0.16					
$-N_r'$	.15	0.24	0.14	0.22	0.18	0.21	0.21	0.15
	.20	0.27	0.16					
$*10^2$	.25	0.27	0.13					

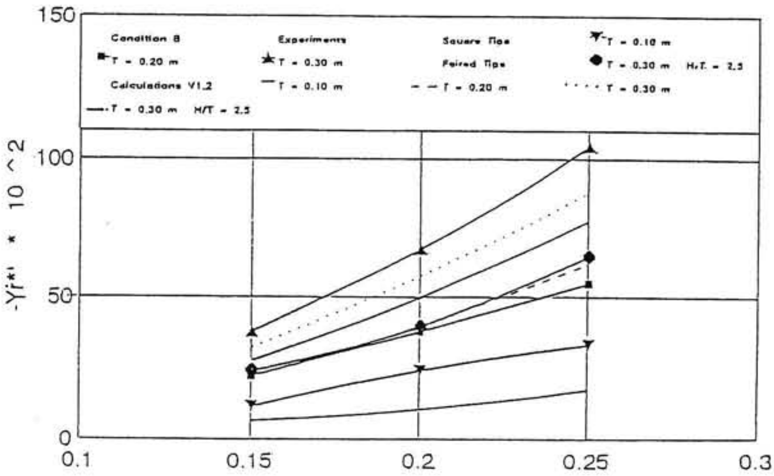

Figure 5. Measured and calculated $Y_{\dot{r}}$' as function of forward speed*

Fig. 5. presents the yaw coefficient $-Y_{\dot{r}}{}^{*\prime}$ as function of forward speed *Fn, H/T* = 2.0. In this case, condition B, there is a counter phase of 180°.

5. Conclusions and recommendations

The presented calculation methods based on the rate of change of fluid momentum are suitable to determine phenomena as

- slamming pressures
- lift production of the hull
- manoeuvring derivatives

Reduction of the waterdepth causes a strong increase of lift and consequently also of manoeuvring derivatives.
The influence of external oscillators such as a rudder and propeller on the hull coefficients needs further investigation. Research into viscous influence due to the curvature of the bilge and/or the influence of bilge keel, is also needed.

6. References

[1] Radev, D. and Beukelman, W. 'Slamming on forced oscillating wedges at forward speed', Part I – Test Results, Part II – Slamming Simulation on Penetrating Wedges at Forward Speed, International Shipbuilding Progress, Volume 39, No.420, 1992 and Volume 40, No.421, 1993.

[2] Jones, R.T. (1945), 'Properties of Low-Aspect-ratio Pointed Wings at Speeds Below and Above the Speed of Sound', NACA-Report 835

[3] Newman, J.N. (1977), 'Marine Hydrodynamics", Book, MIT Press, Cambridge, Massachusetts.
[4] Katz, J. and Plotkin, A. (1991), 'Low Speed Aerodynamics, from Wing Theory to Panel Methods', Book, McGraw – Hill, International Editions
[5] Keil, H. (1974), 'Die Hydrodynamische Kräfte bei der periodische Bewegung zwei-dimensionaler Körper an der Oberfläche flacher Gewasser', Institut für Schiffbau der Universität Hamburg, Bericht No. 305
[6] Dmitrieva, Dr. I. 'Numerical Investigations of Motions and Drift Forces on Different Bodies Using the DELFRAC Program', Report 1016, Ship Hydromechanics Laboratory, Delft University of Technology, The Netherlands
[7] Beukelman, W. (1993), 'Lift and Drag for a Low Aspect-ratio Surface Piercing Wing-Model in Deep and Shallow Water', Delft University of Technology, Ship Hydromechanics Laboratory, ISBN 90-370-0095-9
[8] Beukelman, W. (1995), 'Manoeuvring Derivatives for a Low Aspect-Ratio Surface Piercing WingModel in Deep and Shallow Water', Delft University of Technology, Ship Hydromechanics Lab., (MEMT, ISSN 0925-6555, 35) ISBN 90-370-0127-0
[9] Norrbin, N.H. (1971), 'Theory and Observations on the Use of a Mathematical Model for Ship Manoeuvring in Deep and Confined Waters' Swedish State Shipbuilding Experimental Towing Tank, Publ. 68, 1971
[10] Gerritsma, J., Beukelman, W. and Glansdorp, C.C., (1974), 'The Effect of Beam on the Hydrodynamic Characteristics of Ship Hulls', 10th Office of Naval Research Symp. Boston, USA or Report No. 403-P, Ship Hydromechanics Lab., Delft University of Techn., The Netherlands
[11] Inoue, S., Hirano, M. and Kijima, K. (1981), 'Hydrodynamic Derivatives on Ship Manoeuvring', Int. Shipbuilding Progress, Vol.28, No.321, May 1981, The Netherlands
[12] Clarke, D., Gedling, P. and Hine, G. (1982), 'The Application of manoeuvring Criteria in Hull Design Using Linear Theory', Trans. RINA, 1982
[13] Book: "Principles of Naval Architecture', Volume III: Motions in Waves and Controllability, The Soc. of Naval Arch. and Marine Eng., New York

Optimization of the Propulsion System of a Ship using the Generalized New Momentum Theory

Gonzalo Pérez Gómez
General Director of SISTEMAR, S.A.Titular Professor of Fluids Mechanic at the Escuela Técnica Superior de Ingenerios Navales of Madrid

Juan González-Adalid
Technical Director of SISTEMAR, S.A.

Offered for publication by Association de Ingenieros Navales de España

Abstract

The calculations presented show that the Generalized New Momentum Theory in association with the Equivalent Profile Theory allows to optimize satisfactorely the propulsion system of a ship at a preliminary stage.
Another additional advantage derived from this new mathematical tool is that it can be expected that the future experimental programmes will be shortened and focused onto the development of the selected solution, reducing its execution period and improving the quality of the final product.
The detailed design of the propeller or propellers involved within the adopted solution will be also carried out with the utmost brilliance by means of this new theory.
Some suggestions about the most adecuated procedure to extrapolate the experimental results corresponding to ships with propellers in series are also presented.

Prologue

The Generalized New Momentum Theory allows to calculate the magnitudes of the axial and tangential components of the induced velocities, both at the propeller disk and the infinite downstream, corresponding to any propeller designed to operate inside a liquid vein with a velocities field with axial and tangential components at the infinite upstream.

The first publication of the generalization of the New Momentum Theory was made by the Escuela Técnica Superior of Ingenieros Navales (Chapter 26, Resistance and Propulsion, Ref. 1).

Later on said theory was published by Ingeniería Naval, Ref. 34, and it was also included in the paper presented at the Symposium "Propellers Shafting'94" sponsored by the SNAME, Ref. 35.

As it is indispensable to have a comprehensive understanding of the theory in order to put in practice the type of calculations presented in this paper, a summary of the Generalized New Momentum Theory has been also included as appendix.

The procedure to be followed to optimize the main characteristics of a propeller using the New Momentum Theory in association with the equivalent profile theory, has been described in Refs. 1, 9 and 28. Said procedure is still valid when the Generalized New Momentum Theory is used.

The utility of the generalization done to the New Momentum Theory to value quantitatively the boundary conditions that a nozzle exerts on the propeller which works inside of the nozzle and which are manifested in the values adopted by the thrust deduction fraction and wake coefficients corresponding to the propeller itself, was demonstrated in Ref. 34.

Once said boundary conditions are known and using the Generalization of the New Momentum Theory it is feasible to raise with the utmost guarantee of success and simplicity the detailed design of the propeller that must operate associated to the nozzle in question.

To this regard the authors want to show their surprise because of the mistake made by the "Propulsor Commitee" of the 21st IITC when they affirmed that the authors have extended the combined Momentum and equivalent profile theory to design contrarotating and tandem propellers. They have also informed that the authors did not present model tests and it is not true since in the papers it has been compared the results of the calculations with model tests coming from different model basins.

Within this paper the usefulness of the new theory for the design of propellers working in series (contrarotating and tandem), is shown.

In what follows it will be generically designated by propellers in series not only to the sets of contrarotating propellers but also to those sets constituted by two or more propellers fitted on a same shaft line and hence turning at a same revolutions rate (tandem propellers).

To finalize it will be mentioned that recommendations of high interest related with the extrapolation procedure at full scale of experimental results corresponding to ships with propellers in series, are included in the paper.

1. Generalities

The existing possibilities to optimize the propulsive efficiency of a ship actuating on each one of the propulsive coefficients intervening in said efficiency, were analyzed in Refs. 1 and 2.
Later on, see Ref. 3, the attention was focused in the study of the existing resources to optimize the propeller open water efficiency.
In said paper it was established that there are two alternatives which may be superimposed to improve the propeller open water efficiency which respectively consist on actuating on the basical design parameters of the propeller or on the type of loading radial distribution on the blades.
The actuations on the basical design parameters of the propeller are realized in reducing as maximum the value of the coefficient Bp of the ship's propeller or propellers.
To reach this goal the propulsive power must be subdivided into two or more shaft lines in such a way that both the power supplied to each propeller and its revolutions rate be suitably reduced.
The only negative aspect of the subdivision of the propulsive power comes from the possible reduction of the hull efficiency, which may be produced in case that the propellers be separated from the ship central plan and hence operate in wake fields of low mean values.
In Refs. 2 and 3 it was already pointed out that the contrarotating propellers constitute a solution which combines the advantages coming from a low Bp coefficient and a hull efficiency comparable to the one of a single propeller located at the central plan.
In this paper it is demonstrated that by means of the Generalized New Momentum Theory it is possible to predict through a direct calculations procedure the performance of any ship fitted with single propellers and with propellers in series.
Likewise it is demonstrated that the advantages of the CLT concept (loading radial distributions of very special type on the blades) may be superimposed to the inherent advantages achieved through a favourable actuation directed to reduce the Bp coefficient characteristic of the basical design parameters of each propeller.

2. Basical departing information corresponding to the ship which propulsion system is to be optimized

Once done the generalization of the New Momentum Theory and checked its utility to obtain the boundary conditions that a nozzle exerts on the propeller working inside of it, Ref. 34, it was decided within SISTEMAR to raise the direct calculation of the performances that can be obtained with contrarotating and tandem propellers, and likewise to study the existing possibilities to extend the CLT concept to this type of propellers.

In order to proceed with the optimization of the ship propulsion at a predesign stage it was decided to combine the Generalized New Momentum Theory with MARIN's information, Ref. 27, published by Holtrop relative to the components of the advance resistance of a ship and its deduction fraction, wake and relative rotative efficiency coefficients. Of course, in case that preliminar experimental results be available, these can be used in a completely similar way.

The best way to check the quality of the theoretical developments of Refs. 1, 34, 35 and 40 is, without any doubt, to make an attempt to reproduce by means of direct calculations the characteristics (thrusts and pitches) of a known set of contrarotating propellers for which the respective powers absorbed and revolutions are known and imposing their diameters and blade area ratios.

With the aim to make such an attempt, the interesting paper of Doctor Van Manen and Doctor Oosterveld mentioned in Ref. 29 has been used. Copy of this paper was handed over by MARIN to the authors, and contains abundant information on the tests conducted with propellers in series.

Despite the time elapsed since its publication, the paper was adequated for the purposes of the present paper. It is fair to recognize the merit of Doctors Van Manen and Oosterveld when raising with great skill said experimental task and taking care exquisitely of the results presentation.

In said paper the experimental results obtained with models of a tanker and a cargo liner, are presented.

The results of the experimental works corresponding to the tanker model were used by the authors to prepare the paper entitled "Contrarotating and Tandem CLT Propellers", Ref. 35.

The experimental results corresponding to the cargo liner will be analyzed in this paper which was formerly published by Ingeniería Naval in 1994 (Ref. 40) and which due to the decission of the AINE it is now presented in English.

The main characteristics of the hull and the propellers used in the experimental works described in Ref. 29, refered to real scale, are presented in Table 1.

Table 1. *Tests conducted by Marin with a cargo liner model fitted consecutively with a conventional propeller and with a set of contrarotating propellers.*

MAIN CHARACTERISTICS OF THE SHIP

Displacement at full load: 19,023 tons.

Length between perpendiculars .... 158,5 m.	Mean draught .... 8,839 m.
	Beam .... 22,4 m.

MAIN CHARACTERISTICS AT FULL SCALE OF THE PROPELLERS USED IN THE TESTS

Propeller type	Diameter (m.)	Nº of blades	Pitch at 0.7	H0.7 + D(m).	AE/AO
Single propeller:	6,000	4	5,796	11,796	0,621
Contrarotating propellers:					
Forward:	5,220	4	5,652	10,872	0,432
Aft:	4,880	5	5,838	10,718	0,531

The results of the extrapolations carried out by Doctors Van Manen and Oosterveld of the tests conducted with a single propeller and with a set of contra-rotating propellers, corresponding to a ship speed of 20 knots, are presented in Table 2.

Said ship speed has been choosen as basis for the comparison because it is an intermediate speed within the experimental range.

Within Ref. 29 it is neither described nor mentioned the procedure followed to extrapolate at full scale the experimental results; however, according to the

Table 2. *Comparison between SISTEMAR predictions and the test results.*

	EXTRAPOLATION OF MODEL TEST RESULTS						SISTEMAR PREDICTIONS			
Propeller type	**BHP Forw/Pp**	**RPM Forw/Pp**	**Thrust Forw/Pp**	**W Forw/Pp**	**H0.7 Forw/Pp**	η_0 **Forw/Pp**	**Thrust Forw/Pp**	**W Forw/Pp**	**H0.7 Forw/Pp**	η_0 **Forw/Pp**
Single:	13,821	112,9	87,140	0,243	5,796	0,629	89,958	0,243	5,888 (5,953)*	0,650 (0.644)*
Contrarota.										
Forward:	6,654	111,6	48,180		5,652		47,790	0,243	5,613	0,716
				0,298		0,648				
Aft:	6,273	111,6	44,280		5,838		42,876	0,152	5,829	0,764
	13,927		**92,460**				**90,666**			

Diameter of the single propeller: .... 6,000 m.
Diameter of the forward propeller: .... 5,220 m.
Diameter of the aft propeller: .... 4,880 m.
Speed: 20 knots.

Advance resistance: ....71,190 tons.
Thrust deduction coefficient: 0,183
Relative rotative efficiency: 1,041

The 0.7 pitches are refered to profiles of Walchner type (MARIN) and NACA 65 (SISTEMAR) because the corresponding mean lines are nearly similar. (*) Values deduced using MARIN polynomial expressions corresponding to KT and KQ coefficients of B series propellers.

date in which said paper was written, it is not rejectable to assume that the predicted results for full scale have been deduced supposing that in the tests a complete physical similarity has existed (Froude method).
It is necessary to call the attention on the fact that Doctors Van Manen and Oosterveld have considered that the propeller is constituted by the set of two propellers, because the propeller open water test have been performed with the set of both contrarotating propellers and the effective wake coefficient is refered to the total thrust supplied by both propellers.
This same criterium has been followed in Ref. 30, where a very complete information has been presented on the experimental results obtained with a small systematical series of tandem propellers.
Due to the reasons explained in the following chapter, it is convenient to isolate the contribution of each propeller with the aim to enable the use of Taniguchi's procedure adopted in 1978 by the ITTC to extrapolate the experimental results.
Next the extrapolation procedure suggested to be used to extrapolate the experimental results corresponding to propellers in series is described.

3. Suggestions about the most adequate procedure to extrapolate at full scale the experimental results corresponding to ships fitted with propellers in series

When considering the most adecuated procedure to undertake the design of a propeller it is inavoidable to decide also which are the most adecuated experimental and extrapolation procedures to predict the performance at full scale of this type of propulsion system.
It must be accepted that the most convenient procedure to extrapolate at full scale the experimental results of ships fitted with propellers in series must be characterized by its feasibility to take advantage as maximum of the existing know-how corresponding to ships propelled by single propellers.
Likewise, a detailed knowledge of the boundary conditions which affect to each one of the propeller must be allowed within the procedure, with the aim to enable the correction, if necessary, of the propellers design and furthermore to enable to reproduce during the cavitation test some real operating conditions of the same.
Taking as a basis that the Taniguchi extrapolation procedure Refs. 1 (Chapter 15 of Resistance and Propulsion), 36 and 37, adopted by the ITTC in 1978, is the most rational of the existing extrapolation procedures, because it isolates the scale effects coming from the transgressions of the Reynolds numbers corresponding to the hull and to the propeller models and the scale effect existing into the effective wake coefficient, it will be necessary to tend to use as far as possible said extrapolation procedure.
The extrapolation at full scale of the towing test results will be carried out in

the traditional way nowadays perfectly known and mainly adopted, thus, Hughes's procedure will be used.
To know perfectly the boundary conditions affecting to each one of the propellers which operate in series, it is convenient to conduct open water tests independently for each one of the propellers.
Furthermore, the results of the open water tests will be extrapolated at full scale using the ITTC 1978 procedure, based on Aucher, Bjarne abd Lindgren proposals.
Some similar expressions to the ones proposed by these authors were theoretically deduced in Ref. 38. Said theoretical developments are also included in Chapter 13 of "Resistance and Propulsion", Ref. 1, Vol. II A.
The extrapolation at full scale of the propeller open water tests results conducted with CLT propellers models shall incorporate additional corrections to have into account the scale effects affecting to the viscosity forces which actuate on the tip plates and to the lift coefficients (C_L) of the blades annular sections located above of the non-dimensional station 0.7.
When conducting the selfpropulsion test the torques absorbed by each one of the propellers must be measured as well as the thrusts exerted by these and their respective revolutions.
For each one of the propellers the effective wake fractions at thrust identity will be deduced relating appropriately the results of selfpropulsion and open water tests. Likewise the relative rotative efficiencies corresponding to each propeller will be also deduced.
The thrust deduction coefficient will be defined for the set of two propellers and will be calculated by means of the following expression:

$$t = (T_1 + T_2 + T_F - R_M) / (T_1 + T_2)$$

being T_1 and T_2 the respective thrusts of both propellers, T_F the towing force and R_M the advance resistance of the model.
Of course, it will be accepted that the thrust deduction coefficient previously defined has not been submitted to scale effects.
Likewise it will be accepted that the relative rotative efficiencies corresponding to each one of the propellers have not been submitted to scale effects.
To extrapolate at full scale each one of the effective wake coefficients at thrust identity deduced for each propeller, the ITTC 1978 procedure (Bowden's formula) will be used.
Perhaps the value of the constant (0.04) which intervenes in the estimation of the potential component of the effective wake fraction ($w_p = t + 0.04$) should be revised, as soon as results of regression analysis carried out from sea trials results corresponding to ships with propellers in series be obtained.
Of course, it will not be accepted that the viscous component of the wake fraction at the model field could be negative. In such a case, it would be necessary to reduce the constant term intervening in the evaluation of w_p until making it nule if it were necessary.

To predict the operating conditions at full scale of each one of the propellers, their respective advance degrees must be known, and for this, the following must be taken into account.
Be T the total thrust of both propellers at full scale.

$$T = T_1 + T_2 = R / (1\text{-}t)$$

In general, in the case of contrarotating propellers, the existing ratio between the revolutions of each one of the propellers will be known; for instance it will depend on the characteristics of the reduction gear which drives the inner solid shaft and the outer hollow shaft. In the case of being completely independent both propellers, the power ratio could be known.
Be K_r the propellers revolutions ratio and N_1 and N_2 the revolutions rate of each one of the propellers. Then,

$$K_r = N_1 / N_2$$

In the case of tandem propellers K_r will be equal to one.
To know the respective advance degrees (J_1, J_2) of the propellers corresponding to the ship speed V_B for which the advance resistance is R and the total propellers thrust is T, it will be proceeded as follows.
It will be assumed that N_1 adopts a certain value n and hence the revolutions value N_2 would be equal to:

$$N_2 = n/K_r$$

Knowing the values of the ship speed V_B, the effective wake coefficients w_1 and w_2 of each propeller, and the diameters D_1 and D_2 of both propellers, the advance degrees J_1 and J_2 corresponding to both propellers supposing that the revolutions N_1 were equal to n, will be also known.

$$J_1 = V_B(1\text{-}w_1) / (n\ D_1)$$
$$J_2 = V_B(1\text{-}w_2) / (n/K_r\ D_2)$$

For each one of the values J_1 and J_2, entering into the K_T-J curves of propeller open water tests for each propeller extrapolated at full scale, the coefficients of K_{T1} and K_{T2} corresponding to both propellers will be deduced, verifying:

$$T_1 = K_{T1} \cdot \rho \cdot n^2 \cdot (D_1)^4$$
$$T_2 = K_{T2} \cdot \rho \cdot n^2 \cdot (D_2)^4$$

In general, $T_1 + T_2$ will not be equal to the necessary value of the total thrust T that both propellers should exert in order to achieve the ship speed V_B.
Repeating the calculation process previously described, assuming a new value of N1 different from the previous one, a new value of T_1 and T_2 will be obtained.

Repeating the same process a certain number of times, a correspondence between the supposed values of n and the values obtained for $T_1 + T_2$ will be obtained.
Interpolating in said correspondence with the value of $T_1 + T_2$ equal to T, an appropriated value of n is obtained.
Knowing the value of n, J_1, J_2, K_{T1}, K_{T2}, K_{Q1}, K_{Q2} will be known and consequently the powers absorbed by each one of the propellers will be known.
This calculation process must be done for each one of the velocities values V_B of the ship for which it is wished to predict the propeller performance at full scale.

4. Calculation process that must be followed to carry out the design of propellers operating in series

4.1 Introduction

As it happens when single propellers are designed, to carry out the design of propellers working in series it is necessary to follow a process of succesive approximations so that the thrusts supplied by both propellers be really those requested to achieve ship speed V_B for which the propellers have been designed.
Of course, both the revolutions rate and the power absorption corresponding to each one of the propellers must be respectively equal to their design values.
In what follows, it will be assumed that the second propeller operates at the infinite downstream with regard to the disk of the first propeller.
It is necessary to anticipate that the predictions obtained from this hypothesis match very satisfactorely with the experimental results.
On the other hand, the accuracy of the above hypothesis is endorsed by the fact that the contraction of the fluid vein of a propeller is stabilized at a distance downstream of the propeller disk lower than the propeller radius.
When conducting the cavitation test of a propeller, it is checked that the tip vortices adopt the configuration of cylindrical helix with constant pitch besides very small distances of the propeller blades tips.
In any case, with the aim to mantain the requested rigour within this exposition, it will be accepted that the necessary measures will be taken when doing the design of two propellers to operate in series, in order that the relative axial distance at stations 0.7 of both propellers, be wide enough as to verify the departing hypothesis. For this it will be possible to actuate on the rake radial distributions of both propellers as well as on the axial positions of the respective embedements of the blades of each propeller on their hubs.
Within the calculations carried out it has been also assumed that the clearances at the stern post contour where the propellers in series must operate are wide enough as to enable that the maximum allowable diameter for a single propeller be also acceptable as maximum diameter for the propellers in series.

If the calculations are carried out departing from experimental results coming from tests conducted with a stock propeller, the effective wake coefficient corresponding to the tested propeller will be known. Said coefficient will be transformed into the one corresponding to the diameter of the first propeller in series, by doing the hypothesis that the quotient between the real values of a same coefficient corresponding to different diameters has the same value than the quotient of the analogous values of said coefficient calculated by means of an experimental information of statistical type, as for instance, Ref. 27.
When experimental tests will not be available, the wake effective coefficient corresponding to the first of the propellers in series will be estimated using the interesting information published by Holtrop (Ref. 27) or another similar.
Knowing the ship speed, the design power of the first propeller, its revolutions rate, the number of blades, etc., and once defined the radial loading distribution type wished to be used in the design, it is very simple to optimize the propeller diameter and therefore to undertake its design.
The necessary calculation process to evaluate in a predesign stage the open water efficiency, the components of the corresponding induced velocity at the station 0.7 and the geometrical pitch of said station by means of the New Momentum Theory, has been described in detail in Refs. 1, 9 and 28 so it is not necessary to insist once more on this matter within this exposition.
By using also the New Momentum Theory it will be possible to calculate the axial and tangential components of the velocities induced at the infinite downstream of the propeller, which are of great important for the design of the second of the propellers in series which must be done using the Generalized New Momentum Theory described in the Appendix.

4.2 Description of the iterations of the calculation process

The iterative process of calculations is essentially the same both when the detailed design of propellers in series is undertaken, or when just a predesign of a set of propellers in series is carried out.
From now on, in order to abbreviate, for a set of two propellers operating in series the forward propeller will be designated as propeller 1 and the aft propeller will be designated as propeller 2.
Due to the complexity of the calculation process it is neither feasible nor practical to pretend that the computer program used to carry out the calculations performs authomatically the necessary sequence of calculations to optimize the diameters of the propellers in series.
The curve ship speed-ship advance resistance will be assumed as known.
For the propulsive efficiency of the propulsion system a given value, for instance 0.6, will be assumed as a first estimation.
The propulsive efficiency of the propulsion system is:

$$\eta_p = EHP/[(DHP_1/\eta_{m1})+(DHP_2/\eta_{m2})] = [(1-t)(T_1+T_2)]V/[(DHP_1/\eta_{m1})+(DHP_2/\eta_{m2})] \quad (1)$$

DHP_1 and DHP_2 are respectively the propulsion powers supplied to the propeller 1 and propeller 2; η_{m1} and η_{m2} are respectively the mechanical efficiencies corresponding to each one of the shaft lines.
The designer will have defined the propulsion powers $BHPA_1$ and $BHPA_2$ that must be given to each one of the shaft lines as well as the revolutions rate N_1 and N_2 of each propeller.
Furthermore, the designer must also define the diameters (D_1 and D_2), the number of blades (Z_1 and Z_2), the chord radial distributions and the maximum thicknesses radial distributions of each propeller.
It must be also defined both for the two series propellers the radial distributions of the circumferential mean values of the local effective wake coefficients following the procedure explained.
Finally, the shape of the thrusts radial distributions per unit of radial length of each propeller must be defined.
A first estimation of the curve V-BHP is obtained dividing EHP by the value η_p assumed.
Entering into the curve V-BHP with the value $BHPA_1 + BHPA_2$ a new ship speed V_B is obtained as a first approximation.
For this ship speed, the corresponding thrust is obtained as the addition of thrusts T_1 to T_2 and hence it is fulfiled,

$$T_1 + T_2 = R/(1\text{-}t) \tag{2}$$

being t the thrust deduction coefficient of the propulsion system. As it has been established in the previous section, this coefficient must be the thrust deduction coefficient corresponding to the forward propeller.
In principle, it can be supposed that the values of T_1 and T_2 are respectively equal to:

$$T_1 = BHPA_1(T_1+T_2)/(BHPA_1+BHPA_2)\ ;$$
$$T_2 = BHPA_2(T_1+T_2)/(BHPA_1+BHPA_2) \tag{3}$$

Next, the velocities induced by each one of the annular elements of the actuator disk will be calculated to make feasible the composition of the velocities polygons and consequently the actuating forces and moments may be calculated. Some homotetical transformations of the thrust radial distributions of each propeller will be requested to assure that the following equalities will be verified:

$$BHPA_1\eta_{m1} = 2\pi N_1\int_{rh1}^{R1} Q_{r1}\,dr\ ;\ BHPA_2\eta_{m2} = 2\pi N_2\int_{rh2}^{R2} Q_{r2}\,dr \tag{4}$$

Q_{r1}+ and Q_{r2} are the moments per unit of radial lenght absorbed by the annular sections of radii r_1 and r_2 corresponding to propellers 1 and 2 respectively.
Once achieved the convergence with the accuracy requested, the thrust supplied by each one of the propellers may be calculated as follows:

$$T_1 = \int_{rh1}^{R1} T_{r1}\, dr_1 \; ; \; T_2 = \int_{rh2}^{R2} T_{r2}\, dr_2 \tag{5}$$

Hence, a more approximated value of η_p may be calculated:

$$\eta_p = [(1\text{-}t)\,(T_1+T_2)]V_B/(BHPA_1+BHPA_2) \tag{6}$$

With this estimation of η_p a new curve V-BHP is derived; entering with $BHPA_1$+ $BHPA_2$ into this curve a new value of V_B is obtained and a new iteration of the process of calculations already described starts.
When the equivalent profile theory is used, once known the thrusts radial distribution type per unit of length of each propeller, the value of the constant C of the following expression will be known:

$$T_7 = C\, T/D \tag{7}$$

where D is the propeller diameter; T_7 the thrust per unit of radial length existing in the nondimensional station 0.7 and T the total thrust of the propeller. Thus, the ratio between T_7 and T will be known in each one of the iterations.
Once calculated as a function of T_7 the velocities polygon of the annular section 0.7, the moment per unit of radial length Q_7 may be calculated and therefore the propeller efficiency at the station 0.7 ($\eta_{0.7}$) will be known. By virtue of the equivalent profile theory, this local efficiency will be assumed as equal to the total propeller efficiency; thus, it will be verified:

$$\eta_{0.7} = \eta_o\, \eta_{rr} = T\, V_B[1\text{-}w] \,/\, DHP \tag{8}$$

Being known $\eta_{0.7}$, V_B , w, η_{rr} and T, the value of DHP associated to a given value of the constant C of (7) will be known; so, without being necessary to carry out the integrations (4) and (5), the iterations requested in the thrust distribution of each propeller to assure that it absorbs the BHPA value imposed, may be done.
Once the process has converged and a certain value V_B compatible with the value of η_p assumed has been achieved, it will be necessary to predict the ship performance for propulsive powers below the design power.
In order to be able to do these predictions, it is necessary to define clearly how the propulsion system is going to be used.
If the propellers are driven through two coaxial shaft lines, hollow for the forward propeller and solid for the aft propeller and both shaft lines have a common reduction gear, it is evident that the revolutions ratio corresponding to both shaft lines (n_2/n_1) must be constant.
If the engine driving the forward propeller is completely independent from the engine driving the aft propeller as it is the case for instance when the second propeller is of azimuthal type, infinite combinations of propulsion powers and propeller rpm for forward and aft propeller may be achieved.

If in addition the propellers were of controllable pitch type, there would be double infinite combinations of propeller powers and revolutions rate.
Because of the above and for the sake of simplicity, it will be assumed that the ratio between the revolutions rate of both propellers operating in series remains constant.
Let us consider the ship speed V_B of the ship. Entering into the curve ship speed-ship advance resistance with V_B it is obtained R and hence it is also possible to obtain the total propeller thrusts requested to achieve said ship speed:

$$T_1 + T_2 = R/(1\text{-}t) \tag{9}$$

On the other hand, it must be verified:

$$R/(1\text{-}t) = \rho\ (K_{T1}\ D_1^4 + KT_2\ D_2^4\ (N_2/N_1)^2)n_1^2 \tag{10}$$

K_{T1} and K_{T2} are the K_T coefficients of both propellers corresponding to the design point, and will be assumed as constant all along the V-BHP curve.
The value of n_1 is deduced from (10) and with said value n_2 is calculated by means of the expression:

$$n_2 = n_1\ (N_2/N_1) \tag{11}$$

The total propulsive power corresponding to the ship speed V_B will be:

$$BHP = \rho[(K_{Q1}/\eta_{m1})n_1^2\ D_1^5 + (K_{Q2}/\eta_{m2})n_2^2\ D_2^5] \tag{12}$$

K_{Q1} and K_{Q2} are the K_Q coefficients of both propellers in selfpropulsion conditions at the design point and will be assumed as constant all along the V-BHP curve.

4.3 Analysis of the operating conditions of forward and aft propellers

Two propellers in series have been represented in Figure 1 operating inside the stern post contour of a certain ship and the variations experimented by the axial and angular components of the relative velocity of the water with regard to the set of two propellers in series have been indicated.
At the infinite upstream of the disk corresponding to the forward propeller, the relative velocity of the water with regard to the propeller disk is $V_B(1\text{-}w)$.
In general, at any radius of the disk of the forward propeller, when the detailed design of the propeller be undertaken, or at the radial station 0.7 when the equivalent profile theory is applied, the axial component of the water velocity is:

$$V_B(1\text{-}w) + \Delta V_{11}$$

where ΔV_{11} is the axial component of the velocity induced by the forward propeller.
At the infinite downstream of the forward propeller disk, and therefore, at the infinite upstream of the aft propeller disk, the axial component of the relative velocity of the water is:

$$V_B(1\text{-}w) + \Delta V_{21}$$

where ΔV_{21} is the axial component of the velocity induced by the forward propeller at the infinite downstream.
The axial component before specified corresponds to the case of non viscous fluid.
With the aim to have into account the water viscosity influence onto the axial velocities distribution, the authors have considered convenient to give entrance to a certain empirical corrector coefficient FCV such as to verify:

$$[V_B(1\text{-}w) + \Delta V_{21}] \,.\, FCV = V_B(1\text{-}w_s) \qquad (13)$$

In the preceding equality, w_s represents the virtual wake coefficient corresponding to the hypothetical velocities field that should exist at the infinite upstream of the aft propeller disk. It is quite evident that said coefficient depends on the

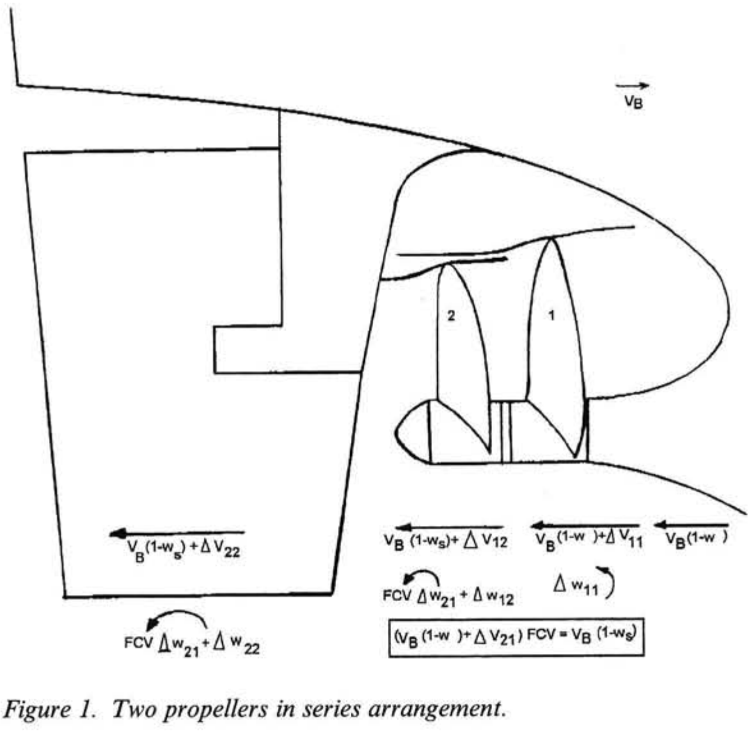

Figure 1. Two propellers in series arrangement.

empirical factor FCV, and hence once assigned a given value to the coefficient FCV, the coefficient w_s will be determined.
FCV must depend on the type of the ship hull lines of the aft body, its block coefficient and the ship size; thus, FCV depends on the effective wake coefficient.
After the experience gained from the calculations presented in Refs. 35 and 40, it can be affirmed that for high block coefficient ships the value of the coefficient FCV may be close to 0.75 while for ships of thin hull lines, said coefficient may be in the order of 0.81.
Of course, the range of variation found for the FCV coefficient is relatively small. Likewise it has been possible to check that small deviations due to a not very fortunated selection of said coefficient, has also a slight influence in the value of the estimated geometrical pitch for the aft propeller, but the value of the estimated thrust for said propeller is affected in a low measure.
It has been assumed that FCV depends on the wake effective coefficient of the forward propeller. If it is accepted that FCV varies linearly with w, it may be established:

$$FCV = 0.72 - 0.5\ (w-0.393) \qquad (14)$$

Once checked that for practical reasons it may be assumed that the aft propeller is located at the infinite downstream of the forward propeller, it is necessary to establish a correspondence between each radius r_1 of the forward propeller and the homologous radius at the disk of the aft propeller, because of the contraction of the fluid vein.
By virtue of the continuity equation it will be verified:

$$\int_{rh}^{r2} [V_B(1-w_r) + \Delta V_{21}]\ .\ FCV\ 2\pi r dr_2 = \int_{rh}^{r2} V_B(1-wr)\ 2\pi r dr_1 \qquad (15)$$

w_r is the circumferential mean value corresponding to the radius r of the local wakes effective distribution existing in the aft body of the ship.
The value of (1-w) corresponding to the nondimensional station 0.7 must coincide with the value of $1-w_T$ being w_T the value of the wake effective coefficient at thrust identity corresponding to propeller 1.
By integrating successively between r_h and r_{11}, r_{12}, r_{13} .... the values of the homologous radii r_{21}, r_{22}, r_{23} .... are respectively obtained at the infinite downstream.
By interpolating into this distribution with the control radial stations choosen to design propeller 2, the local values $V_B(1-w_s)$ which define the velocities field existing at the infinite upstream of propeller 2 are obtained.
If the profile equivalent theory is applied to predict the performance of propeller 2, w_s must coincide with $[V_B(1-w_T) + (\Delta V_{21})_{0.7}]$ FCV.
As it happens with single propellers for which self-propulsion and propeller open water tests are normally conducted with a stock propeller before to carry out its design, in the case of propellers in series it may be of interest to conduct

self-propulsion and propeller open water tests with the aim to know the wake effective coefficients at thrust identity corresponding to the first (w) and second propeller (w_s).
In case of a predesign, the effective wake coefficient (w_s) of the second propeller may be estimated from the value deduced for the first propeller by means of Ref. 27 or another similar and using the expressions (13) and (14).
The angular velocity of the water at the infinite upstream of the first propeller is null.
The relative angular velocity of the water with regard to the disk of the first propeller at its disk plan is $\Delta\omega_{11}$.
$\Delta\omega_{11}$ is the angular component of the induced velocity at the disk of the first propeller.
At the infinite downstream of the forward propeller and therefore at the infinite upstream of the aft propeller, the value of the angular relative velocity is $\Delta\omega_{21}$.
As it happens with the axial components, being the fluid not ideal, it must be taken into account the viscosity which produces a reduction of the angular component of the induced velocity and hence the angular velocity at the infinite upstream of the aft propeller will be assumed as equal to:

$$FCV \, . \, \Delta\omega_{21}$$

FCV is the same corrector coefficient used when calculating the axial components of the induced velocities and for these angular components it adopts, depending on the wake effective coefficient, the same values before mentioned.
When the design of the aft propeller is undertaken it must be taken into account that it works inside a liquid vein with a radial distribution of angular velocities.
When the predesign of a propeller is carried out, according with the equivalent profile theory, it will be enough to consider just the value of the angular velocity corresponding to the station 0.7. However, if a detailed design is carried out, it will be necessary to conduct the calculations for all the control radial stations.
The Generalized New Momentum Theory makes possible the calculation of the axial angular velocities induced by a propeller operating inside a liquid vein which has a radial distribution of angular velocities. Refs. 1, 34 and 35.
The velocities polygons characteristics of a set of contrarotating propellers and a set of tandem propellers have been represented in a schematic way.
It is convenient to stand out the following facts:

a) The relative entrance velocity of the water with regard to the annular section for which the velocities polygons have been represented, is higher in the case of contrarotating propellers.
b) The hydrodynamical pitch angle corresponding to tandem propellers is higher than the angle of contrarotating propellers.

As it is known, (Refs. 1, 3, 6 and 9), the propeller efficiency decreases when its hydrodynamical pitch angles increase. For this reason, a priori, it can be expec-

ted that the efficiency of the set of tandem propellers be lower than the efficiency of contrarotating propellers in spite that the dissipation of energy by viscous forces be higher in the case of contrarotating propellers.
The reasonings presented until now make necessary to call the attention to the following questions:

a) When it is unavoidable to use reduction gears (case of contrarotating propellers and case of tandem propellers with engines not directly coupled) the reduction ratio must be selected so as to optimize the maximum allowable diameters for both propellers.
b) With the aim to avoid that the cavitating flow coming from the blade tip vortices of the first propeller do not erode the blade tips of the second propeller, the diameter of this one shall be suitably lower.
   The diameter reduction of the second propeller will depend both on the sheet cavitation extension and the intensity of blade tip vortex of the first propeller. It will be only known accurately if cavitation tests are conducted. As a general idea, it is necessary to consider for the second propeller reductions in its diameter close to 12%.
c) Having into account the different boundary conditions which affect to both propellers as well as the foreseeable reduction in the optimum diameter of the second propeller in front of the first one, it seems logical to think that an important degree of freedom which must affect to the efficiency of a set of propellers in series must be the distribution of the available propulsive power between first and second propeller.

In Chapter 6 the way to put in practice the ideas already exposed, is described.

5. CLT propellers characteristics

The theoretical fundaments of propellers loaded at the blades tips developed by the authors (TVF and CLT propellers) have been widely described in Refs. 1, 2, 3, 6, 7, 8, 9, 10, 11, 12, 13, 35, 40 and 41, and hence it will be just mentioned herebelow which are the main differences existing between these propellers and conventional propellers.
In Ref. 3 it was established that when the action that the propeller exerts on the surrounding water is modelized by means of the lifting lines theory, the advantage of TVF and CLT propellers is justified by its special radial distribution of the circulation on the propeller blades which has a constant value from station 0.6 approximately up to the blades tips.
According to the lifting lines theory, the magnitudes of the induced velocities are proportional to the radial distribution of slopes of the circulation; therefore, it is deduced that with the circulation radial distribution type described before, the induced velocities obtained must be as low as possible and always lower than those corresponding to conventional propellers for which the radial distri-

bution slopes of circulation, are sensibly higher due to it cuasi-parabolic aspect.
When the action that the propeller exerts on the fluid is modelized using the New Momentum Theory, the advantages of TVF and CLT propellers over conventional propellers are justified by the fact that the special shapes of CLT and TVF blades in association with the end plates as its tip, lead to an overpressure actuating on the blades
aft sides which is considerably higher than the underpressure existing at the forward side.
The end plates already mentioned play also an important role when the advantages of TVF and CLT propellers are explained by means of the lifting lines theory, since said plates are the discontinuity surfaces in which the radial vortices must finalize in order to assure that the mathematical modelization of the action that the propeller exerts on the surrounding water satisfies Helmholtz theorems.
The first contribution of the authors claiming for the advantages derived from this special type of propeller, dates from 1976. Ref. 10. Said propeller type was called TVF (Tip Vortex Free).
Later on, in Ref. 39 the advantages of CLT (Contracted and Loaded Tip) propellers over TVF propellers were established.
The main advantage of CLT propellers over TVF propellers lies on the fact that the tip plates are placed tangent to the revolution surface which envelops the liquid vein which crosses the propeller disk.
By doing so, a reduction of the viscous resistance of the tip plates is achieved because these receive the water flow under free shock entrance conditions.
As the transversal section of the liquid vein is reduced progressively as a consequence of the continuous increase that the water velocity experiences, the radii corresponding to the trailing edges of the tip sections of the propeller blades are lower than those corresponding to the leading edges.
In the case of TVF propellers the tip plates were located tangent to a coaxial surface with the shaft line, and therefore, they were not adapted to the incoming water flow to the propeller, suffering the following inconvenients:

a) The water did not reach to the tip plates under free shock entrance conditions and therefore the viscous resistance was higher than necessary.
b) As the area of the transversal section of the propeller at the axial position corresponding to the trailing edge is higher than the area of the liquid vein, the cylindrical tip plates lead to a detrimental expansion in the fluid, being the pressure actuating in the blades pressure side lower than the one that could be obtained when the tip plate is adapted to the surface which envelops the liquid vein.

The consequences already exposed originated an unnecessary decrease in the propeller open water efficiency.
The New Momentum Theory allows to justify the following additional advantages of the CLT propellers over the conventional propellers:

a) Being the underpressure originated upstream of the propeller disk by a CLT propeller lower than the corresponding one to conventional blades, the cavitation extension in the suction side must be also lower. Likewise, due to the existence of the tip plates, the CLT blades do not have tip vortex cavitation. These facts already mentioned make that the magnitudes of the hull pressure pulses originated by the pressure forces that the propeller exerts on the ship afterbody be lower in the case of CLT propellers.
b) Being the magnitudes of the pressure forces that the CLT propeller exerts downstream, higher than those corresponding to a conventional propeller and being higher the induced velocities at the infinite downstream, it must be concluded that the pressure forces actuating on the rudder when this is turned to one side must be higher than those corresponding to a conventional propeller.

The advantages already stood out are a direct consequence of the fact that the CLT propellers efficiency is higher than the corresponding one of the conventional propellers, because as it is mathematically demonstrated, in order that a CLT propeller can have an efficiency higher than a conventional propeller, it is necessary that the magnitude of the overpressure downstream of the actuator disk be higher than the one of a conventional propeller and likewise, the magnitude of the underpressure upstream of the actuator disk must be lower than the one corresponding to a conventional propeller.

The advantages previously mentioned have been confirmed in full scale usage of different ship types, including tankers, bulkcarriers, ro-ros, container ships, fishing boats of different types, etc.

Up to now, more than 200 CLT propellers have been ordered, both on fixed pitch and controllable pitch types, not only for newbuildings but also replacing conventional propellers/blades.

The experience covers a wide range of applications from large propellers as it is the case of the 7.9 m. diameter CLT propeller installed on the 164.000 DWT bulkcarrier "Comanche" owned by Cargill International to the 1 m. diameter propellers fitted on the hydrofoil "Barracuda" owned by Trasmediterranea.

From comparative trials carried out with the "Comanche" fitted with a CLT propeller and her sistership "Cherokee" fitted with a highly efficient conventional propeller the Owner has concluded that the CLT propeller has improved ship speed at constant power by approximately 0.6 knots and a 12% fuel saving over consumption measured for the conventional propeller achieved at constant ship speed (see Refs. 43 and 44). CLT propellers have been ordered for the "Cherokee" and four other units of the Cargill International fleet.

In the case of the hydrofoil "Barracuda" there are two shaft lines and with the engines at 2238 BHP on each shaft line, the cruising speed of the ship at full load is close to 34 knots. The CLT propellers were installed with the aim to reduce the take-off periods and the engine overloading during said period and both targets were satisfactorily achieved (see Ref. 42).

With regard to the retrofitting of CLT blades on existing CP hubs, the expe-

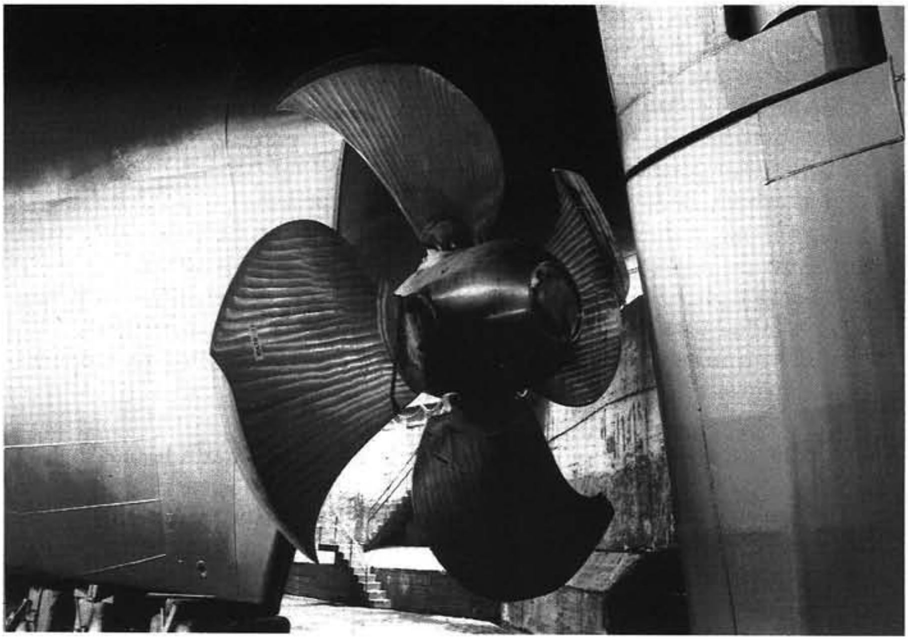

Ro/Ro "Ivan" built by Astilleras Kurveta for Flota Svardiaz

Hydoffoil "Barracuda" owned by Trasmediterranea rience of the shipping companies Trasmediterranea, Flota Suardiaz and W.W. Marpetrol must be highlighted. Said companies have replaced conventional blades in several ships of their fleet.

The best demonstration of the real achievements in service of the CLT propellers is the great number of users who repeat orders for sisterships or other vessels in their fleets. Today there are 18 shipowners with three or more vessels fitted with CLT propellers.

Refs. 13 to 26 both included describe different CLT applications at full scale.

6. Description of the optimization process carried out of the propulsion system of the ship studied

Before to undertake the propulsion optimization process of the ship to be studied, it is necessary to contrast the quality of the mathematical tool developed to carry out the design of different alternatives of propellers to be considered, taking into account its different boundary conditions.

6.1 Verification of the Generalized New Momentum Theory

6.1.1 Performance prediction of a cargo liner with a single conventional propeller.

The departing data of the calculations carried out have been deduced from Ref. 29 and are the following:

V	= 20 knots
DHP	= 13821 HP
RPM	= 112,9
t	= 0.183
w	= 0,243
η_r	= 1,041
D	= 6,000 m
N° of blades	= 4
AE/AO	= 0,621

It has been supposed that the mechanical efficiency of the shaft lines is equal to 1 because the propulsive power is defined in DHP terms.

These calculations have been carried out by means of the already contrasted New Momentum Theory because it does not exist angular velocities at the infinite upstream.

The main results of the direct calculation carried out and MARIN experimental results are the following:

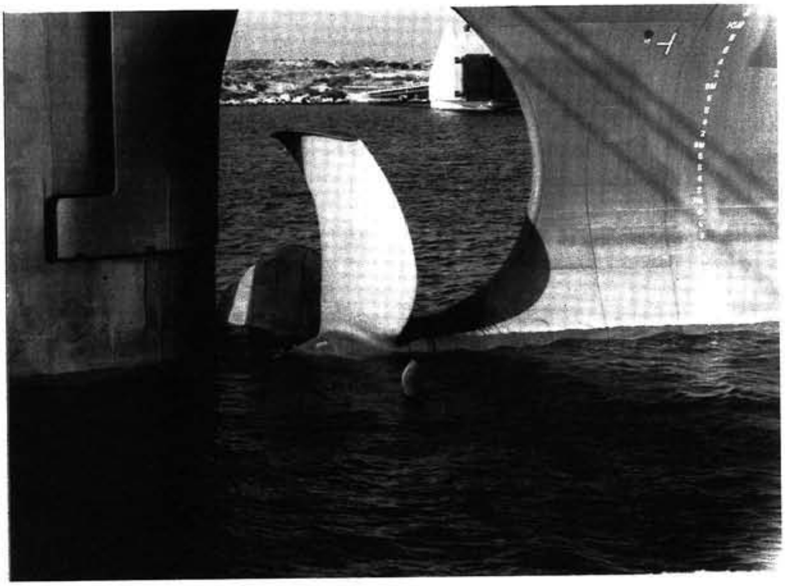

"Comanche" built by Astilleros Español for Cagill International

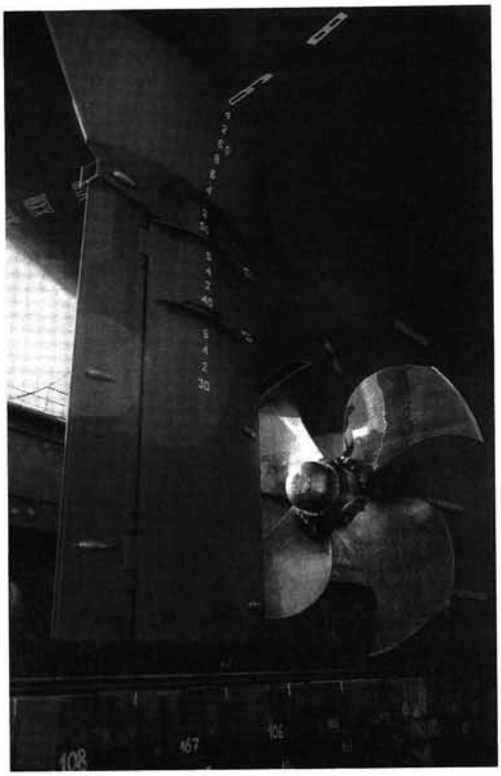

"Mar Almudena" built by Union Naval de Levante for VW Marpetrol

	MARIN	SISTEMAR	
		New Momentum Theory	**MARIN B Series full scale**
η_0	0,629	0,650	0,644
$H_{0,7}$ (m)	5,796	5,888	5,953
T (tons)	87,140	89,958	89,281

$H_{0.7}$ is the propeller blades geometrical pitch at the station 0.7 and T is the thrust supplied by the propeller.

NACA 65 mean line has been used for the calculations because it is quite similar to the mean line of Walchner profiles used by MARIN for radial stations above 0.65R.
The results of the calculations carried out by means of the New Momentum Theory are slightly more favourable than those obtained by means of the polynomial expressions of Doctors Oosterveld and Van Oossanen, Ref. 5, as it happens with experimental results of high efficiency propellers. This conclusion is supported by more than 500 verifications.
The η_0 value obtained experimentally by MARIN (0.629) is slightly lower and has not been extrapolated at full scale.
The difference between the calculated $H_{0.7}$ geometrical pitch and the pitch of the propeller used for the tests is close to 1.6%, figure which is entirely negligible.
Likewise, the difference between the thrust predicted by direct calculation and the one experimentally deduced is close to 3.2%, also relatively small.
It must be concluded therefore that the results of direct calculations carried out corresponding to the single propeller are very accurate, circumstance which is being pointed out since 1986, Ref. 28.

6.1.2 Performance prediction of the cargo liner with a set of contrarotating propellers.

The departing data of the calculations carried out have been the following:

V = 20 knots

V	1st propeller	2nd propeller
DHP (HP)	6654	6273
RPM	111,6	111,6
D	5,220	4,880
z	4	5
AE/AO	0,432	0,531

η_0	1,041	1,041
t	0,183	0,183
w	0,243	0,152

According to the departing hypothesis, the predesign of the first propeller has been done ignoring totally the existence of the second propeller.
Like in Ref. 29, only the values of t (0,230) and w (0,298) corresponding to the set of the two propellers are given. These values are not useful, and for this reason, it has been decided to attribute to the forward propeller the values of t and w corresponding to the single propeller in spite that its diameters are slightly different.
The axial component of the induced velocity at the 0.7 station of the disk of the first propeller is equal to 1,494 m/s and the angular induced velocity corresponding to said station is equal to 0.7602 s^{-1}.
The angle of the geometrical pitch of the station 0.7 of the blades has been calculated using the New Cascades Theory, Refs. 9, 35 and 40. It has been assumed that 90% of the load is obtained under free shock entrance conditions and the remaining load is obtained by angle of attack.
The axial component of the induced velocity, at the inifinite donwstream of the first propeller corresponding to the station 0.7 is 2,987 m/s and the angular induced velocity of said station at the infinite downstream is 2.2381 s^{-1}.
The factor FCV has been calculated by means of the equality (14) obtaining the value of 0.81, so the wake apparent coefficient (w_s) corresponding to the second propeller has been 0.152.
In Table 2, the results of direct calculations and MARIN experimental results are compared.
The geometrical pitches calculated for both propellers are surprisingly in accordance with the real ones, with differences close to just 0.7%. The differences between predicted and calculated thrusts are close to 2%.
The excelent results obtained endorse the validity of the hypothesis which considers that the aft propeller operates at the inifinite downstream of the forward propeller.

Table2.

	MARIN	SISTEMAR
Thrust 1st propeller	48,180	47,790
Thrust 2nd propeller	44,280	42,876
Total thrust	92,460	90,666
η_0 first propeller		0,716
η_0 second propeller		0,764
$H_{0,7}$ 1st propeller	5,652	5,613
$H_{0,7}$ 2nd propeller	5,838	5,829

It is necessary to state that the conclusions presented in Ref. 35 in connection with the verification of the quality of the Generalized New Momentum Theory were so excellent as the ones presented in this paper.
Once demonstrated the quality of the Generalized New Momentum Theory, the conclusions of the propulsion optimization process presented herebelow, must be accepted.

6.2 Criterium to be adopted to compare the different solutions already studied

The predesigns for all the alternatives studied have been performed for a constant ship speed and a same propulsion power.

As the propulsive efficiency increases the thrust supplied to the ship will increase. Of course, in general, there will not exist an equilibrium between the propellers thrust and the ship advance resistance, so the fictitious existence of some trailing forces, F, must be accepted. Said forces have to verify the following equality:

$$T[1-t] = R + F$$

This force allows the ship to sail at the imposed speed of 20 knots whatever be the propellers thrust.
The propulsion system will be as more effective as higher be T, since the thrust deduction coefficient t adopts the same value for all the solutions (exception made of the two shaft lines version).
When direct calculations have been carried out, a global thrust deduction coefficient of the propellers in series equal to the thrust deduction coefficient of the single propeller has been assumed.
As direct calculations made assuming as valid said hypothesis have reproduced satisfactorely both the thrusts and geometry of the propellers used in model tests, it may be concluded that said hypothesis is a consequence of having accepted that the aft propeller operates at the infinite downstream of the forward propeller.
The merits of each solution constituted by propellers in series cannot be judged in terms of the propeller open water efficiencies of each one of the propellers, because in the case of the aft propellers, in spite that they could have efficiencies higher than the forward propellers (depending on the case) the thrust provided may be lower if the axial component of the entrance water velocity to the propeller disk were very high, because the velocity induced at the infinite downstream by the forward propeller were very high.
These inconveniences are avoided using as parameter to judge the quality of each solution, the total thrust produced by the propulsion system.
Being the ship studied of high speed, the single propeller is slightly loaded and hence these experimental data do not constitute an attractive example to stand

out the merits that could be achieved with CLT propellers because its advantages over conventional propellers are directly related with the specific load of the basical conventional propeller.

6.3 Comments on the experimental results obtained by MARIN

From the results of the tests conducted by MARIN it is deduced that at the ship speed of 20 knots, the contrarotating propellers request a propulsion power which is slightly higher than the one corresponding to the single propeller and therefore, the contrarotating propellers would not be advisable.
In spite of the preceding conclusion, the addition of the thrusts supplied by the contrarotating propellers (92.460 Kp) is higher than the thrust supplied by the single propeller (87.140 Kp). The explanation of this fact comes from the thrust deduction coefficient t obtained by MARIN for the set of contrarotating propellers (0.230) which is more pessimistic than the corresponding one of the single propeller (0.183).
Direct calculations carried out assuming a same thrust deduction coefficient both for the contrarotating propellers and the single propeller lead to practically equal thrust for both solutions, concluding therefore that both propulsive solutions offer similar performances. This conclusion coincides with the one deduced from the tests focusing the attention on the propulsion powers.
It is evident that the results of direct calculations and experimental results drive to the same conclusions concerning the merits of each propulsion solution and furthermore the same geometrical characteristcs are obtained.

6.4 Ship performance estimation for different propulsion solutions

The comparisons between performances of different propulsive alternatives studied, have been refered to the modelization by means of the New Momentum Theory of the ship performance with the single conventional propeller.

The main characteristics of the propellers involved within the different propulsive solutions analyzed have been summarized in Table 3 for the sake to facilitate the comparisons.

It has been assumed that the main engine is not directly coupled with the aim to enable the utilization of reduction gears with the most adecuated reduction ratio for each case.

In all the cases it has been considered that the ship speed is 20 knots and the total available power for the propulsion is 13.821 DHP.

6.4.1 Single propeller of CLT type

The optimum diameter of a CLT propeller turning at 112.9 rpm would be 5.8 m. and its thrust would be equal to 94.282 Kp.
As it has been decided to choose in each case the revolutions rate which makes optimum the maximum allowable diameter for the propellers (6 m.) a new pre-design of a 6 m. diameter CLT propeller has been done turning at 100 rpm; its thrust is 95.259 Kp, a 5,9% higher than the thrust of the conventional propeller (89.958 Kp.).

6.4.2 Two shaft lines with conventional propellers of 6 m

The revolutions rate leading to conventional propellers of 6 m of diameter is 80 rpm.
When doing the predesign of these propellers, the values of w (0.12) and of t (0.10) have been rectified to have into account that the propellers are located out of the center line.
The thrust to be obtained with this configuration would be 91.508 Kp; that is, lower than the thrust of a single CLT propeller and relatively close to the thrust of a basical single conventional propeller (89.958 Kp).
The negative repercusion of the displacement of the propellers from the center line has been clearly detected in this solution.

6.4.3 Two shaft lines with CLT propellers of 6 m

Due to the reduced specific load of the conventional propellers as a consequence of its diameter and its revolutions, and to the high ship speed with two shaft lines, it would not be advisable to resort to CLT propellers because the thrust that would be obtained, is just 89.562 Kp.
From the studies presented until now it must be concluded that the best performances would be obtained with a single CLT propeller; furthermore, this solution is much cheaper than the solution of two shaft lines with conventional propellers.

6.4.4 Contrarotating conventional propellers in series

For this type of propulsive solution it is necessary to find out the optimum distribution of propulsive power between first and second propeller, always looking for the revolutions rate which make optimum the maximum allowable diameters for the first propeller (6 m.) and for the second propeller (5.28 m.).
Within this analysis the performances of the set of contrarotating propellers for different propulsive power distributions between first and second propeller have been studied and just slight variation have been found.
A rather weak tendency has been detected to achieve a performance improvement when the load of the second propeller increases above 30%.

Table 3.

RESULTS OF THE OPTIMIZATION CALCULATIONS CARRIED OUT BY SISTEMAR.

Propeller Type	DHP Forw/Aft	N Forw/Aft	Thrust Forw/Aft Total	$H_{0,7}$ Forw/Aft	w Forw/Aft	Ang.Ind.vel produced by forw. prop.*	η_0	Z	D	AE/AO
Single conven.	13,821	112,9	89,958	5,888	0,243	–	0.650	4	6,000	0,621
Single Marin B series with same $H_{0,7}/D$	13,821	112,9	89,281	5,953	0,243	–	0,644	4	6,062	0,621
Single CLT	13,821	112,9	94,282	5,805	0,243	–	0,713	4	5,800	0,621
Single opt. CLT	13,821	100	95,259	6,645	0,243	–	0,721	4	6,000	0,6212
conv. single props. in 2 shaft lines	13,821	80	91,508	8,417	0,120	–	0,768	4	6,000	0,470
2 CLT single props in 2 shaft lines.	13,821	80	89,562	8,506	0,120	–	0,751	4	6,000	0,470
Convs. in series	**70%/30%**									
Forward	9,675	95	68,461	6,769	0,243	–	0,706	4	6,000	0,432
Aft contrarot.	4,146	80	29,809 **98,270**	7,643	0,138	–42,39	0,817	5	5,280	0,531
Aft tandem	4,146	95	18,085 **86,546**	10,676	0,138	39,90	0,495	5	5,28	0,531
Aft tandem with fins	4,146	95	28,182 **96,643**	6,627	0,138	0	0,772	5	5,28	0,531

CLT in series	**70%/30%**									
Forward	9,675	90	70,863	7,212	0,243	–	0,731	4	6,000	0,432
Aft contrarot.	4,146	70	32,109	8,496	0,146	–45,13	0,872	5	5,280	0,531
			102,972							
Aft tandem	4,146	90	21,194	10,052	0,146	35,10	0,575	5	5,28	0,531
			92,057							
Aft tandem with fins	4,146	90	27,643	7,237	0,146	0	0,750	5	5,280	0,531
			98,506							
Convs. in series	**60%/40%**									
Forward	**8,293**	90	59,869	6,971	0,243	–	0,720	4	6,000	0,432
Aft contrarot.	**5,528**	80	39,179	7,959	0,162	–21,09	0,783	5	5,280	0,531
			99,048							
Aft tandem	**5,528**	90	32,156	8,590	0,162	18,70	0,642	5	5,280	0,531
			92,025							
Aft tandem with fins	**5,528**	90	37,489	7,294	0,162	0	0,749	5	5,280	0,531
			97,358							
CLT in series	**60%/40%**									
Forward	**8,293**	90	61,313	6,933	0,243	–	0,737	4	6,000	0,432
Aft contrarot	**5,528**	80	43,619	7,438	0,175	–34,46	0,858	5	5,280	0,531
			104,932							
CLT in series	**60%/40%**									
Aft tandem	5,528	90	31,004	9,311	0,175	+ 30,60	0.610	5	5,280	0,531
			92,317							
Aft tandem with fins	5,528	90	37,837	7,205	0,175	0	0,744	5	5,280	0,531
			99,150							

* In percentage of nominal rpm.
Thrust in tons.
$H_{0.7}$ in m.
DHP in HP.

Table 3. *Continuation*

Propeller Type	DHP Forw/Aft	N Forw/Aft	Thrust Forw/Aft Total	$H_{0,7}$ Forw/Aft	w Forw/Aft	Ang.Ind.vel produced by forw. prop.*	η_0	Z	D	AE/AO
	RESULTS OF THE OPTIMIZATION CALCULATIONS CARRIED OUT BY SISTEMAR.									
Conv. in series	**50%/50%**									
Forward										
Aft contrarot.	6910,5	84	48,593	7,274	0,243	–	0,736	4	6,000	0,432
	6910,5	84	50,980	7,757	0,192	–17,10	0,749	5	6,000	0,531
			99,573							
Aft contrarot with fins	6910,5	84	46,099	8,201	0,192	–	0,710	5	5,280	0,531
			97,079							
CLT in series	**50%/50%**									
Forward	6910,5	84	51,496	7,268	0,243	–	0,743	4	6,000	0,432
Aft contrarot.	6910,5	84	55,409	7,209	0,205	–27%	0,840	5	5,280	0,531
			106,905							
Aft tandem	6910,5	84	41,499	9,816	0,205	+27%	0,629	5	5,280	0,531
			92,995							
Aft tandem with fins	6910,5	84	47,821	8,170	0,205	0	0,725	5	5,280	0,531
			99,317							
Convs. in series	**40%/60%**									
Forward	5,528	80	41,809	7,367	0,243	–	0,754	4	6,000	0,432
Aft contrarot.	8,243	90	57,908	7,358	0,223	—13,2%	0,715	5	5,280	0,531
			99,715							
Aft tandem	8,293	80	48,560	10,106	0,223	+14,8%	0,600	5	5,280	0,531
			90,369							
Aft tandem with fins	8,293	80	53,853	9,067	0,233	–	0,665	5	5,280	0,531
			95,662							

CLT in series	**40%/60%**									
Forward	5,528	80	41,513	7,384	0,243	–	0,749	4	6,000	0,432
Aft contrarot.	8,293	90	67,442	6,816	1,237	–20,05%	0,818	5	5,280	0,531
			108,955							
Aft tandem	8,293	80	52,587	10,284	0,237	+22,60%	0,638	5	5,280	0,531
			94,100							
Aft tandem with	8,293	80	57,040	9,184	0,237	0	0,692	5	5,280	0,531
fins			**98,553**							
Convs. in series	**30%/70%**									
Forward	4,146	78	32,150	7,210	0,243	–	0,774	4	6,000	0,432
Aft contrarot.	9,675	95	67,145	7,083	0,258	–9,73%	0,679	5	5,280	0,531
			99,295							
Aft tandem	9,675	78	56,606	10,584	0,258	+11,9%	0,572	5	5,280	0,531
			88,756							
Aft tandem with	9,675	78	61,132	9,759	0,258	0	0,612	5	5,280	0,531
fins	**93,282**									
CLT in series	**30%/70%**									
Forward.	4,146	78	31,263	7,417	0,243	–	0,752	4	6,000	0,432
Aft contrarot.	9,675	95	79,194	6,583	0,62	–15,89%	0,796	5	5,280	0,531
			110,457							
Aft tanden	9,675	78	62,415	10,890	0,262	+19,40%	0,627	5	5,280	0,531
			93,678							
Aft tandem with	9,675	78	65,224	10,174	0,26	20	0,656	5	5,280	0,531
fins			**96,487**							

* In percentage of nominal rpm.
Thrust in tons.
$H_{0.7}$ in m.
DHP in HP.

The best results have been obtained when the first (forward) propeller receives 40% of the total DHP and the second (aft) propeller receives the remaining 60%. When the percentage power corresponding to the second propeller goes up above 60%, the performance of the set start to decrease.
The total maximum thrust of both propellers is 99.717 Kp.
The optimum revolutions rate for the first propeller is 80 rpm and for the second propeller is 90 rpm.
Within the optimization process, the number of blades and the blades area ratios used have been the very same used by MARIN for both propellers.
It is necessary to remark that the conclusions of a parallel study carried out by the authors in Ref. 35, taking as basis the experimental results obtained by MARIN with the model of a tanker, were different. For this case, the optimum power distribution between both propellers was 60% for the forward propeller and 40% for the aft propeller.
Both in Ref. 35 as in this case it has been concluded that it is feasible to improve the performances supplied by a single conventional propeller resorting to an optimized set of contrarotating conventional propellers.
The percentage of improvement in the performances obtained by the contrarotating propellers depends very much on the specific load of the alternative version of a single conventional propeller.
In the case of the tanker, Ref. 35, the percentage of improvement was higher than the one obtained in this case for the cargo liner.
The percentage of improvement of the thrust that would be obtained with a single CLT propeller in the case of the cargo liner studied in this paper would be 5,9%, while the corresponding one to two contrarotating conventional propellers would be 10,8%; however, the necessary investment to get such improvement would need to be sensibly higher.
In the case of the tanker, Ref. 35, the improvement was higher with a single CLT propeller than with a set of two contrarotating conventional propellers.

6.4.5 Contrarotating propellers in series of CLT type

For this type of propulsive solution it is also necessary to find out the optimum distribution of propulsion power between first and second propeller looking always for the revolutions which make optimum the maximum allowable diameters for both propellers.
As it has been done in the previous case, both the number of blades and the blade area ratios used have been the very same used by MARIN for the contrarotating conventional propellers.
The performance of the set of two CLT contrarotating propellers increases as long as the power supplied to the second propeller increases. When the second propeller receives 70% of the total DHP the thrust of the set of both propellers is 110.457 Kp. The optimum revolutions rate for the first propeller is 78 rpm and for the second propeller is 95 rpm.
The attention is called on the fact that the thrust of the first contrarotating

CLT propeller is 31.263 Kp. while the thrust of the first contrarotating conventional propeller with the same power distribution and turning at the same revolutions rate is 32.150 Kp.
This fact allows to venture that the optimum propulsive solution would be a set of contrarotating propellers with a forward conventional propeller receiving 30% of the available DHP and a CLT propeller as aft propeller receiving the remaining 70% of the available DHP.
The expected total thrust for such a solution would be of 111.344 Kp.
The results obtained do not have anything unexpected since the reduction of power given to the first propeller and the reduction of its revolutions rate, leads to a very unloaded propeller; thus, it may become counterproductive to install a CLT type propeller.
The percentage of improvement that would be obtained in the ship performance with two contrarotating propellers of CLT type would be close to 22,8% (higher than the double that would be obtained with contrarotating conventional propellers).
In case of resorting to the mixed solution of contrarotating propellers (conventional-forward, CLT-aft) the percentage of improvement would be 23,8%.
The most important conclusion deduced from the above is that if the difficult solution of contrarotating propellers is adopted, it would not have any sense not to resort to CLT propellers, being able to arrive, depending on the propellers specific loads to a mixed solution or else to a clearly solution CLT as it happens in the case of the tanker analyzed in Ref. 35.

6.4.6 Tandem conventional propellers in series

The interest of this propulsion system lies on the fact that it is not requested the expensive propulsive installation consisting on two concentrical turning shafts although it takes advantage from the reduction of the B_P coefficient because the propulsive power is subdivided and the propellers revolutions are reduced.
The best results corresponding to this propulsive solution are obtained when the forward propeller receives 60% of the available DHP and the aft propeller receives the remaining.
The thrust of the set of both propellers is 92.025 Kp and the revolutions rate is 90 rpm.
The percentage of improvement with regard to the basical conventional solution would be just 2,3%.

6.4.7 Tandem propellers in series of CLT type

Its interest is due in principle to the reasons already mentioned for the propulsive solution which has been previously analyzed.

The best results corresponding to this propulsive solution are obtained when the forward propeller receives 40% of the available DHP and the aft propeller receives the remaining.

The total thrust is 94.100 Kp. and represents a percentage of improvement on the basical conventional solution of 4,6%.

The improvements percentages obtained for the tandem propellers are not very stimulating; however, these figures can be improved taking into account the ideas presented herebelow.

6.4.8 Tandem propeller in series axially separated by a ring of flow driving fins

The calculations carried out with the Generalized New Momentum Theory allow to conclude that the reason of the poor performance of the aft propeller from a set of tandem propellers is due to its hydrodynamical pitch angle corresponding to the station 0.7 which is very high; much more than the one corre-

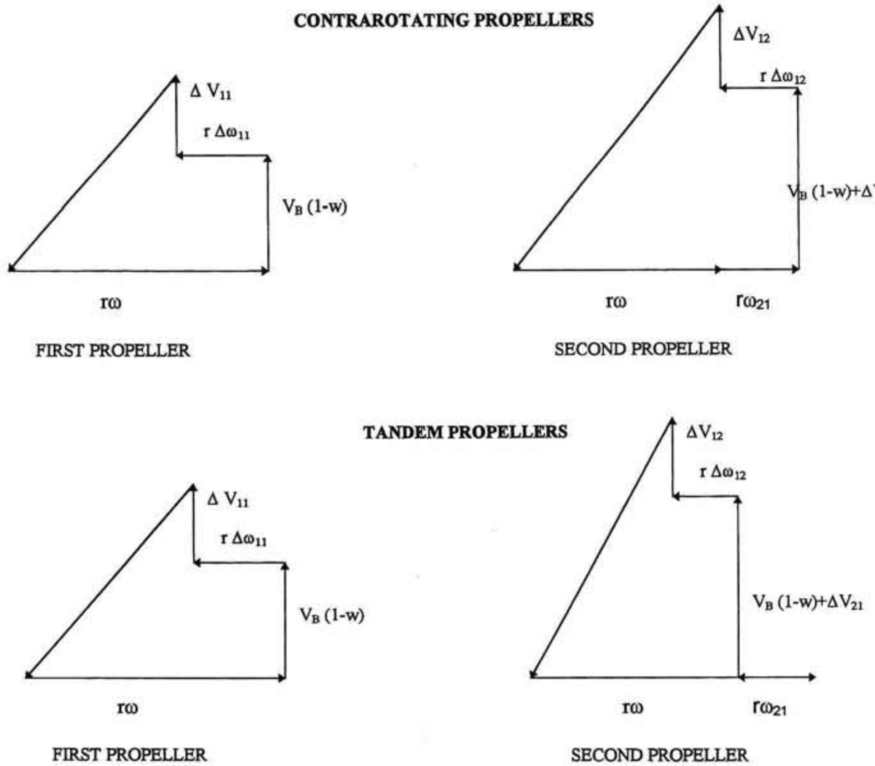

Figure 2. Diagrams of velocities corresponding to forward and aft propellers in contrarotating and tandem arrangements.

sponding to the aft propeller from a set of contrarotating conventional propellers. (See Figure 2).
This fact is due to the influence that the angular component of the velocity induced by the forward propeller at the infinite downstream exerts on the velocities polygon corresponding to the station 0.7 of the aft propeller.
This inconvenient could be eliminated by introducing between forward and aft propellers a ring of fins with the aim to induce into the liquid vein a change in the tangential momentum in order to assure that the water at the infinite upstream of the aft propeller has just a unidirectional axial motion.
When designing the flow driving fins care should be taken to avoid the transmission to the hull of reaction forces with important components in the ship speed direction (negative thrusts).
In Refs. 35 and 40 the authors have proposed to place the fins inside a ring as shown in Figures 3 and 4. The fins are made rigid by means of an internal hub and the outer ring.

In said references the following alternatives have been proposed for the mounting of the ring of fins.

a) To let the ring resting on the tail shaft through a rotating bearing which allows the ring not to be forced to turn driven by the shaft.
b) To let the ring as described in a) but with a fixed connection to the ship hull which prevents to turn.
c) To let the ring be coaxial with the tail shaft but not in contact with it. The ring would be supported by the ship structure through some links.

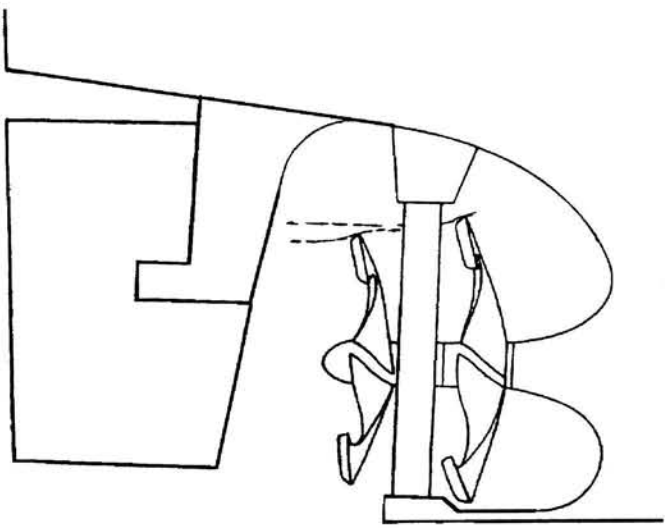

Figure 3. Ring of fins located between forward and aft propellers in a tandem arrangement.

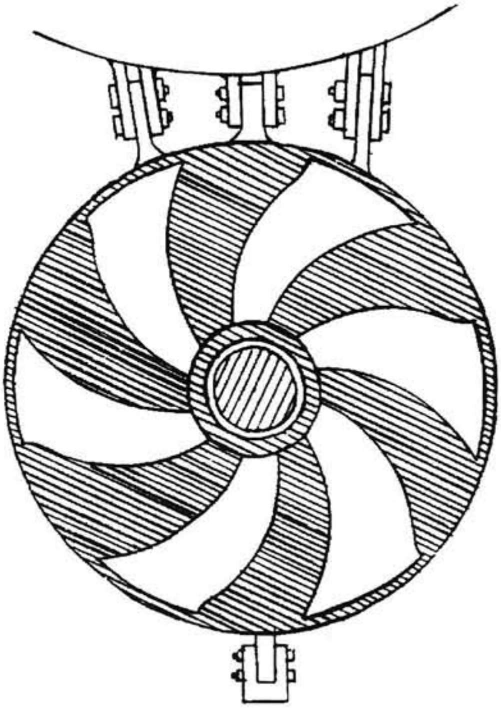

Figure 4. Mounting of the ring of fins located between forward and aft propellers in a tandem arrangement.

In the authors opinion, the alternative c) is the most convenient.
Altenative c) has been represented in Figure 4 characterized because the structural elements that join the ring to the ship structure could be of demountable type (through fixing bolts), with the aim to make feasible the propellers dismounting.
The material used for the construction of the ring could be either bronze or carbon fiber.

The two propellers shown in Figure 4 are right handed seen from astern; for this reason the fins look like left handed propeller blades.
To analyze the advantages that could be obtained with this type of propulsive solution, the calculations corresponding to the alternatives tandem conventional and CLT propellers have been repeated, supposing as null the angular velocities at the infinite upstream of the aft tandem propeller.

a) Tandem conventional propellers.
   The best results are obtained distributing the propulsive power in such a way that the first propeller receives 60% of the available power and the second propeller the remaining 40%.

The total thrust of the set would be 97.358 Kp. which represents an improvement with regard to the basical conventional solution of 8,2%; percentage which is really close to the corresponding one to the solution of contrarotating conventional propellers (10,8).
The optimum revolutions of this version would be 90 rpm.

b) Tandem propellers of CLT type.
The best results are obtained distributing 50% of the available power between the two propellers.
The thrust of both propellers would be 99.317 Kp and their revolutions 84 rpm.
The percentage of improvement on the basical conventional version would be of 10.4%.

Therefore it is concluded that by means of tandem CLT propellers the performance obtained would be similar to the performance achieved with contrarotating conventional propellers but with investments and maintenance costs sensibly lower.

7. Verification of the calculations carried out using the theoretical developments described with the results of an experimental program conducted in Hamburg model basin

As a demonstration of the accuracy of the Generalized New Momentum Theory in association with the equivalent profile theory and also of the quality of the calculation procedure developed, a further comparison between experimental results with CRP arrangement and direct calculations results is presented herein.
The experimental results considered correspond to the case presented by Mr. Praefke, HSVA, in his paper presented at the "Propellers/Shafting's 94" Symposium, September 1994, Virginia, USA.
With occasion of the visit made by one of the authors to HSVA, he met Mr. Praefke and after discussing the experimental program carried out it was agreed to check the calculation procedure presented by the authors.
The information received to be used as input data for the calculations were the speed of the ship; rpm and powers given to the single screw version and to the forward and aft propeller of the CR arrangements; wake fraction corresponding to the single screw version; propeller diameters, number of blades and blade area ratios corresponding to the propellers used in the tests.
The prediction of propeller thrusts and geometrical pitches at the station 0.7 of all the propellers involved constituted the goal of the exercise.
Comparisons between extrapolation of model tests results and calculations results are presented in Table 4.

It must be pointed out that Mr. Praefke gave us the results of his measurements just after receiving the results of our calculations.
The difference in thrust between predicted values and the test results are in the range of 2%. The differences between predicted pitch values and the real ones are in the range of 4%.
The high quality of the results of the calculations prooves also that the assumption made when calculating the induced velocities of the second propeller of the CR arrangement considering that it is located at the infinite downstream of the first propeller is correct.
This comparison was presented in the discussion of Ref. 35.

Table 4

CHECKING OF THE GENERALIZED NEW MOMENTUM THEORY BY COMPARING DIRECT CALCULATION WITH HSVA MODEL TEST RESULTS.

			HSVA test results	SISTEMAR CALCUL.	Difference in percentage
Contrarotating propellers	Forward	Propeller thrust (Kn).	183.2	181.65	0.85
		Geometrical pitch (m).	2.375	2.260	4.8
	Aft	Propeller thrust (Kn).	166.2	168.17	1.19
		Geometrical pitch (m).	2.613	2.496	4.4
	Total thrust	349.4	349.82	0.0	
Single propeller		Propeller thrust (Kn).	323.0	316.2	2.1
		Geometrical pitch (m).	2.335	2.315	0.98

- Ship speed: 26 kn.
- Each contrarotating propeller absorbs 2750 Kw.
- The single propeller absorbs 5500 Kw.
- All the propeller rpm are 400.
- Effective wake coefficient corresponding to the single propeller: 0.180.
- Diameter of forward propeller : 2.200 m. ; Number of blades: 5; Blade area ratio: 0.508
- Diameter of after propeller : 2.000 m. ; Number of blades: 4; Blade area ratio: 0.500
- Diameter of single propeller : 2.400 m. ; Number of blades: 5; Blade area ratio: 0.950

Note:
SISTEMAR calculations corresponding to the propeller thrust, and the geometrical pitches of the propellors tested were carried out without knowing neither the types of the pitch distribution nor the criterium used by HSVA to choose the combinaton of camber and angle of attack.

8. Conclusions

1. The studies carried out have pointed out once more, that using the New Momentum Theory and the equivalent profile theory it is possible to predict with the maximum accuracy the performance of a conventional propeller.
   The extension of these conclusions to the CLT propellers is based on SISTEMAR experience coming from more than 200 applications at full scale conducted with CLT propellers, which conclusions have been progressively published in the papers mentioned in the reference list.
2. It has been checked that the generalization of the New Momentum Theory is very precise and its association with the equivalent profile theory, makes feasible its use in the predesign stage to predict the performance of any ship with propellers in series (contrarotating and tandem).
3. When a set of propellers in series is adopted as ship propulsion arrangement it is indispensable to optimize the power distribution between the first and the second propeller as well as the propeller revolutions. The percentages of power distribution depend on the ship hull lines and the propellers loading.
4. When it has been dediced to do the important investment that the contrarotating propellers request, it is imperative under an economical point of view to optimize the performance of the propulsive system including CLT propellers.
5. Some new lines of investigations have been open to improve the propulsive efficiency of the installations with tandem propellers and likewise it is expected that the applications field of this propulsive solution will increase.
6. In spite of that in this paper the utility of a procedure ellaborated to optimize the propulsive efficiency of the ships through direct calculation has been pointed out, the ideas already presented have contributed also to enhance the role of the model basins, because without any doubt the propulsion systems types which have been analyzed will be progressively introduced into the naval sector and this will require extensive experimental work beyond traditional ones due to the intrinsic complexity of the new propulsive solutions.

List of symbols

EHP	Towing power.
BHP	Propulsive power.
DHP	Power given to the propeller.
η_P	Propulsive efficiency.
η_0	Propeller open water efficiency.
η_r	Relative rotative efficiency.
η_H	Hull efficiency; $\eta_H = (1\text{-}t) / (1\text{-}w)$
V_B	Ship speed.
R	Towing resistance; propeller radius.
t	Thrust deduction coefficient.
w	Effective wake coefficient at thrust identity.
T	Propeller thrust.
N, n	Propeller revolutions.
P	Power absorbed by the propeller.
V_a	Relative water velocity at the infinite upstream.
K_r	Quotient between the revolutions rate of both propellers in a set of contrarotating propellers.
J	Advance degree.
K_T	Non-dimensional thrust coefficient.
K_Q	Non-dimensional torque coefficient.
D	Propeller diameter.
ρ	Water density.
AE/AO	Blade area ratio.
$H_{0.7}$	Geometrical pitch of the blades at 0.7R station.
z	Number of blades.
w_s	Apparent effective wake coefficient at thrust identity.
FCV	Corrector factor of the viscosity action in the axial distribution of velocities.
ω	Angular velocity of the propeller.
ΔV_1	Axial component of the velocity induced at the propeller disk.
ΔV_2	Axial component of the velocity induced at infinite downstream of the propeller disk.
$\Delta\omega_1$	Angular component of the velocity induced in the propeller disk.
$\Delta\omega_2$	Angular component of the velocity induced at infinite downstream of the propeller disk.
ΔV_{11}	Axial component of the velocity induced at the disk of the first propeller.
ΔV_{12}	Axial component of the velocity induced at the disk of the second propeller.
ΔV_{21}	Axial component of the velocity induced by the the first propeller at the infinite downstream.
$\Delta\omega_{11}$	Angular component of the velocity induced at the disk of the first propeller.

$\Delta\omega_{12}$	Angular component of the velocity induced at the disk of the second propeller.
$\Delta\omega_{21}$	Angular component of the velocity induced at the infinite downstream of the disk of the first propeller.

Reference list

[1] Pérez Gómez, G.: "Apuntes de Teoría del Buque". (5 volumes). Escuela Técnica Superior de Ingenieros Navales. Madrid. Different editions during the period 1973-1997.

[2] Pérez Gómez, G.: "Optimización de la propulsión de un buque". Ingeniería Naval, April 1986.

[3] Pérez Gómez, G.; González-Adalid, J.: "Optimización del rendimiento de propulsor aislado de las hélices de los buques". Ingeniería Naval, October 1992.

[4] Pérez Gómez, G.: "Hidrodinámica aplicada a la propulsión del buque". Ingeniería Naval, September 1992.

[5] Oosterveld, M.W.C.; Van Oossanen, P.: "Further computer-analyzed data of the Wageningen B-screw series". International Shipbuilding Progress, Vol. 22, July 1975.

[6] Pérez Gómez, G.; González Linares, F.; Baquerizo Briones, I.: "Some improvements of the Traditional Lifting Line Theory for Ship Propeller". International Shipbuilding Progress. July 1980. Also published by Ingeniería Naval, may 1978.

[7] Pérez Gómez, G.: Seminary entitled "Procedimientos modernos de proyecto de hélices". A.I.N.E. Junta de Zona de Cartagena. October 1979. (5 volumes).

[8] Pérez Gómez, G. "Application of a New Mometum Theory to the Design of Highly Efficient Propellers Having Finite Load at the Blade Tips". WEMT, Paris, July 1984.

[9] Pérez Gómez, G.; González-Adalid, J.: "Tip Loaded Propellers (CLT). Justification of their Advantages over Conventional Propellers using the New Momentum Theory". Presented at the New York Metropolitan Section of the SNAME the 11th of February 1993. International Shipbuilding Progress, 42, nº 429 (1995) pp. 5-60.

[10] Pérez Gómez, G. "Una innovación en el proyecto de hélices". Ingeniería Naval, October 1976.

[11] Ruiz Fornells, R.; Pérez Gómez, G.: "Evolución de los propulsores TVF: Proceso de diseño y primeros resultados experimentales". Ingeniería Naval, May 1981.

[12] Ruiz Fornells, R.; Pérez Gómez, G. and other: "Fuel Saving from a New Type of Propellers". Marine Propulsion. May 1981.

[13] Ruiz Fornells, R.; Pérez Gómez, G.: "Full Scale Results of First TVF Propellers". ISSHES-83. Also published in Ingeniería Naval, May, June 1984.

[14] Ruiz Fornells, R.; Pérez Gómez, G.: "Service Results with the TVF Propeller Duct System". The Sixth International Marine Propulsion Conference. Café Royal, London, March 1984.

[15] "Service Data Back Tip Loaded Propeller Claims". The Motor Ship, July 1987.

[16] Pérez Gómez, G.; González-Adalid, J.: "Comportamiento del Sesermendi

Barri dotado de una hélice convencional en tobera y de una hélice CLT". Rotación, July 1987.
[17] Rial, J.: "Mejora en las prestaciones de un buque palangrero mediante una hélice CLT". Rotación, July 1988.
[18] Pérez Gómez, G.; González-Adalid, J.: "Comportamiento de las hélices en las pruebas de tracción". Rotación, April 1988.
[19] "Reunión sobre ahorro energético en buques. Hélices CLT". Boletín Informativo de ANAVE, December 1990. Also published in Ingeniería Naval, January 1991.
[20] "Owners Endorse CLT Propellers". The Motor Ship, February 1991.
[21] Zatarain, G.: "Comportamiento del buque Guardo equipado con una hélice CLT". Rotación, February 1991.
[22] Zatarain, G.: "Experience with Retrofitting. CLT Propellers". 14th International Marine Propulsion Conference. London. The Motor Ship, March 1992.
[23] Supplement of CLT Propellers. Fairplay, 6th of February 1992.
[24] Supplement on CLT Propellers. Rotación, April 1992.
[25] Sendagorta Gómez del Campillo, I.; Uriarte Elloriaga, R.; Pérez Gómez, G.; González-Adalid, J.: "Mejoras conseguidas en el buque Sierra Guadarrama de Marítima del Norte con una hélice CLT". Rotación, September 1992.
[26] Supplement on CLT Propellers. The Motor Ship, September 1993.
[27] Holtrop, J.: "Propulsion data". International Shipbuilding Progress, Vol. 31, November 1984.
[28] Pérez Gómez, G.: "Nuevo procedimiento para determinar las características de un propulsor convencional de rendimiento óptimo". Ingeniería Naval, January 1986. Also presented in the Sixth LIPS Symposium on Ship Propellers, May 1986.
[29] Van Manen, J.D.; Oosterveld, M.W.C.: "Model Test on Contrarotating Propellers". Seventh Symposium Naval Hydrodynamics, 1968.
[30] Sun Qin; Gu Yunde: "Tandem Propellers for High Powered Ships". 1991, The Royal Institute of Naval Architects.
[31] Pérez Gómez, G.: "Correcciones a la Teoría Clásica de la Impulsión y Habilitación de la misma para el diseño de propulsores". Ingeniería Naval, January 1983.
[32] Pérez Gómez, G.; Baquerizo Briones, I; González-Adalid, J.: "Aplicación de la Nueva Teoría de la Impulsión al diseño de propulsores. Comparación con la teoría de las líneas sustentadoras". Ingeniería Naval, July 1983.
[33] Pérez Gómez, G.; González-Adalid, J.: "Influencia del mayor rendimiento de una hélice CLT frente a una hélice convencional equivalente en las características de maniobrabilidad y en los niveles de vibraciones de un buque". Rotación, December 1989.
[34] Pérez Gómez, G.: "Diseño de hélices que funcionan en la interior de toberas y procedimiento para extrapolar sus resultados experimentales". Ingeniería Naval, January 1994.

[35] Pérez Gómez, G.; González-Adalid, J.: "Contrarotating and Tandem CLT Propellers". Symposium sponsored by the SNAME entitled Propellers/ Shafting'94. September 1994, Virginia, USA.

[36] Taniguchi, K.: "Model-Ship Correlation Method in the Mitsubishi Experimental Tank". M.T.B. December 1963.

[37] Taniguchi, K.: "Model-Ship Correlation in Propulsive Performance". Japan Shipbuilding and Marine Engineers, May 1967.

[38] Pérez Gómez, G.: "Comentarios sobre algunos temas de interés del campo de la hidrodinámica aplicada al buque". Ingeniería Naval, February, 1978.

[39] Pérez Gómez, G.: "Adaptación de los propulsores con carga en los extremos de las palas a la vena líquida que atraviesa el propulsor". Sixth Symposium on marine propellers sponsored by LIPS, May 1986. Ingeniería Naval, August, September, 1986.

[40] Pérez Gómez, G.; González-Adalid, J.: "Optimización del sistema propulsor de un buque utilizando la Nueva Teoría de la Impulsión Generalizada". Ingeniería Naval, May and June 1994.

[41] Pérez Gómez, G.; González-Adalid, J.: "Consideraciones sobre la modelización matemática de la acción que una hélice ejerce sobre el agua". Ingeniería Naval, May and June 1996.

[42] Boeta, R.: "Trasmediterranea fits first Hydrofoil". The Motor Ship supplement, September 1996.

[43] Hollstein, H.J.: "Performance Improvement of the Orange Juice Carrier Bebedouro by means of a CLT Propeller". The Motor Ship supplement, November 1995.

[44] Hollstein, H.J.; Pérez Gómez, G.; González-Adalid, J.: "Bulkcarrier Speed Trials with a Sistemar CLT Propeller". The Naval Architect, February 1997.

Appendix

Generalization of the New Momentum Theory

The New Momentum Theory has been based on the assumption that the water upstream of the propeller disk has a unidirectional motion (the fluid has velocities with just axial components).
In the case of nozzle propellers this assumption is not true. Also in the case of contrarotating and tandem propellers arrangements this assumption is not true for the second propeller. Therefore, with the aim to design properly these types of propellers it has been necessary to generalize the theory in order to admit that at the infinite upstream of the propeller disk the velocity field of the fluid may have angular components.
The generalization of the New Momentum Theory was published formerly in Refs. 1 and 34 and later on it was published in Ref. 35 in English.
Let us assume that the fluid vein passing through the propeller disk has velocities with both axial and angular components at the infinite upstream.
Be such components at the generic station r, $V(1-w_r)$ and ω_o, being V the ship speed and w_r the effective wake at the radius r.
Let us consider a generic annular section of radius r of the actuator disk which modelizes the action that the propeller exerts on the water, with a width equal to dr.
The axial components of the propeller induced velocities are not affected by the existence of the tangential components of the water velocities at the infinite upstream of the propeller disk and so the theoretical developments corresponding to the New Momentum Theory, Ref. 9, are still valid.
The angular induced velocities, on the contrary, are specially affected by the existence of the new components of water-velocities at the infinite upstream of the propeller disk.
Let us name $\Delta\omega_1$ the angular induced velocity produced by the annular element of actuator disk of radius r and width dr at the propeller disk.
$\Delta\omega_2$ is the angular induced velocity at the infinite downstream of the propeller disk.
The relative angular velocities with respect to the actuator disk are obtained as the addition of ω_o and the angular induced velocity ($\Delta\omega_1$ at the actuator disk and $\Delta\omega_2$ at the infinite downstream).
The differential moment $M_1(r)dr$ exerted by the annular element of the propeller disk on the water passing through the propeller disk per unit of time, is:

$$M_1(r)dr_o = I_{-\infty}(r)\, dr_{-\infty}\, (\omega_o + \Delta\omega_2) - I_{\infty}(r)\, dr_{\infty}\, \omega_o \qquad \text{(A.1)}$$

$I_{-\infty}(r)$ is the inertia moment at the infinite downstream of the mass of water passing per unit of radial length through the annular element of the actuator disk per unit of time.
$I_{\infty}(r)$ is the similar water property at the infinite upstream of the propeller disk.

Due to the conservation of the kinetic moment between the actuator disk and the infinite downstream of the propeller disk, the following identity shall be accomplished:

$$I_{-\infty}(r)\, dr_{-\infty}\, (\omega_o + \Delta\omega_2) = I_o(r) dr_o\, (\omega_o + \Delta\omega_1) \tag{A.2}$$

$I_o(r)$ is the inertia moment at the actuator disk of the mass of water passing per unit of radial length through the annular element of the actuator disk per unit of time.

From (A.1) and (A.2) it is concluded:

$$M_1(r) dr_o = I_o(r) dr_o\, (\omega_o + \Delta\omega_1) - I_{\infty}(r)\, dr_{\infty}\omega_o \tag{A.3}$$

The following equalities are obvious:

$$I_{\infty}(r)/\ I_o(r) = (2\pi\ r_{\infty}^3\ dr_{\infty}\ V(1\text{-}w_r)\rho)\ /\ (2\pi r_o^3\ dr_o\ [V(1\text{-}w_r) + \Delta V_1]\rho) =$$

$$= r_{\infty}^3\ dr_{\infty}\ V(1\text{-}w_r)\ /\ (r_o^3\ dr_o\ [V(1\text{-}w_r) + \Delta V_1]) \tag{A.4}$$

By virtue of the continuity equation it can be established:

$$2\pi\ r_{\infty}\ dr_{\infty}\ V(1\text{-}w_r) = 2\pi r_o\ dr_o\ [V(1\text{-}w_r) + \Delta V_1]$$

$$dr_{\infty} = r_o\ (dr_o\ /\ r_{\infty})[V(1\text{-}w_r) + \Delta V_1]\ /\ (V(1\text{-}w_r)) \tag{A.5}$$

From (A.5) and (A.4) it is deduced:

$$I_{\infty}(r)dr_{\infty}/(I_o(r)dr_o) = (r_{\infty}^3 r_o dr_o)/(r_o^3 dr_o r_{\infty})(V(1\text{-}w_r)+\Delta V_1)/(V(1\text{-}w_r))V(1\text{-}w_r)/$$

$$(V(1\text{-}w_r)+\Delta V_1)\ I_{\infty}(r)dr_{\infty}/\ (I_o(r)dr_o) = r_{\infty}^2\ /\ r_o^2 \tag{A.6}$$

From (A.6) and (A.3) it is obtained:

$$M_1(r)dr_o = I_o(r)dr_o\ (\omega_o + \Delta\omega_1 - r_{\infty}^2\ /\ r_o^2\ \omega_o)$$

$$M_1(r)dr_o = I_o(r)dr_o\ [\Delta\omega_1 + \omega_o\ (1 - r_{\infty}^2\ /\ r_o^2)] \tag{A.7}$$

The relationship between r_o and r_{∞} corresponding to each annular blades element can be deduced by means of continuity equation,

$$\int_{rh}^{r\infty} 2\pi r_{\infty}\ dr_{\infty}\ V(1\text{-}\omega) = \int_{rh}^{ro} 2\pi r_o\ dr_o\ [V(1\text{-}\ w_r) + \Delta V_1] \tag{A.8}$$

Knowing the value of the second member of (A.8) it can be deduced the value of r_{∞}.

At the preliminary stage of the design of a propeller, it is very convenient to use the Generalized New Momentum Theory in association with the equivalent profile theory, so as a consequence of the above mentioned theory it can be established:

$$\pi (R^2 - r_h^2) [V(1-w_r) + \Delta V_1] = \pi (R_\infty^2 - r_h^2) V(1-w_r)$$

$$(R_\infty^2 - r_h^2) / (R^2 - r_h^2) = [V(1-w_r) + \Delta V_1] / (V(1-w_r)) \tag{A.9}$$

In these expressions R is the propeller radius, r_h is the propeller hub radius and R_∞ is the radius at the infinite upstream of the propeller disk and w_r is the wake fraction.
By neglecting r_h^2 in front of R^2 and R_∞^2, (A.9) is transformed in the following expression:

$$R_\infty^2 / R^2 = [V(1-w_r) + \Delta V_1]/(V(1-w_r)) \tag{A.10}$$

It can also be established:

$$r_\infty^2 / r_o^2 = [V(1-w_r) + \Delta V_1] / (V(1-w_r))$$

From (A.7) it is deduced:

$$M_1(r)dr_o = I_o(r)\, dr_o\{\Delta\omega_1 + \omega_o [1 - (V(1-w_r) + \Delta V_1) / (V(1-w_r))]\}$$

$$M_1(r)dr_o = I_o(r)\, dr_o[\Delta\omega_1 - \omega_o\, \Delta V_1 / (V(1-w_r))] \tag{A.11}$$

This expression is only valid in association with the equivalent profile theory. In a general case, (A.7) must be applied.

Next it will be assumed that (A.7) and (A.11) have the following expression:

$$M_1(r)dr_o = I_o(r)\, dr_o(\Delta\omega_1 - C\omega_o) \tag{A.12}$$

In case of (A.7), C has the following expression:

$$C = -1 + (r_\infty/r_o)^2$$

In case of (A.11), C has the following expression:

$$C = \Delta V_1 / V(1-w_r)$$

Be $M(r)dr_o$ the elemental torque that the annular element of the propeller blades receives from the tail shaft.
As the energy that z blades annular elements receive from the tail shaft when

the propeller turns with an angular velocity equal to ω must be equal to the energy that the annular element of the actuator disk gives to the water, it is possible to establish the following identity:

$$M(r)dr_o\ \omega = T(r)\ dr_o\ [V(1\text{-}w_r) + \Delta V_1\ ] + M_1(r)dr_o\ (\omega_o+\Delta\omega_1) \qquad \text{(A.13)}$$

By replacing in (A.13) the expression of dM_1 from (A.12) and doing operations, it is obtained:

$$[M(r)dr_o\omega\text{-}T(r)dr_o(V(1\text{-}w_r)+\Delta V_1)]/(I_o(r)dr_o)=(\Delta\omega_1)^2+\Delta\omega_1(\omega_o\text{-}\ C\omega_o)\text{-}C\omega_o^{\ 2} \qquad \text{(A.14)}$$

When ω_o is null, the expression of $\Delta\omega_1$ is:

$$\Delta\omega_{1o} = \{(M(r)\omega - T(r)[V(1\text{-}w_r) + \ \Delta V_1\ ]) / I_o(r)\}^{\ 1/2}$$

As it should happen this equation is equal to the equation deduced in the New Momentum Theory (Ref. 9).

Thus,(A.14) is converted to the following equation:

$$(\Delta\omega_1)^2 + \Delta\omega_1.\ \omega_o\ (1\text{-}C) - C\omega_o^{\ 2} - (\Delta\omega_{1o})^2 = 0$$

$$\Delta\omega_1 = 1/2\ \{-\ \omega_o\ (1\text{-}C) + [\omega_o^{\ 2}\,(1+C)^2 + 4(\Delta\omega_{1o})^2\ ]^{1/2}\ \} \qquad \text{(A.15)}$$

The relative angular speed of the water with respect to the actuator disk is:

$$\Delta n = \omega_o + \Delta\omega_1\ = \omega_o/2\ (1+C) + \{[\omega_o\,(1+C)\ /\ 2]^2 + (\Delta\omega_{1o})^2\ ]\}^{1/2} \qquad \text{(A.16)}$$

Once $\Delta\omega_1$ is known, to calculate $\Delta\omega_2$ it is necessary to consider that the kinetic momentum does not change between the actuator disk and the infinite downstream,

$$I_{-\infty}(r)dr_{-\infty}\ (\omega_o + \Delta\omega_2) = I_o(r)dr_o\ (\omega_o + \Delta\omega_1)$$

It is accomplished:

$$I_o(r)dr_o\ /\ (I_{-\infty}(r)dr_{-\infty}) = r_o^{\ 2}/r_{-\infty}^{\ 2}\ ;\ \Delta\omega_2 = I_o(r)dr_o\ /\ (I_{-\infty}(r)dr_{-\infty})\ (\omega_o + \Delta\omega_1) - \omega_o$$

In the case of a predesign by means of the equivalent profile theory, it is obtained:

$$\Delta\omega_2 = I_o(r)\ /\ I_{-\infty}(r)\ (\omega_o + \Delta\omega_1) - \omega_o = [V(1\text{-}w_r) + \Delta V_2]\ /\ [V(1\text{-}w_r) + \Delta V_1]$$

$$(\omega_o + \Delta\omega_1) - \omega_o$$

$$\Delta\omega_2 = \{[V(1\text{-}w_r) + \Delta V_2]\ \Delta\omega_1 + \omega_o\ (\Delta V_2 - \Delta V_1)\}\ /\ [(V(1\text{-}w_r) + \Delta V_1)] \qquad \text{(A.17)}$$

A Reanalysis of the L. Ashton and Victory Experiments

C.W.B. Grigson
MA, PhD FRINA

Offered for publication by Royal Institution of Naval Architects

Summary

The resistance tests of the L. Ashton and Victory geosims are analysed by a fairly accurate friction law. Scale effect on form factor should be a weak decrease with scale. No effect could be detected with the Victory design, possibly a small one on L. Ashton. k was found by Prohaska's method applied not only to the models but also at full scale.

The boat DC Endert jr was hydraulically smooth. The ship L. Ashton, faired, filled, and coated with aluminium paint, was hydraulically smooth up to 8 knots. Resistance at full scale is predicted consistently with different sizes of model, and with quite good accuracy.

An increase in k with scale, and considerable drag attributed to roughness when the ITTC 1957 friction line is used, are nothing but a consequence of the error in that formula in which C_{FM} is too large and C_{FS} is too small.

1. Introduction

If the 1957 ITTC correlation line

$$C_{FITTC} = 0.075/\,(\log R_n - 2)^2 \tag{1}$$

is compared with a fairly accurate planar friction law, it is found to give values of drag coefficient which are too large at model scale and too small at ship scale, Fig. 1. Estimates of the form factor k_m obtained at model scale, and of full-scale viscous drag coefficient C_{VS} are appreciably affected. This Note is a reanalysis of the L. Ashton experiments made by BSRA and Ship Division, NPL [1,2] and of the Victory experiments made by NSMB [3]. The hope was that reliable information would be obtained on the prediction of hull resistance from models, on any effects of scale on form factor, on Froude's hypothesis that the wave-making drag coefficient is invariant with Froude number, and on the roughness function determined from the observed behaviour with speed of $\Delta C(U)$ from a complete hull at full-scale. The L. Ashton experiments were themselves repeated [2] and the repeat data have been recently reanalysed by Nakatake *et al* [4] using the ITTC 1957 line.

Even a vessel with a ten-percent form factor like the slender L. Ashton, Fig. 2(a), should be analysed by form-factor methods. After removing the effects of air resistance from the measurements, one may write at full scale:

$$C_{TS} = C_{FR}(1 + k) + C_R \tag{2}$$

where

$$C_{FR} = C_{FS} + \Delta C \tag{3}$$

is the planar drag coefficient of the rough surface of the ship.

By writing C_{TS} in this way we are in fact comparing the actual drag coefficient in the three-dimensional flow with that of a two-dimensional time-mean flow along a plane having the same surface area and roughness and the same Reynolds number as the ship. If we do this then we ought on principle to use an accurate friction equation to give C_{FR}; a correlation line is not necessarily the same thing or accurate enough.

The wave-making coefficient of L. Ashton and of both sets of Victory geosims, for a wide range of speeds, was accurately given by

$$\begin{aligned} &C_R = cF_n^4, \\ &F_n < 0.25. \end{aligned} \tag{4}$$

Combining (2) and (4) at full scale according to Prohaska's method [5].

$$C_{TS} / C_{FR} - 1 = k + cF_n^4 / C_{FR}, \quad (5)$$

which is a line in coordinates of $(cF_n^4 / C_{FR}, C_{TS} / C_{FR} - 1)$.

At model scale the surfaces are smooth and C_{FR} is replaced by C_{FM}.

Fig. 1 shows the Reynolds numbers of the models and of the full scale hulls (in the Victory family, the boat DC Endert jr). At model scale the ITTC line will lead to values of k_m which are too small (consider the run-in point where $C_{TM} = C_{VM} = C_{FM}(1+k_m)$). If at full-scale the hull were hydraulically smooth, or if C_{FR} in equation (5) were calculated from the roughness function Δ_{u+} representing the actual surface, then the ITTC Line would lead to values of k at ship scale which would be too large.

In this note Prohaska's method is applied to all the models, using either an accurate law or the ITTC 57 line, and the results are compared. A full-scale prediction of the smooth drag is obtained from each model; they are compared for consistency which is good, and with the full-scale drag coefficients. The latter are predicted accurately in the case of L. Ashton at speeds up to 8

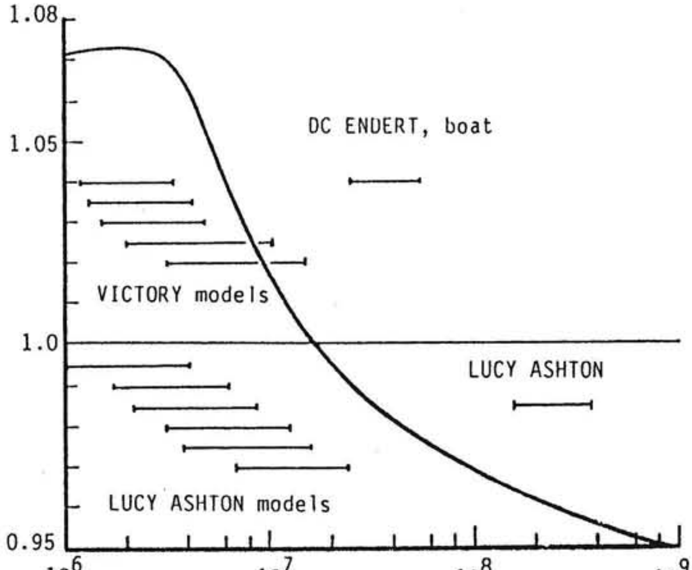

Figure 1. Ratio of the ITTC 1957 formula to an accurate, smooth planar friction law.

knots; and in the DC Endert are predicted with rather more scatter over the whole range of trials speed. In her best finish L. Ashton is hydraulically smooth up to 8 knots; and the DC Endert jr is hydraulically smooth at all speeds tested.

k is then found from the full-scale measurement of C_{TS}.

At speeds above 8 knots, L. Ashton is in an intermediate flow condition, and $\Delta C(U)$, as U varies, has a smooth maximum. The corresponding roughness function Δu_+ is deduced and is of a type frequently observed in painted surfaces.

2. Particulars of the designs

The lines of L. Ashton are rather fine and well streamlined, as may be seen in Fig. 2. The Victory dry cargo ship is fuller with a good deal of parallel mid body. The Victory geosims were tested at two different draughts and trims,

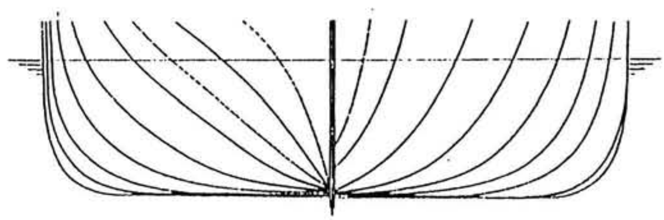

(a) LUCY ASHTON

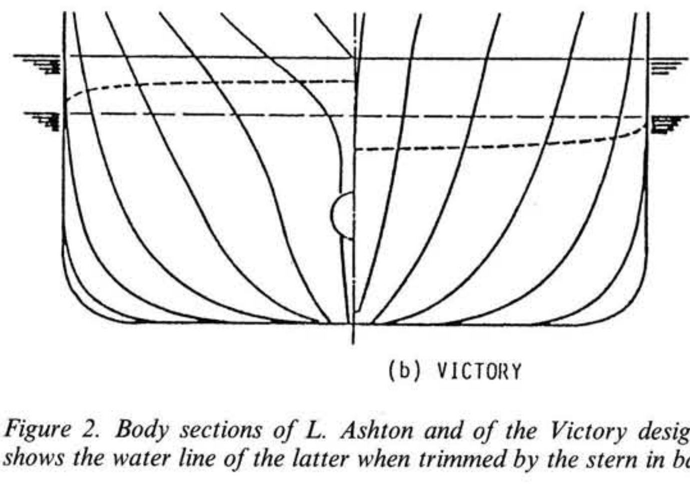

(b) VICTORY

Figure 2. Body sections of L. Ashton and of the Victory design. The dotted curve shows the water line of the latter when trimmed by the stern in ballast.

providing results from two bodies which hydrodynamically are quite different from each other. Table 1 gives data on the hull shapes.

Model measurements of the L. Ashton were made by Ship Division, NPL, and also for the largest model by AEW, Haslar. The Victory geosims were tested by NSMB. Table 2 gives model sizes and the scale ratios.

L. Ashton, propelled by four aircraft jet engines, ran trials on the Gare Loch, with four different hull finishes, aluminium paint with and without filled seams, and the rougher red-oxide paint with and without filled seams.

The trials of DC Endert were run in ideal conditions of calm in the Bay of Rijeka, in the Adriatic. DC Endert was towed by a line sufficiently long for the ship itself to be clear of the wake of the tug, as is borne out by the results below.

Table 1. *Parameters of the three hull shapes*

	L. Ashton	Endert(B)	Endert(L)
L	58.06m	22.2	22.6
B	6.42m	3.15	3.15
T_F	1.42m	0.95	1.45
T_A	1.42m	1.32	1.45
S	416.9 m^2	87.89	102.4
∇	386.5 m^3	52.64	69.53
$10S/L^2$	1.237	1.783	2.005
$10^3\nabla/L^3$	1.975	4.811	6.023
∇/LBT_{mean}	0.730	0.663	0.674
L/B	9.044	7.048	7.175
B/T_{mean}	4.52	2.78	2.17

L is waterline length

Table 2. *Size of the models*

L. Ashton		Endert(B)		Endert(L)
l_m	λ	l_m	λ	l_m
9ft	21.17	2.66m	8.334	2.71
12	15.88	3.33	6.667	3.39
16	11.91	4.44	5.0	4.52
20	9.525	5.77	3.833	5.89
24	7.921	7.40	3.0	7.53
30	6.35			

3. Treatment of the measurements

The coordinates of $X = cF_n^4 / C_{FM}$

$$Y = C_{TM} / C_{FM} - 1$$

were calculated for all the model data using the expression for the smooth planar model drag coefficient

$$C_{FM} = [0.93 + 0.1377(\log R_n - 6.3)^2 - 0.06334 (\log R_n - 6.3)^4] \cdot C_{FITTC}, \qquad (6)$$

see Ref. [6]. It is essential to draw the graphs of Y(X) and some of them are shown in Fig. 3. The graphs for the Victory series in ballast are very similar to the ones laden and are not shown.

Corresponding calculations were made for all the models using the ITTC formula (1).

For Froude numbers between 0.1 and 0.25 excellent straight lines are obtained. But at too low speeds measurements become erratic and above $F_n = .25$ the lines tend to be a broad maximum (L. Ashton) or rise steeply. One has therefore to exercise judgement about which data may be accepted as belonging to the linear sets. The data accepted are of course the same whether equation (6) or equation (1) has been used for C_{FM}. The accepted points are then analysed statistically so as to find the intercepts, k, and the slopes, c, and to get the ±95% limits of confidence on the values of k and c.

A small correction to speed has been made with the aid of Lackenby's equation

$$\Delta u/u = a/ (A-a-bu^2/g) \qquad (7)$$

where A is the cross section of the tank, a the mean cross-section of the model and b is the width of the tank at the surface of the water [1, Appendix]. When Prohaska's method is used the effect of the correction on the values of k and c is detectable on the 20ft, 24ft and 30ft sizes.

A prediction of the full-scale smooth drag coefficient

$$C_{TS\text{-smooth}} = C_{FS}(1+k_m) + cF_n^4 \qquad (8)$$

was made at speeds up to $F_n = .25$ for all the models using the accurate friction law, and also using the ITTC line, which at the full-scale is nearly the same at Schønherr's law. When the Prohaska function is accurately linear, it seems that if a slightly larger value of the intercept k_m is deduced, it is accompanied by a

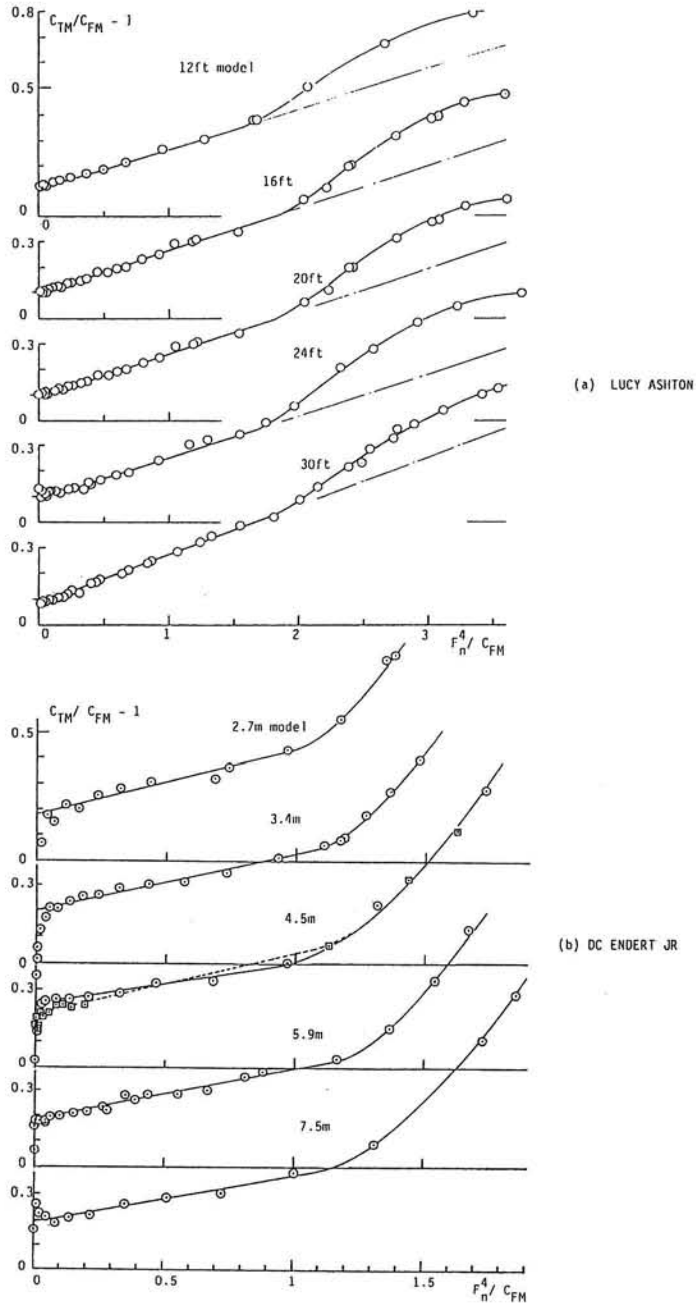

Figure 3. Prohaska functions of (a) the L. Ashton, (b) the DC Endert jr with C_{FM} from equation (6). All the data are from models fitted with trips.

slightly smaller estimate of the slope c and vice versa. With the result that the calculated full-scale smooth drag is nearly the same for all the models.

4. Results

Determination of k and c

Table 3 shows the values of form factor and slope based on equation (6); Table 4 the values found from the ITTC 1957 line.

Table 3. *Analysis by accurate friction law*

Length	k	±95%CL*	c	±95%C	L*size of sample
(a) L. Ashton					
2.743m	.128	.010	.158	.012	8
3.656	.120	.0055	.152	.0077	12
4.877	.103	.0051	.160	.0065	21
6.096	.098	.0043	.160	.0066	23
7.315	.087	.0084	.158	.013	20
9.144	.069	.0046	.185	.0056	21
58.06	.081	.046	.191	.13	5(smooth)
58.06	.074	.019	.169	.027	9 (rough)
(b) Victory, trimmed in ballast					
2.66	.229	.015	.151	.031	12
3.33	.205	.011	.160	.020	10
4.44	.217	.046	.143	.084	5
4.44	.186	.030	.191	.20	7
5.79	.216	.015	.130	.027	12
7.40	.220	.016	.149	.026	14
22.2	.219	.028	.173	.031	12
(c) Victory, laden					
2.71	.186	.021	.257	.040	8
3.39	.203	.015	.221	.027	11
4.52	.250	.014	.151	.030	8
4.52	.214	.022	.228	.042	5
5.89	.183	.012	.214	.022	14
7.53	.192	.017	.166	.035	9
22.6	.225	.025	.176	.085	20

* The ±CL are the ±95% confidence limits

Table 4. *Analysis by ITTC Line*

k	±95%CL	c	±95%CL	size of sample
(a) L. Ashton				
.048	.0098	.165	.012	8
.044	.0047	.169	.0069	12
.036	.0054	.181	.0071	21
.042	.0045	.189	.0071	23
.043	.0063	.188	.0099	20
.049	.0069	.203	.0083	21
.186	.051	.211	.136	5
(b) Victory, trimmed in ballast				
.143	.014	.153	.031	12
.120	.0098	.175	.020	10
.145	.047	.169	.090	5
.104	.027	.250	.20	8
.156	.015	.162	.028	12
.173	.017	.187	.029	14
.244	.031	.181	.033	12
(c) Victory, laden				
.103	.019	.261	.040	8
.118	.014	.234	.027	11
.172	.012	.187	.027	8
.135	.017	.254	.034	5
.126	.012	.246	.022	14
.154	.013	.211	.027	9
.262	.025	.191	.084	20

Except for the 16, 20, 24 and 30ft models of L. Ashton, the size of the sets of data accepted as belonging to the straight part of Y(X) was quite small, mostly between 8 and 12. The limits of confidence on k and c are then rather wide, a purely statistical consequence of the small size of the samples of data.

DC Endert jr was specially built for the experiments:

> 'The shell plating was finished with the greatest care. The seams of the skin which is entirely welded, are ground flush...'

Under water the hull was given: one coat of primer, anti-corrosive; then priming with motor-car primer; wet-polishing of the surface with waterproof emery paper; finally two coats of antifouling. [3, pp173-5]. Great effort was put into making the hull of the 72ft boat quite smooth.

L. Ashton was destined for the breakers when she was selected for experiment. Her steel bottom was pitted and rough to the touch; it was therefore carefully treated to make it comparable with the freshly painted hull of a new ship of that time, a time before shop-blasted and shop-primed plates became the rule in shipbuilding. Two layers of filler were applied followed by two coats of red oxide paint. The result was considered comparable with a newly finished ship. In the course of the trials a bituminous aluminium paint became available, reputed to give a smoother surface than the red oxide. The aim was now to achieve the smoothest possible surface for comparison with the predictions from smooth models. What remained of worn rivet heads was smoothed with filler and the longitudinal plate seams were faired over by a composition; the hull was then given two coats of the aluminium paint. The result was hydraulic smoothness up to 8 knots, see Fig. 4(a).

Thus Prohaska lines can be obtained from the trials of both DC Endert and L. Ashton. But in Table 3, C_{FS} and C_{FR} must be calculated from the form of the friction law accurate at full scale, see [6] and [7]. Take the averages of the results for the larger models, the 16ft to 30ft geosims of L. Ashton and the 4½ to 7½m models in the Victory series: one may compare the results with full-scale, Tables 5 and 6.

Table 5. *Accurate friction law*

	L. Ashton	Victory(B)	Victory(L)
$\bar{k}_m$	.089	.210	.211
k_s full scale	.081	.220	.225

There is no scale effect on k when the accurate friction equation is used, and a marked one according to the 1957 ITTC Line, with k larger at full-scale, in discord with what should be expected from the physics of the flow.

Table 6. *ITTC 1957 Line*

	L. Ashton	Victory(B)	Victory(L)
$\bar{k}_m$	.044	.15	.15
k_s full scale	.186	.244	.262

The wave making component

In the models of the L. Ashton the slopes c and the wave making drag coefficients are nearly the same for all but the largest model, the results of which are out of line. But at 30ft size in the NPL tank, the largest model could feel the bottom and the wave-making would have been enhanced, leading to the larger value of c in Table 3.

The value of c for the ship are not inconsistent with the model values, because of the wide limits of confidence.

As to the Victory series, within the wide limits of confidence on c, the values found are in agreement. But the scatter in the data as well as the small sample sizes preclude an accurate test. Moreover the wave-making is quite small compared with the viscous component.

Drag coefficients at full scale

Fig. 4 shows the smooth drag coefficients, equation (8), predicted from the models and based on the accurate friction relation and the corrected observations listed in [1] and [3]. The bars represent ±3% about their midpoints. If the flow is hydraulically smooth there is quite good agreement.

L. Ashton is smooth up to 8 knots and the DC Endert is hydraulically smooth at all trial speeds. In prediction from the models, and in the trials measurements, the results from the L. Ashton seem to have a higher consistency and a smaller scatter than those of the Victory series.

If the ITTC line is used all the values of k_m are smaller and C_{FS} itself is smaller so that equation (8) is a good deal less than when the accurate law is used. And so one would conclude, as the authors of [1] and [3] did, that despite all the effort to produce a really smooth skin, there was still an appreciable increase in drag due to roughness.

The points shown in Fig. 5 are the corrected trials observations. The worst finish, unfaired pits and seams and red oxide paint, is that of curve (a); curve (b) is the red oxide paint after the pits and seams had been faired; and the best finish is curve (c), bituminous aluminium paint with faired pits and seams.

The effect of the pits and sharp seams in (a) is to add $\Delta C_r = 0.13E\text{-}3$ to the drag coefficient C_{FR} at all speeds. But when the pits had been stopped and the seams faired, both (b) and (c) show hydraulic smoothness up to about 8 knots.

The full-scale smooth predictions are based on the 20ft model, with k_m and C_{FS} obtained from the accurate friction law, the dotted curves in the figure. The

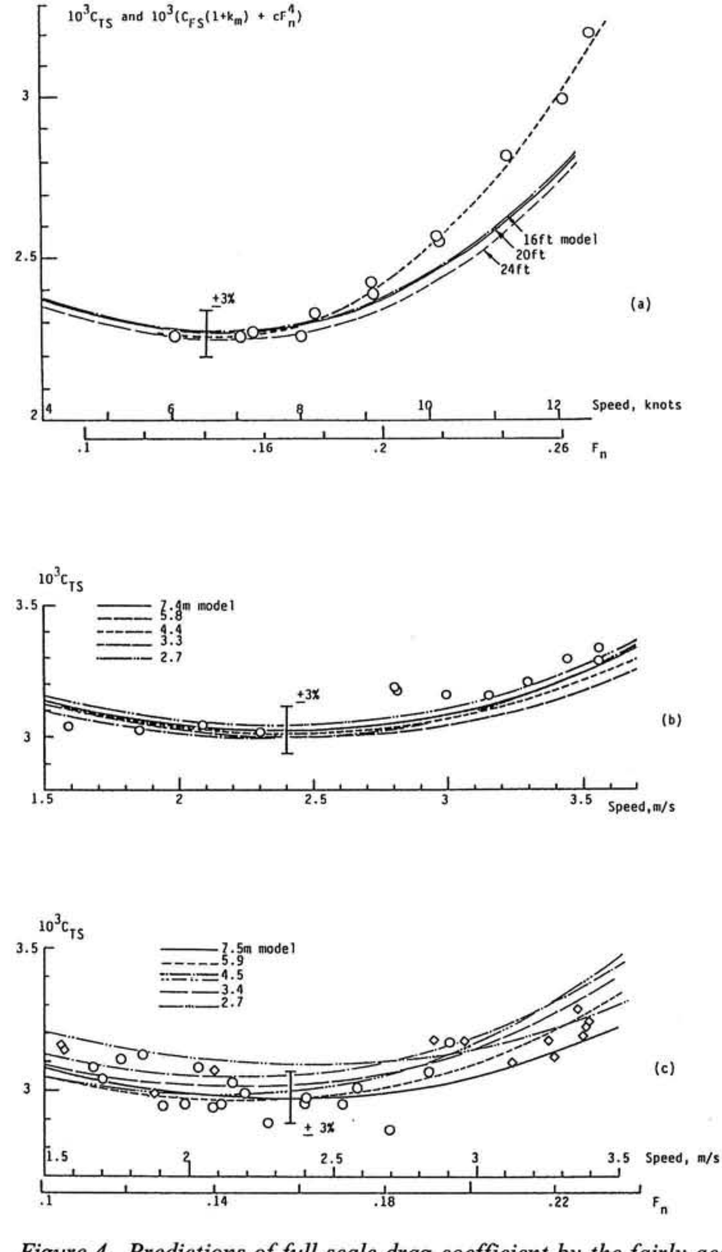

Figure 4. Predictions of full-scale drag coefficient by the fairly accurate friction law. (a) L. Ashton, (b) DC Endert trimmed in ballast, (c) DC Endert laden. L. Ashton is hydraulically smooth up to 8 knots; DC Endert at all test speeds.

difference between the trials data and the smooth predictions provides an experimental curve of ΔC as a function of speed. A roughness function, Δu_+, a function of the friction velocity u_τ, is then postulated and C_{FR} and $\Delta C(U)$ are calculated from $\Delta u_+(u_\tau)$.

By trial-and-error the roughness function is modified until $\Delta C(U)$ as calculated agrees with $\Delta C(U)$ as observed. The final curves of C_{TS} corresponding with the actual ship surfaces should then agree with the trials observations. The trial-and-error process is continued until the discrepancy between the calculated

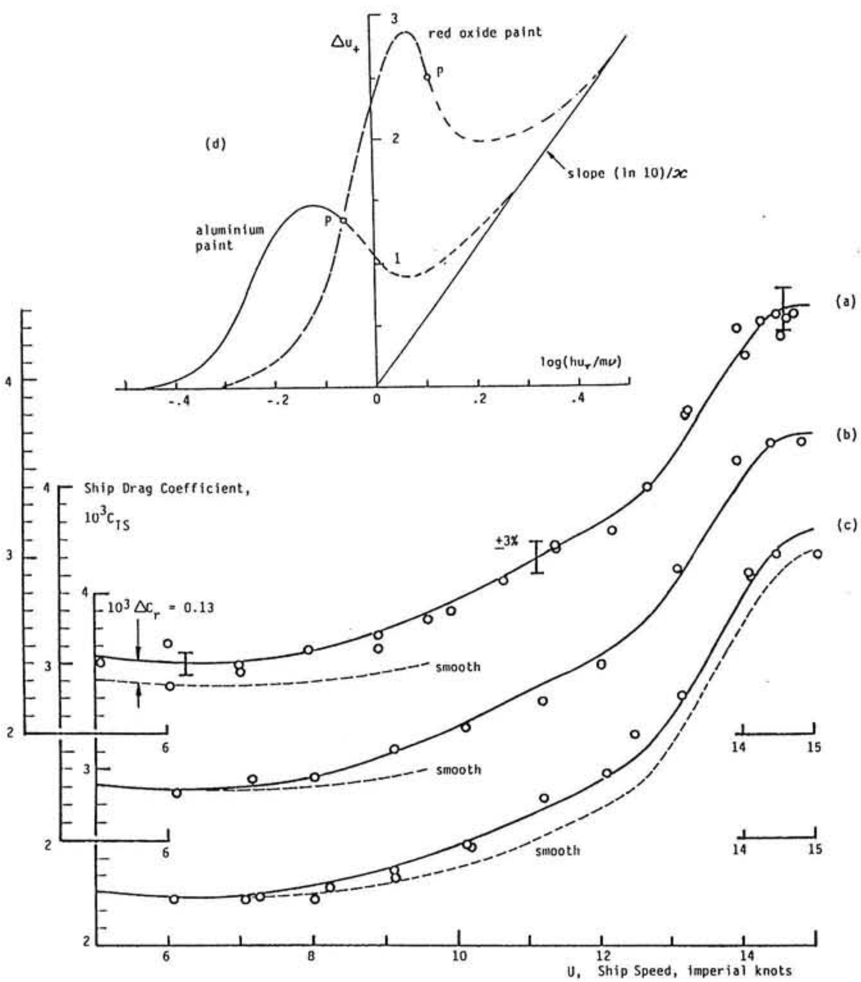

Figure 5. (a)-(c) shows curves of $C_{TS}(U)$ calculated with the aid of the roughness functions given in Fig. 5(d).

curves and the trials results is no greater than the scatter of the observations. The r.m.s. discrepancy between the curves and the observations is less than 2%.

The roughness functions of the two finishes are experimentally defined only up to the point P corresponding with 15 knots. But were the speed increased above this point, the curves must pass through a minimum and then approach the fully rough asymptote, the line of slope (ln $10/\kappa$.)

Let us compare the predictions by the accurate law and by the ITTC 1957 line in hydraulically smooth flow, Table 7. They are based on the 20ft model.

Table 7. *Predictions of the drag coefficient of L. Ashton in hydraulically smooth flow*

Speed (knots)	Predictions by		%error
	accurate law	ITTC 57	
4	2.368E-3	2.180E-3	7.9
6	2.282	2.100	8.0
8	2.297	2.135	7.0

Thus the error in k_m at model scale, and in C_{FS} at full scale, brings about considerable inaccuracy when the ITTC formula is used in calculating ship drag.

Roughness of L. Ashton

The corrected trials observations of C_{TS} are shown in Fig. 5 for the three conditions of hull roughness. The lower curve of Fig. 5(c) (dotted) is the full-scale drag coefficient calculated for a perfectly smooth shell. The upper curve is for the actual roughness and is obtained from the equation.

$$\begin{aligned} C_{TS} &= C_{FR}(1+k_m) + cF_n^4 \\ Fn &< 0.25 \end{aligned} \tag{9}$$

$$\begin{aligned} C_{TS} &= C_{FR}(1 + km) + C_{FM}(Y - k_m) \\ F_n &> 0.25. \end{aligned} \tag{10}$$

Equation (10) is used when the Prohaska function Y(X) goes non-linear, since it is more accurate to draw a smooth curve through Y(X) than to try to draw one through the steeply rising function $C_R(U)$. C_{FR} is calculated using the roughness functions for bituminous aluminium and red oxide paint respectively shown in Fig. 5(d). To predict the worst case, curve (a), a constant addition $\Delta C_r = 0.13E\text{-}3$ is added at all speeds to C_{FR}.

ΔU_+ must be found by trial and error as already explained above. The postulated roughness function is expressed as the logarithm of a cubic spline, as function of u_τ. No information about the geometry of the hull surface is involved, for ΔU_+ is a non-dimensional fluid-mechanical quantity. For justification see [8, 10 and 11] in which the full-scale planar drag of many surfaces is worked out from measurements of $\Delta C(U)$ made at model scale.

Each of the three curves of Fig. 5 is an independent comparison of predicted C_{TS} with full-scale observations.

5. Discussion and conclusions

The measurement of k

All the designs investigated here had an extensive range of speed in which the wave making drag coefficient was proportional to F_n^4. In most cases a sample of 8 measurements or more defined the intercept and slope of the Prohaska line. Yet when model basin reports of new vessels are studied, it is rare today to find as many as 8 measurements in the linear region. Moreover, it seems never to be the practice to work out the confidence limits on k.

Unfortunately, one must conclude even with a data sample as large as 8 with which to fix the line, the 95% confidence limits are rather wide, ±10% of the value of k or worse. This means that the accuracy with which k in current practice is obtained is unnecessarily poor. Many series of runs are made in developing a new design: how can an improvement really be assessed if the value of k_m is never measured accurately?

Scale effect on k

In conceiving of form factor the actual drag coefficient is compared with that of a smooth plane having the same Reynolds number as the ship. In the actual case the time-mean flow is three-dimensional; in the plane it is two dimensional (the turbulent fluctuations are of course similar and fully three-dimensional in both cases). The time-mean flow around the ship can be derived in principle partly from a set of sources and sinks, and partly from a turbulent boundary layer growing thicker from stem to stern. The potential flow scales perfectly, but the streamlines of this flow are displaced outwards by the boundary layer which does not scale perfectly. The relative displacement thickness (δ_1/L) decreases with scale; relatively the flow becomes less 'full' as scale increases. Thus a weak scale effect on k ought to be observed, *decreasing* as the scale increases.

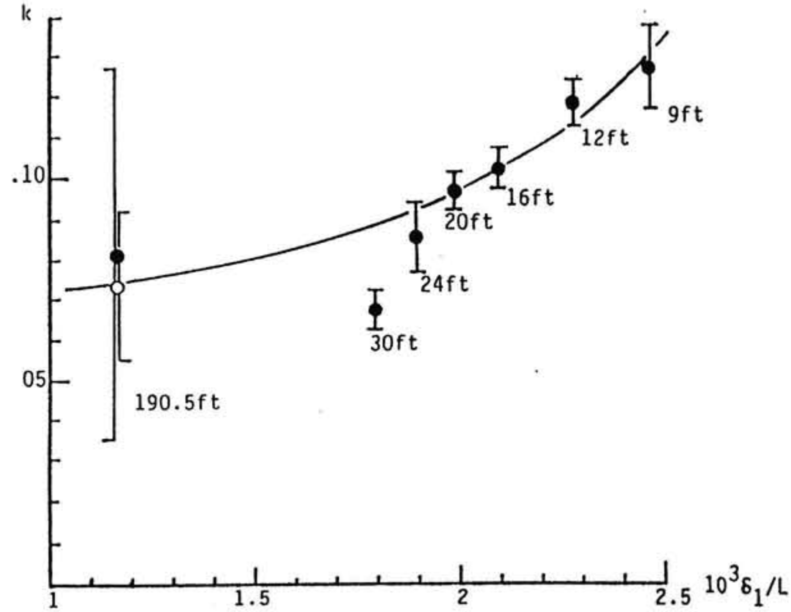

Figure 6. LUCY ASHTON: form factor v. relative displacement.

The values of δ_1 have been calculated in accord with [7] and Fig. 6 shows the measured values of k versus (δ_1/L). If the measurements on small models are included, then the graph may indicate a scale effect, which would be of the expected kind: but if the results from the larger models only are thought reliable, then any scale effect is slight.

The results from the Victory families do not show a scale effect. If it exists it is hidden in noise.

Using the ITTC rule for C_F, the Performance Committee of the 20th ITTC have tried to obtain [4] the full-scale form factor of the L. Ashton from her models. They were recut, towed naked and then were fitted with bossings; they were recut a second time and again towed, after which they were fitted with shaft brackets. It is the two series of repeat towing tests, naked with trips, which have been used by the Committee [2]. The samples of data in the later series are a good deal smaller than those done originally [1]. Table 8 compares the PPC results with those of Table 4.

The values obtained from the repeated towing tests are comparable with but more scattered than those of Table 4.

The Report of the PPC does not give sample sizes or the limits of confidence on the estimates of k_m. But those limits must be rather wider than those of Table 4 since the samples of data were smaller. One cannot from these results claim that a scale effect of k_m versus λ is observed. But what the Committee did was to put regression lines through their two sets of data and extrapolate to $\lambda = 1$, a procedure for which no justification is attempted. Their value of k_s is larger than the model values.

Table 8. *Estimates of k_m based on the ITTC line*

Tests from	[1]	[2]	[2]
λ	Table 4	Estimates of the PPC	
21.17	0.048	0.056	0.045
14.88	0.044	0.042	0.016
11.91	0.036	0.034	0.029
9.525	0.042	0.030	0.018
7.938	0.043	0.050	0.039

Roughness of the L. Ashton

Curves of $\Delta C(U)$ showing maxima were first obtained by Couch [9] in 1951. He towed friction planes in a model basin, with different kinds of paint on the planes. The corresponding hydrodynamic roughness functions were worked out long afterwards [8, 10 and 11] and also have maxima.

The roughness functions Δu_+ (u_τ) of many irregular surfaces have humps or even true maxima like those of Fig. 5(d). The common geometric property seems to be arrays of elements of roughness in which the ratio of the average spacing, $\bar{l}$, to the average height, $\bar{h}$, is quite large and there is not much spread in the distributions of $\bar{l}$ and $\bar{h}$. Examples also occur which are quite regular: surfaces spark-machined to represent sinusoidal waves in three dimensions, arrays of hemispheres or of cones; or painted surfaces wavy in two dimensions. See [8 and 11].

However, the physical explanation of the maxima in Δu_+ is not understood. Therefore examples which are the aggregate effect of the flow near the skin of actual full-scale hulls, are very interesting.

Accuracy of prediction of the drag coefficients

When the hull is hydraulically smooth the present friction law gives quite accurate predictions of C_{TS} for all three shapes of hull. Furthermore in L. Ashton at higher speeds, the roughness function deduced is of a quite normal type. But using the Schønherr line and ignoring form factor, Lackenby found a strange curve for $\Delta C(U)$, having one weak hump and one quite sharp maximum, which would imply a loss function Δu_+ of a type never yet observed.

Prediction using the ITTC 1957 rule, nearly the same as Schønherr's equation at ship scale, underestimates C_{TS} between 5 and 10% This is true of the DC Endert both laden and in ballast as well as L. Ashton. Consideration of Fig. 1 makes clear that this will happen quite generally.

Need for an accurate friction equation

The results of the paper depend on the claim that the friction law used is indeed accurate. The claim is based on the agreement between the predicted skin friction and several hundred observations of c_f made in several laboratories using floating-element balances in flows which were at constant pressure and time-mean two dimensional. Between $1.5E6 < R_n < 7E8$ the predicted curve of c_f lies satisfactorily in the midst of the observations. The theory which gives c_f is then applied to calculate C_F. Measurement of C_F itself is not practicable with sufficient accuracy because of edge effects.

Unfortunately measurements of c_f become rare when the Reynolds numbers are very large. However there is at NACA Langley a subsonic wind tunnel in which flat plates can be tested to $R_n = 1E9$. Experiments like the extremely thorough and careful measurements of Smith and Walker [12] could there be done at the Reynolds numbers of ship scale.

Conclusions

1. When models of length 5m or more are used in predicting the full-scale drag of a ship, agreement with the prediction can be within 1%. This accuracy seems to have been attained in the experiments with L. Ashton, provided a fairly accurate friction law is used to find form factor and the full scale viscous drag.

2. If any scale effect of form factor occurs it is very small. And if anything, k is smaller at full scale than with the model.

3. Use of the ITTC 1957 line leads to errors of 5-10% in predicting C_{VS}, which will be underpredicted. This is because at model scale the estimates of k_m, and at ship scale the estimates of C_{FS}, are too small.

Acknowledgement

Mr David Bailey is thanked very much for discussions about form factor and the L. Ashton which persuaded the author to try the present friction law on families of geosims.

References

[1] Conn *et al*: 'BSRA Experiments with the L. Ashton II, Trans INA, Vol 95, pp350-436, 1953.
[2] Lackenby: 'BSRA Experiments with the L. Ashton III', Trans INA, Vol 97, pp109-166, 1955.
[3] Van Lammeren *et al*: 'Scale effect experiments on Victory ships and models' Pt I, Trans INA, Vol 95, pp167-220, 1953.
[4] Nakatake *et al*: 'Report of the PPC to the 20th ITTC, 1993.
[5] Prohaska: A simple method for evaluation of the form factor, Proc ITTC, 1966.
[6] Grigson: 'An accurate smoothfriction line for use in performance prediction', Trans RINA Vol 135, pp149-162, 1993.
[7] Grigson: 'An accurate turbulent velocity profile for use at ship scale', J. Ship Res., Vol 33, pp162-168, 1989.
[8] Grigson: 'Full-scale drag of actual ship surfaces....', J. Ship Res., Vol 31, pp189-206, 1987.
[9] Couch: 'Friction plane resistance tests on antifouling paints', DTMB Report 789, 1951.
[10] Grigson: 'The drag at ship scale of planes having any quality of roughness', J. Ship Res. Vol 29, pp94-104, 1985.
[11] Grigson: 'Drag losses of new ships caused by hull finish', J. Ship Res. Vol 36, pp182-196, 1992.
[12] Smith and Walker: 'Skin friction experiments in incompressible flow', NACA R-26, 1959.

Notation

B	beam
C_F	smooth planar drag coefficient, C_{FS} ship, C_{FM} model
C_{FITTC}	C_F by the 1957 ITTC formula
C_{FR}	rough planar drag coefficient
C_R	residuary drag coeff. equals $C_T - C_F(1 + k)$
C_T	total drag coefficient
C_V	viscous drag coefficient
ΔC	$C_{FR} - C_{FS}$
ΔC_r	increase in ΔC due to pits and seams
k	form factor

$\bar{l}$	mean spacing of elements of roughness
L, l_m	length on the waterline
S,s	hull wetted surface, ship or model
T	draught, T_F forward, T_A aft
X,Y,c	coordinates and slope of Prohaska line
U,u	speed, ship or model
Δu	increment in u due to blockage
Δu_+	hydrodynamic roughness function
u_τ	friction velocity
δ_1	displacement thickness of boundary layer
λ	scale factor
κ	von Karman's constant
∇	volume of displacement

Suffices: S,s quantities at ship scale, M,m model.

Written discussion

Mr R J Stenson: Dr Grigson has written a detailed reanalysis of the L. Ashton and Victory experiments using his "fairly accurate planar friction line" which he introduced in the Transactions of RINA, 1993. In that instance the new friction line was applied to calculate the form factors of five full ships and the values attained were higher than those obtained using the ITTC57 correlation line. Similar results are obtained in the current contribu-tion. A statement is made that "there is no scale effect on k when the accurate friction equation is used and a marked one according to the 1957 ITTC line, with k larger at full scale, in discord with what should be expected from the physics of flow." It would seem that Table 3 in the case of L. Ashton, and Figure 6, of Dr Grigson's current paper would tend to contradict this statement.

With regard to the comments by Dr Grigson about the analysis carried out by the Performance Committee of the 20th ITTC, he is probably correct about the procedure used to determine k_s values. However, from a practical point of view, this analysis showed the ship prediction obtained using this full scale form factor to have better agreement with full scale results. In the 1993 paper use of the new friction line showed increases in RPM and P_D compared with estimates based on the ITTC line. It would be interesting to know the results of ship performance predictions using the results in the current paper. Also regarding sample size in the 20th PPC analysis, if the sample size was not given in the report as Dr Grigson rightly points out, how can he conclude that the limits of confidence on estimates of k_m must be rather wider than those in his Table 4? It is agreed, however, that increased sample size would help to increase our confidence in the accuracy of estimating k_m.

As is often the case in reanalysis, a number of gremlins have appeared in the paper. In Table 2 the scale ratio of 7.921 should be 7.937 for L. Ashton. Neither l_m of 2.66 or l_m of 2.71 results in a scale ratio of 8.334 for Endert, and l_m of 5.77m should be 5.79m based on a scale ratio of 3.833. In Table 8, the scale ratio of 14.88 should be 15.88 and 7.938 should read 7.921. On page 7 in the version this reviewer received there are some missing words in the first sentence under "Scale effect on k". This reviewer found it somewhat difficult to compare tables and figures that fluctuated between English and metric measurements, especially when comparing the same series of experiments as in the L. Ashton. I am also curious as to the definition of an Imperial Knot as shown in Figure 5. Other than these minor difficulties, I found the paper to be most interesting and I congratulate Dr Grigson on yet another meaningful contribution to the literature regarding form factor.

Dr A M Kracht: The author has carefully analysed the results of model and full scale tests with L. Ashton hull form with respect to form factor and scale effect. For a serious discussion of scale effects, results of accurate and corresponding measurements at model and full scale are necessary. But because such tests are expensive they have been executed very seldom. Therefore, the L. Ashton tests are like bench-mark tests which have been reanalysed very often.

The author states that in the case of hydraulically smooth surfaces and based on his "accurate planar friction law" (equation 6) the form factor of k is independent of model scale if the model length is greater than 5.0m. This may be desirable but is not reasonable because the form factor depends on hull form geometry and on the relative boundary layer thickness which is a function of scale as demonstrated by Fig. 6.

A question is the general applicability of the author's friction law for other hull forms. The results of an analysis of the rearranged equation 6

$$C_{FM} / C_{ITTC} = 0.93 + (0.1377 - 0.06334x^2)x^2,$$

where

$$x = \log R_n - 6.3,$$

is summarised in Table 9.

Maxima, minima and zero crossings are marked. The table demonstrates that the author's friction law yields reasonable C_F- values only in the range of $10^5 < R_n < 6.10^7$ and, therefore, it is not adequate for high-block hull forms.

Table 9

R_n	$\log R_n$	C_{FM}/C_{FITTC}	Remarks
10^4	4.000	–0.113	
	4.048	0.000	zero passage
10^5	5.000	0.982	
	5.132	1.000	
	5.257	1.005	maximum
	5.400	1.000	
10^6	6.000	0.942	
	6.300	0.930	minimum
10^7	7.000	0.982	
	7.200	1.000	
	7.343	1.005	maximum
	7.468	1.000	
10^8	8.000	0.800	
	8.552	0.000	zero passage
10^9	9.000	–1.400	

Mr H Vreedenburgh, MSc (Fellow): Dr Grigson has produced a very interesting paper and it is with considerable diffidence that I venture to query his equation (6) purporting to give the smooth planar model drag coefficients. I compared these coefficients with the flat plate friction coefficients according to Lap-Troost for values of log R_n from 6.0 to 9.0 and also calculated the ratios of the values according to equation (6) with the ITTC values.

The results as given in Table 10 make me wonder if equation (6) as printed in the paper is correct and I should be obliged if Dr Grigson would clarify this point.

Mr D Bailey (Fellow): Dr Grigson has given us an interesting paper with interesting conclusions concerning form factor. Results from geosim models provide an excellent opportunity to examine scale effect on form factor but ideally a wider range of data than that used in this paper is desirable, provided of course that enough measurements at low (tripped) speeds are available.

The great debate on friction lines that reached its height some 30 years ago included in 1963 an extensive analysis of geosim data by Hughes [13] which has relevance to the current paper. Hughes took 40 sets of geosim results obtained from different towing tanks. These covered a wide range of ship types including L. Ashton and Victory, the data now examined by Dr Grigson. However, in recognising the almost certain effects of tank blockage on larger models, Hughes who had earlier derived a blockage corrector, applied it to all 40 models before starting on his own analysis. In addition he repeated the NPL tests on the larger L. Ashton model in the newly built tank at Feltham the extreme dimensions of which precluded blockage. Hughes' paper makes inte-

Table 10

$LogR_n$	10^3C_F ITTC	10^3C_F Eqn(6)	10^3C_F Lap-Troost	(6)/ ITTC57
6.0	4.687	4.415	3.590	0.942
6.2	4.252	3.960	3.301	0.931
6.4	3.874	3.608	3.042	0.931
6.6	3.544	3.338	2.813	0.942
6.8	3.255	3.127	2.611	0.960
7.0	3.000	2.947	2.429	0.982
7.2	3.774	2.774	2.263	1.000
7.4	2.572	2.582	2.115	1.004
7.6	2.392	2.348	1.980	0.982
7.8	2.229	2.049	1.857	0.919
8.0	2.083	1.664	1.745	0.602
8.2	1.951	1.174	1.642	0.602
8.4	1.831	0.559	1.547	0.305
8.6	1.722	–0.196	1.462	–0.114
8.8	1.622	–1.109	1.381	–0.684
9.0	1.531	–2.192	1.309	–1.432

resting reading today, particularly as it culminated in the definition of his own proposed friction line and a recommended determination of form factor, the latter sadly forgotten by later workers.

I do not know whether Dr Grigson would conclude differently if he had (a) been able to enlarge his analysis to include other geosim data and (b) whether the use of refined data as used by Hughes would influence results but I would be interested to have his views.

Reference

[13] Hughes: 'Correlation of model resistance and application to ship', Trans RINA 1963.

Mr G E Gadd, MA, PhD (Member): In the first part of Section 5 the author makes a plea for model testing establishments to make more use of Prohaska's method to define form factor. Unfortunately modern merchant ships very often have large bulbous bows, and this makes it much more difficult to determine form factor in this way. This is because at low speed the bulb often sucks down the flow at the bow, causing local wave breaking, with adverse effects on resistance. At higher speeds the water surface height increases at the bow, leading to a smoother flow over the bulb, but it is then difficult to assess whether or not there is a range of speeds where wave resistance can be assumed to vary as the fourth power of Froude number.

Mr J Holtrop: Dr Grigson is to be commended for this paper on ship resistance. By turning to the results of classical geosim research, Dr Grigson shows how the consistency of the resistance is affected by the extrapolation line and the form factor concept.

On most points I feel inclined to corroborate Dr Grigson. In particular I share his concern about the accuracy of the form factor as it is determined from low-speed resistance experiments. Hence, I fear that the debate on scale effects on 1+ k, if any, will continue for a considerable period of time, despite Dr Grigson's attempts to resolve this issue. Another point of concern is the slope of the ITTC-1957 line at model Reynolds numbers, rendering it less suitable as an extrapolator of viscous resistance.

As to this second point I feel pleased to report some supporting preliminary conclusions of a statistical study on a large sample of 325 random model-ship correlations of both single and twin-screw ships of all types and sizes. In this study the level and scatter of the correlation coefficients for power and propeller rotative speed were examined when a number of changes were made in the extrapolation procedure. Challenged by the discussions of two other RINA papers by Dr Grigson of recent date, some of these changes consisted of substituting the ITTC-1957 line by either the Schönherr mean line or by Dr Grigson's smooth planar friction law. In doing this, the form factors were adjusted to the changed level of the friction coefficent by other extrapolation parameters as the model-to-ship correlation allowance and the wake scaling were kept the same.

It appeared that this substitution rendered a slight but distinct reduction of the scatter of the power correlation coefficient, thus furnishing evidence in an indirect manner as to the supposed insufficiency of the ITTC-1957 line. As expected, the substitution of the ITTC-1957 line was accompanied by a change of the average level of the power correlation coefficient Cp, Table 11.

Table 11

	Sample size N = 325 data		
	ITTC1957	Schönherr	Grigson
Average Cp	1.012	1.004	0.986
%standard deviation	7.5	7.3	7.3

It is noted that the relatively large scatter is probably due to mixing up the sub-samples of twin and single screw ships.

Mr D G M Watson, BSc (Fellow): Whilst the 1957 ITTC correlation was just about acceptable when it was used as a correlation line it clearly became a nonsense when form factors were introduced in 1978 and the 1957 line was treated as though it was a planar friction line.

By that time one was starting to wish that testing tanks would revert to Froude even if this meant the use of ship-model correlation factors which, with values less than unity, postulated the absurdity of ships smoother than models.

From significantly reducing the proportion of frictional to total resistance (from Froude) using the 57 ITTC line, the 1978 introduction of (1 + k) took the viscous resistance back to near the proportion it used to have in a Froude calculation.

The next thing to happen was a change in the approximate formula for k which saw this factor starting to have a different value for ship and model. Whilst this may have enabled testing tanks to produce better power estimates it left ship designers with a very low confidence in power estimates made pre model testing – and it must be remembered that in most cases it is the power calculation at this stage which determines what machinery is fitted and therefore whether the specified speed is attained.

With this background I was readily converted to the need for an accurate friction line and think that the industry owes Christopher Grigson a considerable debt for all the work he has put into developing this and the many excellent papers he has written on this and related subjects.

This new paper which applies the line to some of the best available data provides further proof of the correctness of the Grigson line and – joy of joys – gets rid of the absurd anomaly of different k values for ship and model.

ALL CHANGE TO THE GRIGSON LINE.

Author's reply

Mr Stenson is thanked very warmly for finding the author's mistakes in Table 2 and 8. The missing word in Section 5 was 'length'. For predictions of performance using the present friction equation, may I refer him to Ref. 14. The confidence limits in the 20th PPC analysis are dependent on the sample sizes given in [2] which are smaller than in [1]. The imperial knot is 6080ft/hr, the international 1852 metres/hr, respectively .51477 and .51444 m/s. American as well as British tanks used always to work in imperial knots, and perhaps some still do.

Dr Kracht and Mr Vreedenburgh quite rightly doubt equation (6). However, section 3 does say that the equation is applied at *model* scale and 'see Ref. 6': in which the origin of that formula and the restrictions on its use are explained. Ref. 6 derives an algorithm from a modern version of von Karman's theory of turbulent time-mean two-dimensional flow on a plane. Modern data – Patel's – must be used for the constants of the boundary layer and the wake term of the velocity profile must be made to vary correctly with R_n when Reynolds numbers are below 45E6. But all the data for the calculation are hard, got from measurement, and there are no adjustable factors anywhere to 'tune' the theory in order to obtain agreement. This is an important point. Predicted values of c_f, the skin friction coefficient, are within about ±1% of the centroid of several hundred observations. Having given c_f, the theory at once gives the drag coefficient, which is unsuitable for direct comparison with the drag of planes because there is no accurate way to correct for edge effects.

It is preferable to use the algorithm to get C_F but for those who do not wish to do so, two polynomial approximations are stated [6, eqns 21 and 22]. The first of these is equation (6) above and applies to models: it should not be used outside the range of validity, $1.5E6 < R_n < 2E7$.

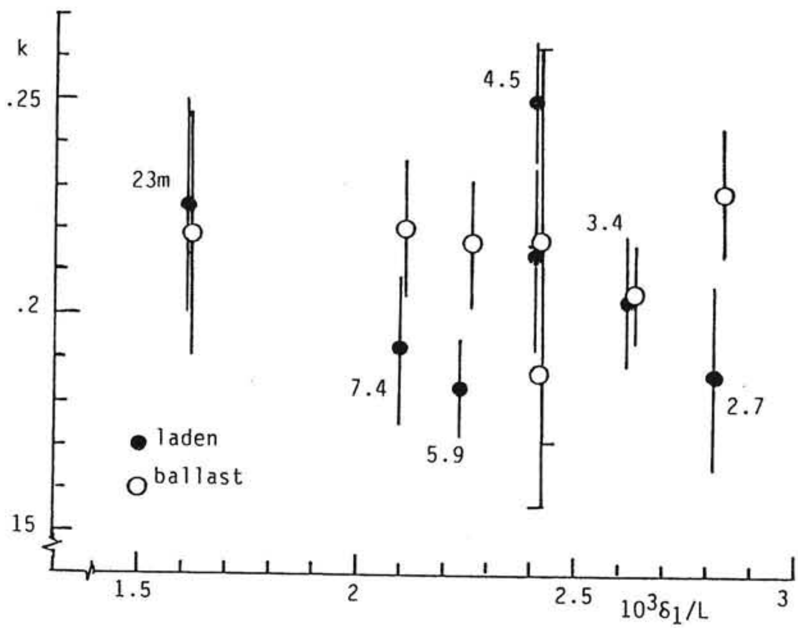

Figure 7. k versus relative displacement thickness for VICTORY series

Mr Stenson and Dr Kracht think that the results for L. Ashton, Fig. 6 and Table 3, mean that k varies with scale. But the errors in finding k must be considered, particularly those of the full scale in hydraulically smooth flow. Table 12 shows the spreads in the full-scale estimates of k.

Model values bracket these limits. Remember, also, that these confidence limits are those associated with random errors and tell nothing about systematic ones. Results for the two Victory shapes are shown in Fig. 7, with no suggestion of a scale effect. The curve in Fig. 6 seems to be evidence of systematic error with decrease of model size. Because theory, see below, shows that C_V scales with C_F.

Table 12

Spread in k at full scale in hydraulically smooth flow

	Lower CL	expected value	upper CL
L. Ashton	.035	.081	.127
Endert (B)	.191	.219	.247
Endert (L)	.200	.225	.250

In reply to Mr Bailey: (a) no, (b) rather doubtful. In [13] Hughes plots C_{TM} versus $(1/.075)C_{FITTC}$, keeping Fn constant. Variation of $(1/.075)C_{FITTC}$ is brought about by changing the size of the model. If the ITTC formula were accurate, then since $C_{TM} = C_{FM}(1 + k) + C_w$ and C_w is fixed at a constant speed, the graph would be a straight line of slope dependent on $(1 + k)$. Each new speed would lead to a new line, all having this same slope. Some of Hughes' data are from untripped models; some have excessive scatter; but some – TINA ONASSIS and SIMON BOLIVAR for example, fall on parallel lines and are solid evidence (i) that $C_T = C_V(R_n) + C_R(F_n)$, and (ii) that C_V scales with C_F.

Hughes gave the equation

$$C_F = 0.0620 / (\log R_n - 2.18)^2$$

on page 187 of [13]. I think it is in serious disagreement with experiment in planar turbulent flow.

Dr Gadd makes a practical objection to Prohaska's method. Addition of a bulb to a parent form must certainly modify the waves at the bow, since it is the purpose of the bulb to reduce wave-drag. If successful $(C_T - C_F)/C_F$ must be appreciably diminished and the scatter of Prohaska's function will be in-

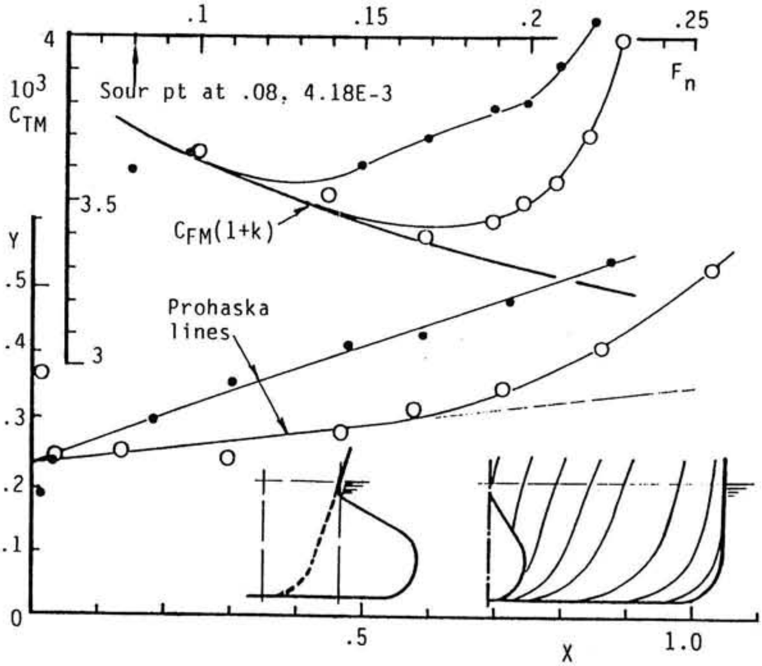

Figure 8. Determination of form factor. • for parent form, o with bulb added.

creased. The form factor ought to be close to that of the parent body. Tests to determine k should be done at speeds when the waves are small. A chief reason for the difficulty in finding k from the results of commercial towing tests is surely that the model basins run the tests at speeds corresponding with the service and maximum speeds of the ship, speeds often beyond the linear part of the Prohaska curve.

Fig. 8 shows towing tests of a merchantman displacing 92000m^3, C_B = .75, service speed 20.5 knots, F_n = 0.2 approximately, results of the parent form, and with a large bulb added. Although commercial tests, these were run over a wide range of speed. More runs should have been made near F_n = 0.1, but there is nothing to suggest any difficulty in the measurement of k with the large bulb. Note that the values of k without and with the bulb are the same.

Mr Holtrop's latest correlations are disappointing. Not only because use of the author's friction equation produces no improvement, but because the addition of 100 new trials measurements has had no effect on the scatter of Cp. The 325 data were, I believe, all from trials run by MARIN and correlated with model tests done by MARIN, that is, by one of the most outstanding ship test establishments. Thus the standard errors in Cp which Mr Holtrop reports are very discouraging; and mean that the 95% confidence limits on the prediction of power are plus-or-minus 14%.

However, there are serious errors of principle in the methods generally used to predict performance from models. Six of them are listed in [14]. Each kind of error will vary in importance from design to design, so that their effects are just like random errors. One of the six is inaccuracy in C_F. Removing just one of these errors may have little effect. What is needed is that they should all be eliminated or reduced by changes in method of prediction, as demonstrated in [14].

Mr Watson's support for the author's friction equations is very welcome, though a change of track by the model basins is improbable, as witness the many models analysed using traditional 'two dimensional methods of extrapolation' even though an important part of the measured resistance is then scaled incorrectly.

I would like to emphasise the difference between 'two-dimensional extrapolation' and the method of the paper. The latter is dictated by laws of fluid physics all believed to be correct to a good approximation, even though it may not be possible to derive them from the Navier-Stokes equations.

(1) By Froude, $C_T = C_V(R_n) + C_R(F_n)$.

(2) By von Karman, the equations of the planar turbulent boundary layer are solved.

(3) By Young, C_V scales with C_F.

(4) By Michell, when wave-making is small, $C_R = F_n^4$.

Prohaska's method follows, but to determine k with accuracy:

> Model trim and scaled displacement must be the same as the ship throughout the speed range of the tests; many runs at low F_n must be made; and the model must have a well-designed trip (If the drag of the trip is too high, or if there remains laminar flow abaft the trip, the fact shows conspicuously on the Prohaska graph).

Having obtained k at slow speed, model tests must continue up to maximum speed to give C_R, from

$$C_R = C_{TM} - C_{FM}(1 + k)$$

At full scale in hydraulically smooth flow, at the same F_n as the model,
$C_{TSsmooth} = C_{FS}(1 + k) + C_R$

The only way that the drag added by roughness can be included is to find a representative loss function by the method of Lewkowicz and Musker [15] and from the Δu_+ of the actual hull surfaces, to calculate the rough planar drag coefficient.

In 'Principles of Naval Architecture' [6, Vol 2, pp57-62] the form factor method is presented as though it were an extrapolation technique comparable with two-dimensional extrapolation. But it is different in principle because the viscous part of the drag is correctly treated. The fact matters, because when the viscous part is dealt with correctly, it turns out that the proportion of wave-making drag on most merchant ships is a good deal smaller than had been supposed.

The method used in the paper *ought* to give fairly accurate estimates in hydraulically smooth flow without the use of any correlation factor. At all test speeds with the two shapes of Endert, and at speeds below 8 knots with L. Ashton, it does so, fig. 4. The accuracy, about ± 3%, is as good as is claimed with aircraft [17, Table IV, p 127]. These results are the only ones at present available, simply because full-scale towing trials are extremely rare. The author also tried to predict the full-scale drag of YUDACHI, WRANGEL, ALDEBARAN and PENELOPE [18-21]. He failed because of roughness and in the last two ships, because of high appendage drag.

In 1939 Young showed [22, 23 pp198-208] that C_V scales with C_F, so that there is no scale effect on k_o, a fact long accepted by aerodynamicists [17, p140]. But k_o is not identical with k, and Young's proof applied to streamline axisymmetric bodies.

If R_t is the sum of the tangential and R_p the sum of the normal forces resolved along the axis of motion, then the drag $R = R_t + R_p = R_t(1 + k_o)$, making $k_o = R_p/R_t$. But $k = (C_V/C_F - 1)$ in the limit as wave making goes to the negligible.

Compare the streamline axisymmetrical body with a plane representing a hull, the body, the plane and the hull all having the same drag, length and wetted surface area. One finds

$$k = k_o + (1 + k_o)\, \Delta R/R_f, \tag{11}$$

where ΔR is the increase in the frictional resistance of the curved body compared with the plane of resistance $R_f(1 + k)$. ΔR and R_f are both smooth frictional forces of the same nature. It is most improbable that ΔR could scale in a way appreciably different from R_f. Moreover the second term in (11) is small compared with k_o. So, the scaling laws of k and k_o will be the same.

Young's result will also apply to a half-body with semi-circular sections. The scaling behaviour cannot change if the sections were changed to semi-ellipses, or even (in the absence of wavemaking) by the body sections of a streamline hull. Thus the fact that C_V scales with C_F, proved by Young for an axisymmetrical body, must also hold for a ship.

The author thanks Mr Bailey, Dr Gadd, Mr Holtrop, Dr Kracht, Mr Stenson, Mr Vreedenburgh and Mr Watson. He is very grateful for their contributions to the paper.

References

[14] Grigson: 'An improved method of predicting the performance of merchant ships from models', Trans RINA, Vol 137, 1995.
[15] Lewkowicz and Musker: Papers 9 and 10, Proc. International Symposium on the viscous resistance of ships, SSPA, Gothenburg, 1978.
[16] Lewis, Ed: 'Principles of Naval Architecture', 3 vols, SNAME, Jersey City, 1988.
[17] Covert, Ed: 'Thrust and Drag, its prediction and verification', AIAA, New York, 1985.
[18] Hiraga, Admiral: 'Experimental investigations on the resistance of long planks and ships', Trans INA, Vol 76, 1934.
[19] Nordstrøm: 'Full-scale tests with WRANGEL and comparative model tests', SSPA Pub. No. 27, Gothenburg, 1953.
[20] Retali and Bindel: 'Étude á la mer de la résistance á la marche et de la propulsion', Bulletin de L'ATMA, No. 54, 1955.
[21] Canham: 'Resistance, propulsion and wake tests with HMS PENELOPE', Trans RINA, Vol 116, 1974.
[22] Young: 'Calculation of total and skin friction drag of bodies of revolution at zero incidence', ARC R&M 1874, 1939.
[23] Young: 'Boundary Layers', BSP, London, 1989.

Noise Prediction and Correlation with Full Scale Measurements in Ships

C.G. Holland, BSc, CEng, MIMarE
Lloyd's Register

S.F. Wong, BEng, CEng, MIMarE
Lloyd's Register

Offered for publication by the Institute of Marine Engineers

Summary

The demand for a comfortable environment on cruise vessels and the stringent habitability standards recommended by authorities to protect shipboard personnel against hearing damage prompt the necessity of an accurate noise prediction at the ship design stage. Whilst it is recognised that noise prediction is a continuous research and development activity in many institutes and universities throughout the world, the intention of this paper is to discuss noise prediction techniques in a general manner and to describe the approach to noise prediction developed and used by Lloyd's Register (LR). There is no guarantee of absolute accuracy in any noise prediction technique. This paper first briefly outlines the problems and factors affecting the degree of accuracy. The development of LR's own noise prediction programme is then addressed. In order to demonstrate the correlation between predicted and measured results, two practical cases, which have been completed recently on a modern containership and a luxury yacht, are discussed. The final section of the paper is devoted to a discussion of how future developments may improve the accuracy of noise prediction.

Introduction

Shipboard acoustics have been transformed in recent years due to fundamental changes in ship design. In the 1950s and 1960s shipping was dominated by general cargo vessels featuring an accommodation block situated amidships and this design resulted in low levels of propeller generated noise in the accommodation. The general adoption of steam propulsion plant, rather than diesel engines, provided a relatively quiet working environment and also was beneficial in terms of accommodation noise. In addition, ships were not generally equipped with heating, ventilation and air conditioning (HVAC) systems. Modern cargo vessels normally feature diesel engine propulsion, an aft accommodation block and comprehensive HVAC systems. Although these design changes do not necessarily mean that the living quarters in modern ships are more noisy, it is clear that ambient noise levels are more likely to be affected by the propeller, diesel engine and HVAC system noise sources. The demands in some ship types for high installed power and for hulls featuring minimum scantlings have also resulted in more onerous design conditions for the noise control engineer.

The widespread awareness of noise-related health problems and the need to protect personnel against hearing damage have prompted the introduction of stringent habitability standards. Table I presents the noise levels recommended by the International Maritime Organisation (IMO) and the UK Department of Transport, now the Marine Safety Agency.[1,2] Noise levels specified for recent

Table 1. *Recommended noise levels for specified areas*

Location	Noise levels onboard ships IMO A. 468 (XII) dB(A)	Code of practice for noise levels in ships UK Depent of Transport dB(A)	Noise levels specified for recent passengerships dB(A)
Passenger cabins	–	–	40-55
Public area	–	–	55-60
Shopping areas	–	–	60-70
Crew cabins	60	60	55-60
Crew mess room	65	65	60-65
Hospital	60	60	55-60
Conference room	–	65	50-60
Offices	65	65	55-60
Recreation rooms	65	65	60-65
Open recreation area	75	75	65-70
Galleys	75	75	65-75
Lifeboat sations	–	–	65-70
Wheelhouse	65	65	60-65
Radio room	60	60	55-60
Engine control room	75	75	70-75
Workshop	85	85	80-85

passenger ships are included for comparison. Although the application of the standards to passenger accommodation is not a legislative requirement, they are often used as guidelines during negotiations between shipowners and shipbuilders.

In recent years the cruise industry has enjoyed increased popularity and this is reflected by the level of newbuilding orders. Passengers who join cruise ships for vacation purposes are, to a large extent, conditioned to expect noise levels similar to those of hotels ashore or of their own homes. None of the standards mentioned above define limits for passenger accommodation, but confine their attention to the working and crew resting and recreation spaces of the ship. In hotels noise levels in the range 30–40 dB(A) can be expected for the better standard rooms. In contrast, from LR's experience of conducting field measurements, modern passenger cabins have noise levels in the range 50–55 dB(A) in general, reducing to 40–50 dB(A) in the case of some luxury cabins.

The changes in ship construction, the emergence of noise regulations and the increasing demands of passengers, have reinforced the importance of noise control considerations as early as possible in the design stage in order to avoid any costly remedial actions that may be required after construction. The formulation of an effective noise control strategy will involve noise prediction calculations and this paper describes this process.

Main elements of noise prediction

The process of noise prediction involves consideration of three related elements: the noise source, the transmission path and the receiver. While each element appears to be independent, they can, jointly or individually, affect the prediction results significantly. As such, the understanding of each element, and particularly the input data required, is essential before proceeding with the calculation.

Noise sources

The major noise sources in a ship are: the main propulsion machinery, the auxiliary engines, the propeller and transverse propulsion unit, and the HVAC system. The relative sensitivity of one source, with respect to the noise level at the receiver, will depend on the ship type, machinery arrangement and the receiver location. A cabin at a location far from the main engine and propeller will more likely be affected by any HVAC noise. The majority of main and auxiliary machinery is driven either by diesel engines or steam turbines. Generally speaking, steam turbines generate less noise than diesel engines with similar output power, and are thus less likely to produce annoying background noise in accommodation areas.

Machinery generates noise into the surrounding air and also induces vibration into any structure to which it is connected. The levels of noise and vibration that are generated will be governed by the acoustic power and mechanical force of the machine itself. For propellers the main difficulty is the evaluation of cavitation generated noise, whereas the calculation of HVAC noise is relatively straightforward.

Machinery

The acoustic output power of a particular machine is expressed by the sound power level, which describes the rate at which energy is radiated (energy per unit time) from the sound source, but is independent of the nature of the space surrounding the source – the sound field. If the sound power level is known, the sound pressure level corresponding to the characteristics of a particular sound field may be deduced. Empirical formulae have been used for many years to estimate the sound power level of certain types of machinery, depending on the physical size, output mechanical power, operating speed etc, but the results are, in general, unsatisfactory. In fact, the traditional approach is to measure the sound pressure level directly and derive the sound power level. However, careful interpretation is required as the measured sound pressure level will be affected by:

1. the distance at which the measurement was carried out;
2. the difference of the acoustic properties between the spaces where the machine was tested and its final housing environment;
3. the presence of other significant noise sources.

Ideally, the machine under test should be placed in an anechoic chamber, but in practice this is not always possible.

The availability of sound intensity meters in the late 1980s enabled the direct measurement of sound intensity. The determination of sound power through sound intensity measurement is more direct and accurate than the determination through sound pressure measurement. This is due to the fact that the intensity meter takes account of the direction of the power flow as well as the magnitude. Thus measurements can be taken in any sound field without being influenced by background noises from other machinery. Standard methods of taking sound intensity measurements are still being formulated and these will be required to ensure a consistent approach.

Turning to the subject of mechanical force determination; ideally the mechanical force generated by the source should be measured and the vibration levels that could be induced into the structure calculated, based on the mobility of the seating (mobility is a frequency response function to describe the vibration response of a structure to an input force). In practice, however, it is not possible to measure the force directly and, instead, vibration levels at the foot of the machine are normally measured at the test bed and the results used as the input data in noise prediction. Unless the mobility of the test bed seating is the same as that installed on the ship, test bed results should only be treated as experimental data. This method also does not make any allowance for the flexible nature of the ship structure, compared to the solid floor at the test site.

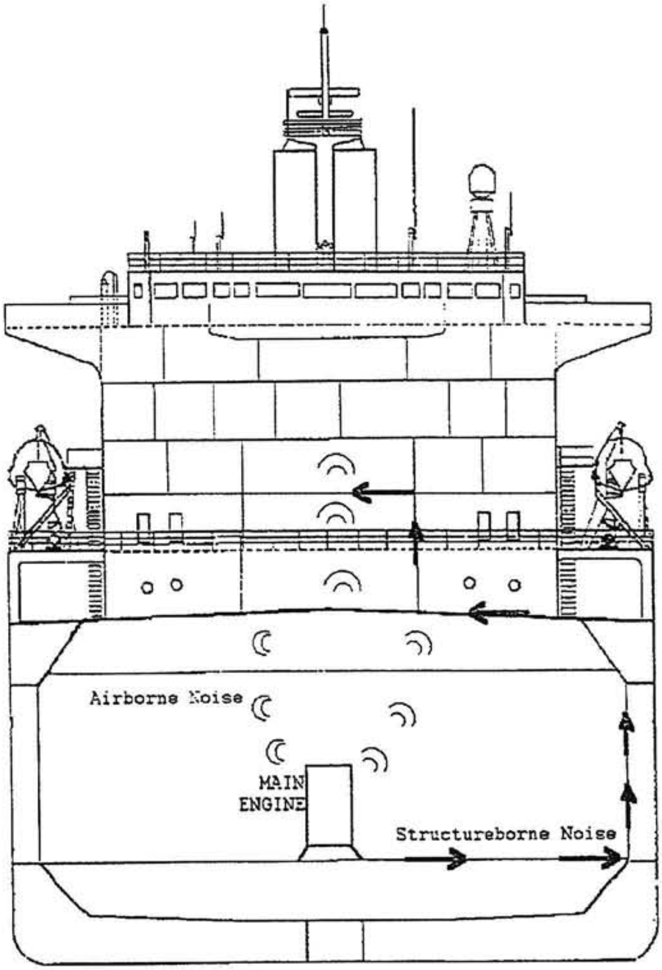

Figure 1. Noise transmission path

Propellers

The main difficulties in determining propeller noise are associated with uncertainties in the description of cavitation growth and collapse on the propeller blades, the calculation of wake field distribution around the aft end of the ship, and the shell plate response to waterborne sound pressure. Although there exist both semi-empirical formulae derived from model experiments and prediction models of the equivalent acoustical source strength (based on the speed of revolution, transmitted power and the propeller geometry), the results do not compare favourably with practical measurements. The lifting surface

Table 2. *Insertion loss of common contruction materials*

Material	Mean value	63	125	250	500	1000	2000	4000	8000
		Octave band centre frequency (Hz)							
Steel plate									
3.2 mm thick	32	16	22	28	34	40	44	32	41
6 mm thick	37	22	28	34	40	45	37	42	51
12 mm thick	42	28	34	40	45	37	41	51	60
Mineral wool (120 kg/m^3)									
25 mm thick	19	4	9	14	19	24	29	34	39
50 mm thick	24	9	14	19	24	29	34	39	44
75 mm thick	27	12	17	22	27	32	37	42	47
100 mm thick	29	14	19	24	29	34	39	44	49
Mineral wool (200 kg/m^3)									
25 mm thick	22	7	12	17	22	27	32	37	42
Cement									
20 mm thick	37	22	27	32	37	42	47	52	57
40 mm thick	42	27	32	37	42	47	52	57	62
Calcium silicate board									
6 mm thick	23	8	15	19	23	24	24	34	35
9 mm thick	27	11	18	22	26	27	27	37	38
13 mm thick	29	14	21	25	29	33	40	41	41
19 mm thick	32	17	24	28	32	33	33	43	44
Glass wool (17 kg/m^3)									
50 mm thick	12	0	2	7	12	17	22	27	32
Swedac on steel deck	59	32	43	50	52	67	67	76	90
TNF on steel deck	49	22	38	46	55	53	59	60	60

method, normally used in propeller analysis, is potentially capable of estimating the radiated pressure field of a cavitating propeller in the low frequency range. The method is predominantly based on a time domain analysis of cavitation growth and collapse, for propellers operating in a known wake field. It is adequate for estimating pressure sources at blade passing frequency, but the quality of correlation between measured and predicted pressures at higher multiples of blade passing frequency reduces as the harmonic number increases.
Transverse propulsion units are recognised as a major noise source when they are used for docking manoeuvres. A unit of this type is normally integrated into the hull structure rather than having a fluid medium between it and the hull surface, as in the case of the propeller. A noise prediction method developed by the Institute of Applied Physics, Delft, is based on a large number of measurements onboard different types of ships and is described in Ref 3.

Transmission path

Noise transmission can either be waterborne, airborne or structureborne. External, waterborne noise transmission is mainly of concern to specialised vessels such as seismic survey ships, oceanographic research ships, fishery ships and naval vessels. For merchant ships, the internal noise environment is of greater concern and is affected primarily by airborne and structureborne noise. Figure 1 shows typical airborne and structureborne noise transmission paths.

Airborne noise

Airborne noise is transmitted by exciting the surrounding air particles. As the noise propagates, part of the energy will be lost through the barriers it crosses and the distance it travels. Generally, the noise level will drop by 6 dB for every distance doubled and the amount of noise attenuated through barriers will depend on the total insertion loss (IL) through the barriers (insertion loss is a measure of the decrease in transmitted power in decibels). In the ship environment, the barriers include decks, bulkheads and cabin partitions. Table II lists the IL of some common construction materials. It should be noticed that the IL is higher at high frequencies and with thicker material. This is

Table 3. *Radiation factor of common construction materials*

Construction	Octave band centre frequency (Hz)							
	63	125	250	500	1000	2000	4000	8000
Steel plate (20 mm thick)	25	22	15	10	6	−2	0	0
TNF floor	16	17	13	10	1	−4	0	0
Swedac floor	19	18	17	16	13	5	−5	0
Cement on steel	19	18	15	2	−2	0	0	0
Cabin wall/lining	19	16	15	10	5	0	0	0

Table 4. *Absorption coefficients of common construction materials*

Description		Octave band centre frequency (Hz)							
	Mean coefficient	63	125	250	500	1000	2000	4000	8000
Room partition	0.04	0.10	0.09	0.05	0.02	0.01	0.01	0.01	0.01
Room ceiling	0.64	0.45	0.50	0.60	0.65	0.75	0.80	0.75	0.65
Floor with vinyl tile	0.05	0.02	0.02	0.04	0.05	0.05	0.10	0.05	0.05
Floor with carpet	0.20	0.05	0.10	0.15	0.25	0.30	0.30	0.30	0.20
Tiled deck	0.03	0.02	0.02	0.03	0.03	0.03	0.03	0.02	0.02
Steel plate	0.02	0.01	0.02	0.03	0.03	0.03	0.02	0.02	0.02

because the wavelengths of high frequency components are shorter and are thus more easily interrupted. In fact, noise at remote areas is normally dominated by low frequency components which, in practice, are very difficult to eliminate.
As stated, airborne noise is attenuated by bulkhead partitions and distance from the source. It is, therefore, found to be the main transmission mechanism in spaces where excitation sources are located but its influence on remote areas is negligible. A typical example is the domination of airborne noise generated in an engine room.

Structureborne noise

Structureborne noise is the propagation of vibratory energy through the structure. In contrast to airborne noise, an insignificant amount of energy will be lost through 'untreated' steel structures in the transmission process, due to low inherent damping. In fact, energy could well be gained in the transmission process due to coupling and due to resonances of sub-systems as the structureborne noise passes through. Because the reduction of structureborne noise is mainly achieved through the process of diversification of energy at structural discontinuities rather than distance from the source, it is the main cause of noise levels in spaces remote from excitation sources.
Vibratory energy travels through structures in several types of waveforms, mainly bending, longitudinal, transverse and even torsional. Of all the waveforms considered, bending waves are by far the most important type for structureborne noise transmission as they are found to be well coupled to the radiation of airborne noise. However, this does not necessarily mean that bending waves carry more vibratory energy than other types of waveforms. In fact, the wave types are interrelated because bending waves at structural joints could be transformed into other wave types and vice versa. Although it is known that waveform transformation takes place at joints, the method by which the energy is distributed in the process is still uncertain. This uncertainty is compounded when considering a complicated ship structure involving a large number of discontinuities.

Receiver

The receiver is the area or enclosure where the final noise level due to the noise sources considered is to be determined. This could be any indoor or outdoor space of interest in a ship.

Enclosed space

The noise level in an enclosed space is affected by the total acoustic power entering the space and the acoustic properties of the space itself. The total acoustic power entering the space is a combination of both airborne noise and radiated airborne noise due to structureborne noise transmission. When structureborne noise reaches the receiver, part of the energy will excite the surrounding air to generate airborne noise. This mechanism is called radiation. As structureborne noise will travel along all surfaces of the enclosure through solid connections, the radiation factor of each surface will contribute to the total power radiated. The radiation factor is primarily a function of the material of the structure and also depends on the mounting condition. Its values are frequency dependent and, preferably, should be determined by measurement on site. Table III lists the radiation factors for some construction materials used in ships. For a 20 mm thick steel plate, the most effective radiation will occur at a 2000 Hz centre frequency, increasing the noise level by 2 dB. At a 63 Hz centre frequency, the radiated noise level will be reduced by 25 dB.

The acoustic properties of an enclosure are generally expressed as the 'room constant'. The room constant is defined by the amount of exposed surface area in the enclosure and the acoustic absorption properties of the surfaces. The larger the room and the more absorptive area the surfaces have, the larger will be the value of the room constant and the smaller will be the noise level in the enclosure. Table IV presents the absorption coefficients of common materials used in accommodation areas. Again, the values of these coefficients are frequency dependent.

Outdoor area

An outdoor area is normally treated as a 'free-field' condition such that any noise transmission will not be reflected from solid surfaces and will not encounter any barriers. For example, the calculation of the noise level on a navigation bridge wing due to funnel exhaust gas considers only the direction of the source and the distance between the source and receiver.

Noise prediction methods

Over the years a number of noise prediction techniques have been developed, based on various hypotheses and theories. Three main approaches can be identified. These are: the finite element method (FEM), statistical energy analysis (SEA) and the semi-empirical method. The first two approaches aim to address the propagation of structureborne noise from theoretical stand points. The last approach uses existing well-developed empirical formulae to calculate airborne and structureborne noise attenuation.

Finite element method

The application of the FEM in engineering appeared as early as the mid-1950s. The basis of this method is to subdivide a complex structure into a finite number of discrete parts or elements. Structural relationships can then be derived

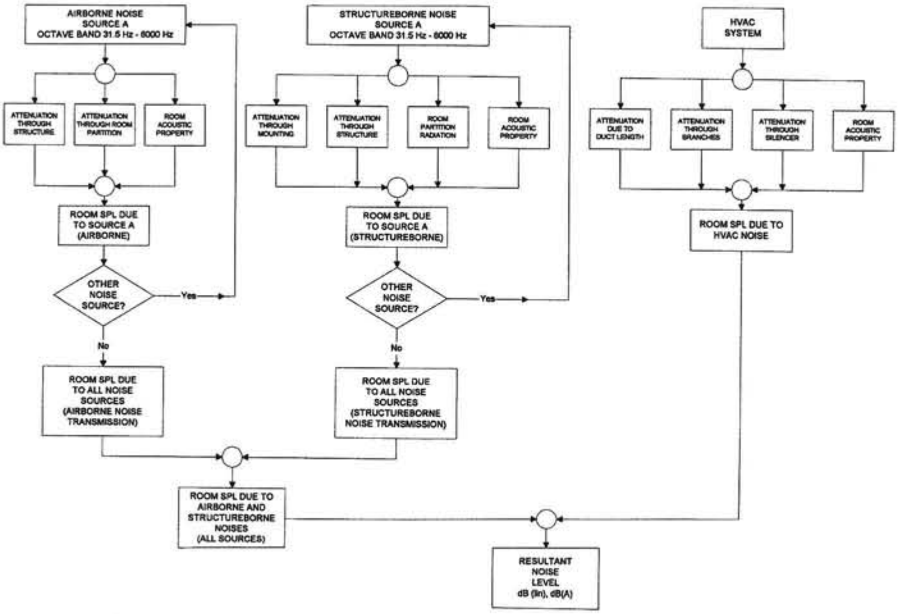

Figure 2. Noise prediction programme flow chart

for each finite element which link force and displacement components at the nodal points. Although the great strength of the FEM is its versatility, as there is virtually no limit to the type of structure that can be analysed, the competence required to select suitable elements in building up the model can only be gained through research work and/or practical experience. Technically, providing the element types are suitably selected, an increase in the number of elements that are used to represent a structure will give better results. However, the use of more elements implies longer computing time and, as such, a balance has to be drawn between these two conflicting criteria. Experience gathered in the past suggests that FEM is particularly suitable for problems concerning low frequency vibrations.

Statistical energy analysis

This method involves the evaluation of vibration energy dissipated between connected resonant structures by a statistical method, and is based on the assumption that the flow of acoustical energy between two subsystems is proportional to the difference in energy levels between these subsystems. The major conditions under which SEA can be applied are that the coupled systems are resonant and that the modal density (the number of resonant vibration mode shapes within a frequency bandwidth) of each system is sufficiently high. The higher the number of mode shapes that appear in each system, the better is

Table 5. *Structureborne noise attenuation of various abatement measures*

Description	Mean attenuation	63	125	250	500	1000	2000	4000	8000
		Octave band centre frequency (Hz)							
Resilient mount	18.5	12	16	20	20	20	20	20	20
Floating floor	17.4	2	6	12	17	18	24	30	30
Cement floor	6.4	–2	2	3	6	9	10	11	12
TNF floor	24.1	0	3	12	14	22	37	50	55
Swedac floor	26.1	17	24	23	23	26	26	34	36

Table 6. *Particulars of a 4410 TEU containership*

Length (BP)	263m
Breadth (Mld)	37.1m
Depth (Mld)	21.7m
Draught (Mld)	12.5m
Main engine	mcr: 41 310 kW at 93 rev/min ncr: 36 170 kW at 89 rev/min Mounting: solid
Auxiliary machinery	4 off: 1880 kW each at 720 rev/min Mounting: elastic
Propeller	1 x 5-bladed Diameter: 8400 mm Mean pitch: 9156 mm

the accuracy. The method generally provides fairly good results at high frequency bands but not in the low frequency bands, and it is normally used on structures which are less complex than ships.

Semi-empirical method

Perhaps this is still the most commonly adopted method for noise prediction. The method uses empirical formulae for the calculation but the accuracy of the results will ultimately be determined by the quality of the input data. The input data could be obtained from various sources. With respect to the noise source data, manufacturers are usually able to supply noise data associated with the machinery supplied, in terms of both airborne and structureborne noise levels. Even without this information, however, data can be interpolated from noise measurements on similar machinery, or even calculated approximately from empirical formulae. Regarding the data for the receiver, the acoustic properties of the structure are normally well determined either by laboratory tests or site measurements. The characteristics of the transmission path present the most problems in terms of the calculation of structureborne noise attenuation. Over the years, LR has carried out extensive measurements on various kinds of ships to establish the characteristics of noise attenuation through different types of construction. These experimental results are stored in a data bank, together with noise source and receiver data. Because of the large amount of information available, the semi-empirical method is used as the basis for the LR's inhouse noise prediction programme.

LR noise prediction programme

Figure 2 shows the flow chart of the programme. It is built up from three modules to cover airborne, structureborne and HVAC noise calculations separately. The merits of using a modular structure are that the effects of each module on the noise level at the receiver can be evaluated easily and the dominant sources causing any excessive noise can be identified.

Airborne noise calculation module

The calculation is based on the assumption that the airborne overall sound pressure level in the receiving space is equal to the combined effect of the sound power levels emanating from all significant noise sources. The partition insertion loss in way of the noise transmission path and the acoustic properties of the receiving space are considered in the process. After the sound pressure level at the receiver has been calculated, due to each noise source in every octave band (centre frequency of 63 Hz to 8000 Hz), the resultant noise level can then be obtained by logarithmic addition to obtain the overall airborne noise level within the space or compartment.

Structureborne noise calculation module

The major assumption underlying this calculation is that vibratory energy transmits into the structure from noise sources in the form of acoustic frequency vibration, which is attenuated through discontinuities and with distance from the source. For convenience of calculation, the attenuations are considered to be concentrated at structural discontinuities along the path between the source and the receiving end. The discontinuities accounted for in the calculations are: deck plate stiffening, junctions of deep frames and bulkheads, and junctions of shell plating with decks.

The degree of structureborne noise attenuation through each junction is not the same for all ships due to differences in the geometry of construction. Studies of data collected through measurements, however, provide nominal values, and as a rough guide, structureborne intensity reduces on average by about half a decibel per frame. Structureborne noise also falls with vertical distance from the source; for example, the noise reduction on the first two decks is approximately 5 decibels per deck and on subsequent decks is approximately 2 decibels per deck.

Noise abatement measures are widely applied in a ship to control the noise

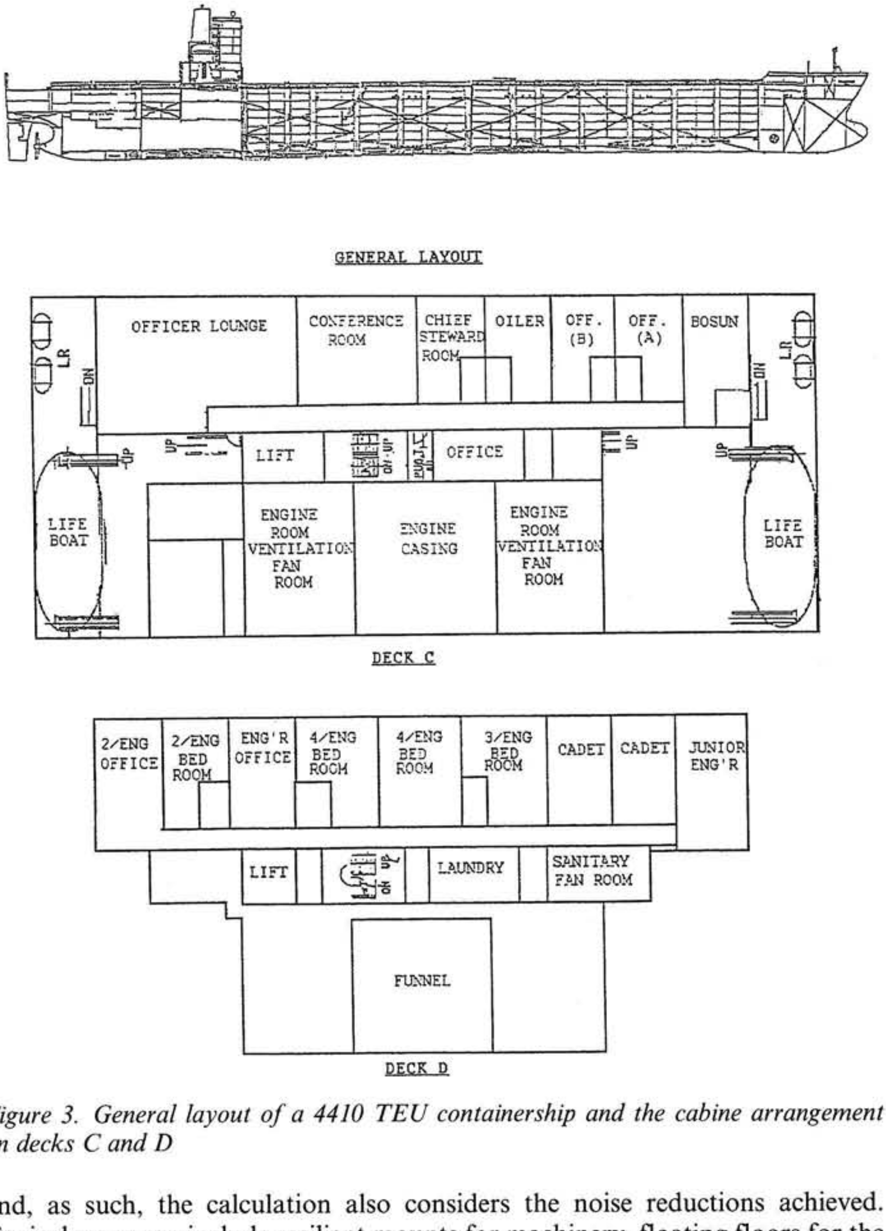

Figure 3. General layout of a 4410 TEU containership and the cabine arrangement on decks C and D

and, as such, the calculation also considers the noise reductions achieved. Typical measures include resilient mounts for machinery, floating floors for the accommodation, silencers for ventilation outlets and damping materials applied to steel structures. The attenuation data for some general abatement measures are given in Table V. It should be noted that the effectiveness is frequency dependent and, as such, the selection of measures proposed requires careful consideration.

Table 7. *Comparison of predicted and measured noise levels (4410 TEU containership)*

Deck	Space	Noise level, dB(A)	
		Predicted	Measured
2nd	Workshop	86	82
	Engine control room	72	76
Upper	Suez crew	64	63
	Deck control room	66	64
	Shipper's office	66	61
A	Hospital	59	56
	Crew recreation room	62	57
	Galley	70	68
	Crew mess room	57	61
B	Gymnasium	66	66
	Chief cook	58	56
	Crew (K)	59	54
	Officer mess room	62	58
C	Open swimming pool	74	77
	Bosun	59	55
	Chief steward office	62	58
	Conference room	63	*56
	Officer lounge	62	*56
D	Cadet (A)	66	*51
	4th engineer	62	*52
	Engineer office	59	55
	2nd engineer dayroom	58	53
E	Chief engineer dayroom	64	55
	Chief engineer	54	53
F	Radio room	53	49
	Captain bedroom	61	*55
	Radio officer	53	51
Navigation	Bridge	52	*60

* More than 5 dB(A) deviation

Table 8. *Particulars of a 70m yacht*

Length (BP)	61.25m
Breadth (Mld)	12.4 m
Depth (Mld)	5.75m
Speed	17.5 kn at mcr
Main engine	2 x Caterpillar type 3516 2 off: 1432 kW each at 1800 rev/min Mounting: elastic
Auxiliary machinery	3 off: 145 kW each at 1500 rev/min Mounting: elastic
Propeller	2 x 4-bladed highly skewed cpp Diameter: 1700 mm Mean pitch: 20 094 mm

The sound pressure level radiated from the vibrating surface of each boundary in the receiving space is calculated in a similar manner to the airborne noise calculation, taking into account the acoustic properties of the receiver. The calculation is repeated for all noise sources in all selected octave bands. The resultant sound pressure level can then be used to evaluate the overall airborne noise levels in the space due to the structureborne noise.

HVAC noise calculation module

The calculation of HVAC noise depends on a knowledge of the sound power output of the fans in the air conditioning system. The noise emitted from air outlets in the receiving space will depend on the amount of noise attenuation due to the length of ducting, types of duct branches, air flow rates and the characteristics of any silencers fitted. The resultant sound pressure level in the space is then calculated, taking into account the acoustic properties of the space itself.

Once the sound pressure levels in the receiving space due to the airborne, structureborne and HVAC noise sources have been calculated, the overall noise level can be obtained by logarithmic summation. The results are expressed in linear and A-weighted values for every octave centre frequency band. The overall A-weighted noise level at the receiver is also given.

Case studies

Case 1: 4450 TEU containership

A noise prediction was carried out during the ship's early design stage. The principal particulars of the ship are listed in Table VI and the general layout is shown in Fig. 3.

The first step in any noise prediction process is to identify the sources. An examination of the general layout revealed that the accommodation block was located between frames 70 to 90 and, therefore, propeller induced noise was not expected to have any significant effect on the background noise levels, even though it was included in the calculation. Also, the accommodation block was not expected to be affected by noise from the bow thruster, which was located remotely at frame 151 and is only operated intermittently during manoeuvring. Further examination of the submitted drawings concluded that accommodation area noise would be caused by the main engine, auxiliary machinery, ventilation and exhaust fans, and the air conditioning units. The fans and the air conditioning units were located within the accommodation area. The starboard side of the accommodation was expected to be exposed to higher noise levels in comparison with the port side, due to the positioning of the machinery.

There were no special acoustic treatments applied to the ship and cabin construction was typically based on the following elements:

1. steel deck covered by a thin layer of concrete and polyvinyl tiles;
2. cabin lining rigidly connected to the decks and the bulkheads;
3. cabin lining surface made of steel sheet covered by a PVC film.

It was expected that a void space introduced immediately below the superstructure would reduce airborne noise transmission but have little effect on structureborne noise propagation.

A summary of the predicted and measured results is given in Table VII. The accuracy of the calculated overall noise levels was expected to be within 5 dB(A). In general, the predicted noise levels correlated well with the measurement results, with the exception of cabins on decks C and D. The accommodation arrangements of decks C and D in Fig 3 show that the engine room ventilation fans and the sanitary exhaust fan are located on these decks. Frequency analysis of the predicted results indicated that the major influence on the overall noise levels of spaces on these two decks was the structureborne noise emitted by these fans. The problem was related to the fact that information on these fans was not supplied by the makers, and so the input data used in the calculation were extracted from a data bank based on similar types of equipment. As only the cabins in the vicinity of the fans displayed disappointing

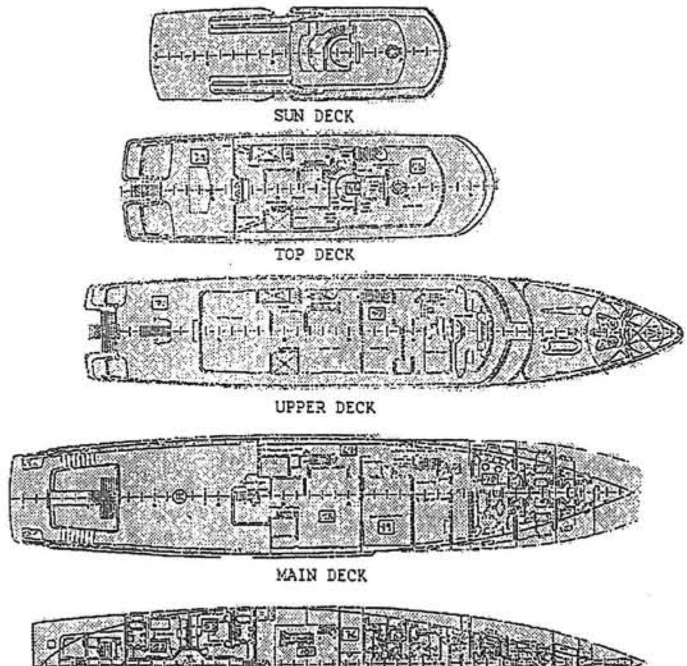

Figure 4. General layout of the 70m yacht

Table 9. *Comparison of predicted and measured noise levels (70m yacht)*

Deck	Space	Noise level, dB(A)			
		Alongside		Underway	
		Predicted	Measured	Predicted	Measured
Lower	Engine control room	56	57	76	*55-60
	Engine room	96	93-98	101	98-103
	Crew cabin (IV L2)	46	50	63	*50
	Guest cabin, P fore	45	43	53	*46
	Guest cabin, P aft	45	42	52	50
Main	Crew mess	45	46	48	49
	Dining room	45	44	49	47
	Main saloon	45	43	55	*48
Upper	Owner's suite	45	43	47	44
Top	VIP suite	45	46	46	45
	Outside sitting area	57	59	72	67

* More than 5 dB(A) deviation

results, it is suspected that the data extracted from the data bank did not truly represent the actual acoustic power of the machinery.

Case 2: 70m yacht

Particulars of the yacht are given in Table VIII and Fig. 4 respectively. The noise prediction was performed under two conditions : alongside and underway.

The alongside noise calculation was carried out assuming the operation of two generator sets, one engine room ventilation fan and the air conditioning system. The underway noise prediction was based on the running of both main engines and propellers, plus the noise due to the engine room ventilation fan and air conditioning system. In contrast to Case 1, propeller noise was considered as a significant noise contributor because of the location of the cabins and recreation areas. The diesel generators were, however, excluded from the underway noise calculation as the noise levels were found to contribute at least 9 dB per octave less noise and 18 dB per octave less vibration than the main engines.

Extensive noise and vibration attenuation measures were applied to the yacht, with most accommodation areas being fitted with floating floor arrangements. The application of special acoustic treatment on small vessels is quite common practice in order to achieve maximum noise attenuation in the light of the comparatively short transmission path between noise sources and receivers.

The comparison between the predicted and measured results is given in Table IX. Under the alongside condition the correlation is very impressive, suggesting that the quality of the input data with respect to the noise sources considered in this calculation was good. However, the predicted results for the underway condition for some areas are generally higher than the measured data, mainly at the lower deck. Frequency analysis reveals that the noise in the Engine Control Room was generated mainly by propeller airborne noise, while the noise in crew and guest cabins was affected by structureborne noise from both main engines and propellers. It is believed that the input data for the noise sources, especially propellers, could well be overestimated.

The above two case studies demonstrate the influence that the input data has on the accuracy of the final results. However, deviation between the predicted and measured results is also governed by how well the final construction agrees with the design drawings.

Future developments

The target of any future development is to improve the accuracy of noise prediction results. Technically, three areas in the noise production process can provide scope for improvement: determining the sound power levels of excitation sources accurately; improving the accuracy of estimating propeller noise; and understanding better the behaviour of structureborne noise propagation in ship structures.

Until recently, sound power output from machinery could only be derived from sound pressure measurement and the results are influenced by the various factors discussed earlier. With the introduction of the sound intensity meter, sound power can now be determined more confidently from the results of intensity measurements. Techniques for using the equipment and the measurement procedures to be followed are still at the development stage. LR is working with major engine builders to formulate standard measurement procedures in marine applications.

Propeller noise calculations using the combined lifting surface and bubble-cloud collapse method are available. The volume of cavitation computed in the wake peak is related to the distribution of free bubbles generated during the collapse phase of blade sheet cavitation. Comparisons with ship and model scale data show encouraging results, although the complexity of the approach is not ideal for preliminary design studies.

Regarding structureborne noise transmission, although the semi-empirical method can give good results if the analysed structure is similar to previous designs stored in a data bank, adjustment of parameters such as frame spacing, steel thickness etc, cannot be studied for different designs. In response to the rapid change in ship design concepts, the feasibility of using an SEA technique to address the structureborne noise transmission is currently under investigation.

Acknowledgements

The authors would like to express their thanks to the Committee of Lloyd's Register for permission to publish this paper. Thanks are also extended to the many colleagues in the Technical Investigation, Propulsion and Environmental Engineering Department who have contributed to the content of the paper.

References

[1] *Noise Levels On Board Ships*, International Maritime Organisation (IMO) Resolution A.468 (XII) (1982).

[2] *Code of Practice for Noise Levels in Ships*, UK Department of Transport, Second Edition (1990).

[3] Carlton, J.S. *Marine Propellers & Propulsion*, Butterworth-Heinemann Ltd (1994).